HAW HAMBURG

Master Thesis

Calculating the Power of Wind Turbines with the Blade Element Momentum Theory

Author: Laura Salcedo Campoamor

Supervisor: Prof. Dr.-Ing. Dieter Scholz, MSME
Submitted: 2017-08-18

Faculty of Engineering and Computer Science
Department of Automotive and Aeronautical Engineering

DOI:
https://doi.org/10.15488/xxxxx

URN:
https://nbn-resolving.org/urn:nbn:de:gbv:18302-aero2017-08-18.015
Associated URLs:
https://nbn-resolving.org/html/urn:nbn:de:gbv:18302-aero2017-08-18.015

Any further request may be directed to:
Prof. Dr.-Ing. Dieter Scholz, MSME
E-Mail see: http://www.ProfScholz.de

This work is part of:
Digital Library - Projects & Theses - Prof. Dr. Scholz
http://library.ProfScholz.de

Published by
Aircraft Design and Systems Group (AERO)
Department of Automotive and Aeronautical Engineering
Hamburg University of Applied Science

This report is deposited and archived:
- Deutsche Nationalbiliothek (https://www.dnb.de)
- Repository of Leibniz University Hannover (https://www.repo.uni-hannover.de)
- Internet Archive (https://archive.org)
  Item: https://archive.org/details/TextSalcedoCampoamor.pdf

This report has associated published data in Harvard Dataverse:
https://doi.org/10.7910/DVN/BI1LSE

Abstract

Purpose – Conversion of a FORTRAN program of the Blade Element Momentum Theory (BEMT) into an Excel program and to show how Excel (with the Solver) can be used to optimize the geometry of the blade geometry (pitch angle, taper ratio, number of blades).
Methodology – Literature review, work with fundamental wind energy equations, spread sheet programming.
Findings – Various free tools are available to calculate the aerodynamic power output of wind turbines. However, a spread sheet opens up all methods and equations and offers easy access to check and change the code and to adapt to a given problem. Cone and axis angle are usually parameters to be freely chosen, because classical Horizontal Axis Wind Turbine (HAWT) have 90° cone angle and 0° axis angle. Beyond the fundamental $C_P - \lambda_t$ curves also the curve power versus wind speed is of importance including stall behavior of the plant.
Research Limitations – Although the aerodynamic coefficients are from 2D measurements they can be used successfully in a quasi 3D setting. Realistic results require the lift coefficient to be known well beyond the stall angle of attack.
Practical Implications – The BEMT is made available via a spread sheet including optimization.

HAW HAMBURG

DEPARTMENT OF AUTOMOTIVE AND AERONAUTICAL ENGINEERING

Calculating the Power of Wind Turbines with the Blade Element Momentum Theory

Task for a *Master Thesis*

Background

For the past decades, wind power is the leading source of renewable energy. It is the world's fastest growing energy source due to its reliability and cost-effectiveness. The dominant wind turbine design is the Horizontal Axis Wind Turbine (HAWT). A closer look reveals that HAWTs often have an axis with a small angle to the horizon (axis angle). Furthermore, the blades may show an angle with the axis not exactly 90° (cone angle). Almost all engineering-level aerodynamic design calculations for HAWT are done with the Blade Element Momentum Theory (BEMT). Available for work on this task is a FORTRAN program for the BEMT that allows also the introduction of cone and axis angle.

Task

Task is to convert the FORTRAN program of the BEMT into an Excel program and to show how Excel (with the Solver) can be used to optimize the rotor geometry. The subtasks are:

- Review of available free tools to calculated the aerodynamic power output of wind turbines.
- Summary of the fundamental equations of the Blade Element Momentum Theory (BEMT).
- Introduction to the different wind turbine configurations.
- Help to get started with the blade element momentum spread sheet.
- Investigation of generic $C_P - \lambda_t$ curves.
- Trial to optimize disk geometry.

The report has to be written in English based on German or international standards on report writing.

Table of Contents

Page

List of Figures

List of Tables

List of Symbols

A	Cross-section area or surface area
a	Distance between blades
B	Placeholder
b	Strip width of wind affected by a single blade
C_d	Drag coefficient of a single blade element
C_l	Lift coefficient of a single blade element
C_P	Power coefficient
C_{P_i}	Power coefficient of a blade element
C_T	Thrust coefficient
D	Diameter
E	Energy
F_d	Drag force on a blade element
F_l	Lift force on a blade element
F_S	Total thrust force
L	Blade length
m	Mass
P	Power
Q	Change of twist angle along the blade for linear distribution
R	Effective radius
R'	Non-dimensional distance over the blade
r	Blade distance from the root
U	Change of blade chord along the blade
u	Circumferential speed
V	Volume
v	Axial speed
w	Composed speed
z	Number of blades

Greek Symbols

α	Angle of attack
β	Twist angle
β_S	Pitch angle
ε	Glide ratio
η	Efficiency
θ	Angle of rotation within the rotor plane

κ	Cone angle
λ	Speed ratio
ξ	Axial flow reduction factor
ρ	Density
σ	Tangential flow reduction factor
τ	Axis angle
φ	Angle of flow incidence on a blade element
ω	Rotation speed of the rotor

Subscripts

∞	Conditions upstream
0	Forces and powers without rotor, related to effective speed or related to the blade root element
1	Conditions upstream
2	Conditions on the actuator disc
3	Condition in the downstream
d	Conditions on the actuator disc
eff	Effective measure
i	Blade element number i
m	Related to the value between elements
min	Minimum value
opt	Conditions for maximum power
P	Related to friction
r	Related to the circular root of the blade
s	Perpendicular to the blade element chord
t	Tangential to the blade element chord or conditions on the tip
w	Condition in the wake or related to wind
z	Related to number of blades

List of Abbreviations

CAD	Computer-Aided Design
BEMT	Blade Element Momentum Theory

List of Terms and Definitions

Wind turbine

The American Energy Department describes it as follows: “A machine that converts wind energy to mechanical energy; typically connected to a generator to produce electricity.” This term is the focus of this thesis and will be presented and analysed during the whole text. Wind turbines are the main tool to extract power from wind and are the basis of wind energy and wind engineering.

Rotor

The Thesaurus dictionary defines it as: “The rotating armature of a motor or generator”. In a wind turbine is the part that transforms the aerodynamic forces generated by wind into a torque used in the electric power acquisition.

Actuator Disc

Circular area influenced by the rotor of a wind turbine through the wind crosses without taking into account rotating effects.

Rotor Disc

Circular area influenced by the rotor of a wind turbine through the wind crosses taking into account rotating effects, which disturb the wake.

Blade Element

Result of dividing a blade into several parts. This element is the aerodynamic unit within the rotor calculations.

1 Introduction

1.1 Motivation

Nowadays, wind energy has become a useful source of energy, and, as it is a relative new industry, since its first development it has carried different further challenges and difficulties which needed a new field of study. It was based on propeller engineering, although it has proved to involve distinct objectives. As the main aim of a wind turbine is to generate energy, all its design has to be focused on extracting power from the wind. For that reason, wind energy challenge is oriented to control the rotor and generator performance at every wind condition.

This thesis seeks to help wind industry in the preliminary design of the rotor and its blades in order to support wind energy.

1.2 Objectives

The final objective of this thesis is to give a solution to maximise the aerodynamic efficiency for certain wind conditions and given geometrical parameters being based on the Blade Element Momentum Theory. This calculation will help the preliminary design of a wind turbine rotor, supporting the initial step within wind turbine and wind energy calculation.

To that point, it is necessary to adopt a set of equations and theoretical base. For that reason, they will be derived some mathematical statements that will help the comprehension of the aerodynamics of a wind turbine. This will be done through the Blade Element Momentum Theory.

As a second step, it is necessary to use or implement a tool that can support all the calculations and give the sought results. This implicates the complete understanding of the tool for a correct use.

Furthermore, it will be implemented an additional wind turbine configuration that the user will be able to introduce in the analysed wind turbine. This new configuration will be composed of two installation angles based on the Wagner-Rotor (**Wagner**).

1.3 Literature and Researches

Since its beginning, aerodynamics has been the central science in wind energy; in 1915, Lanchester (**Lanchester 1915**) was the first to predict the maximum power output of an ideal wind turbine. A major study was achieved by Glauert (**Glauert 1935**), by formulating the Blade Element Momentum Theory (BEMT). This method is still the basis for all rotor design codes. Recently, first results of complete Navier-Stokes calculations for the most simple wind turbine operational mode have been reported.

Progress within this technical area has been significant in the 30-year history of modern wind energy. For example, a better understanding of the aerodynamics improved the aerodynamic efficiency from 0.4 to 0.5 (out of a maximum of 0.592).

Nevertheless, many phenomena are still not fully understood or quantified. This is due to several aspects that are unique for wind turbine aerodynamics:

- Wind turbines operate in the lowest part of the earth boundary layer, which leads to the fact that steady wind is an off-design condition (aircraft try to fly high enough to avoid turbulence and extreme winds). All aerodynamic phenomena are essentially unsteady, which, however, is still beyond the scope of current design knowledge.
- The very successful “Danish concept” for wind turbines relies on stall for aerodynamic power limitation in high wind speeds: the increase in drag due to stall limits the torque produced at the rotor axis. All other aerodynamic objects avoid stall as much as possible because of the associated high loads and the possible loss of aerodynamic damping.
- The flow in the blade tip- and root region is three-dimensional, while the flow just outside the layer is chord wise. The relevance of two-dimensional data for wind turbine performance prediction is very limited.

The aerodynamic research for wind turbines has contributed significantly to the success of modern wind energy. For most unsolved problems, engineering rules have been developed and verified. All of these rules have a limited applicability, and the need to replace these rules by physical understanding and modelling is increasing. This is one of the reasons that the world wide aerodynamic research on wind energy shows a shift towards a more fundamental approach.

1.4 Structure of Work

In order to present the information and analyses in this thesis, the text is organised in six chapters:

Chapter 2 gives a review of the theoretical concepts related to wind turbine aerodynamics and presents different codes and tools within the field developed in this thesis.

Chapter 3 explains the basis of the Blade Element Momentum Theory.

Chapter 4 presents several configurations and design options used in actual wind turbines.

Chapter 5 gives a detailed description of the Excel tool developed in this thesis.

Chapter 6 presents and explains general results and comparisons between diverse configurations and conditions.

Chapter 7 describes a possible optimization procedure to implement in order to maximize the power coefficient of a given wind turbine.

Annex A shows the numeric results for different rotors

2 Literature Review

Below there is an explanation of some of the basis of the aerodynamics that are followed up in this project. First, it is presented a summary of how a wind turbine works in order to achieve its objectives. Secondly, they are presented some actual examples of codes used to analyse wind turbine performances that are relevant for the conducted research.

2.1 Review of Aerodynamics for Wind Turbines

2.1.1 Introduction

To understand the performance of a wind turbine is necessary to set out the energy of the wind itself, seen as a moving body. This energy is given by

$$E = \frac{1}{2}mv^2(Nm) \qquad (2.1)$$

The mass of the wind is determined by its density and volume

$$m = \rho V\ (kg) \qquad (2.2)$$

To explain the point, it is suggested a circular window in a wall. This window will have a cross section of 1 m^2 and will be subjected to a flow of 10 m/s. With these data, 1/10 s are required to allow 1 m^3 of air to pass through the window. It is showed then, how the performance of the wind is related to the unit of time. (**Wagner**, Page 2**)**

Therefore, it can be applied the following expression derived from (2.1)

$$P = \dot{E} = \frac{1}{2}\dot{m}v^2\ (W) \qquad (2.3)$$

Knowing that $\dot{m} = \rho\dot{V}$ and $\dot{V} = Av$

$$P = \frac{1}{2}\rho Av^3\ \ (W) \qquad (2.4)$$

Therefore and however, the power output obtained from a wind turbine is given by the following expression s it will be seen

$$P = \frac{1}{2} C_P \rho A v_2^3 \qquad (2.5)$$

Where v_2 is the wind speed which the wind turbine rotor is subjected to, and C_P is the power coefficient, which describes the power in the wind that is converted by the turbine into mechanical work. This coefficient varies with the tip speed ratio (the ratio of blade tip speed to natural wind speed), and has a theoretical maximum of 0.593 (the Betz limit according to **Betz 1927**), so lower peak values are achieved in practice. By operating at variable speed, it is possible to maintain the maximum power coefficient over a range of wind speeds. However, these measures will give modest increases in the power output. Major increases in the output power can only be achieved by increasing the swept area of the rotor plane or by locating the wind turbines on sites with higher wind speeds (**Burton 2001**, Page 7).

The density of air is low compared to other elements as water, which leads directly to the large size of a wind turbine. Depending on the design, for 1,5 MW wind turbines may have a rotor that of more than 60 m diameter. (**Burton 2001**, Page 6)

Hence, during the last years, there has been an increase in rotor diameters from approximately 30 m to more than 60 m. This enlargement of the rotor diameter leads to a four-times increase in power output. On the other hand, the influence of the wind speed is more pronounced, leading to an eight-fold increase in power. Thus, it is ensure that wind farms are developed in areas of the highest wind speeds and the turbines optimally located within wind farms. Moreover, very high towers are being used (more than 60–80 m) to take advantage of the increase of wind speed with height. (**Burton 2001**, Page 7)

Studies have determined that the ‘optimum’ size of a wind turbine (regarding costs of manufacture, installation and operation against the revenue generated) is a diameter in the range of 35–60 m (**Burton 2001**, Page 7).

All modern electricity-generating wind turbines use the lift force derived from the blades to drive the rotor. So a high rotational speed of the rotor is desirable in order to reduce the gearbox ratio required.

Wind turbines are effective energy concentrators and as a result the energy recovery period is less than 1 year, i.e., the energy used to manufacture and install the wind turbine is recovered within its first year of operation (**Freris 1990**).

2.1.2 The Actuator Disc Concept

A wind turbine extracts kinetic energy from the wind by slowing down the mass of air which passes throw the rotor plane or actuator disc. Assuming that the affected mass of air remains separated from the air which does not pass through the actuator disc, a boundary surface can be drawn extended upstream and downstream forming a long stream-tube of circular cross section. No air flows across the boundary, so the air flowing will be the same for all positions along the stream-tube. The air within the stream-tube slows down, but is not compressed, so the cross-sectional area of the stream-tube must expand to accommodate the slower moving air, Figure 2.1, (**Burton 2001**, Page 42)

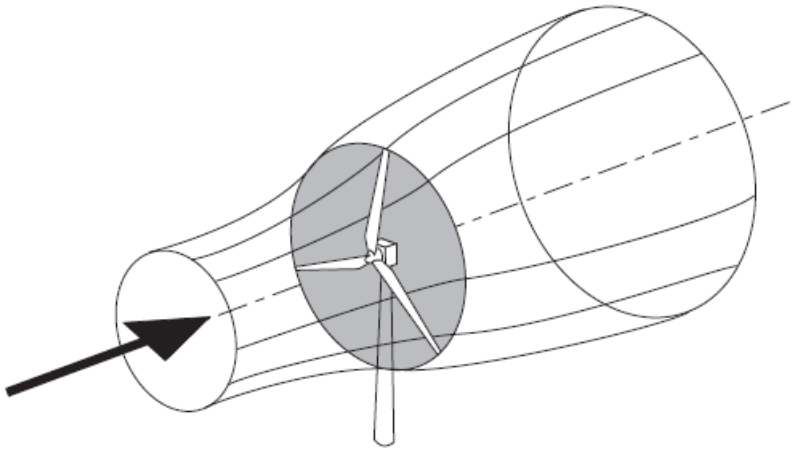

Figure 2.1 Stream-tube of air mass affected by an actuator disc (from **Burton 2001**)

The presence of the turbine causes the air upstream gradually to slow down such that when the air arrives at the actuator disc its velocity is already lower than the free-stream wind speed. The stream-tube expands as a result of the slowing down and, as the air passes through the disc, there is a drop in static pressure such that, when leaving, the air is below the atmospheric pressure level. The air then proceeds downstream with reduced speed and static pressure (that is, the wake), Figure 2.2.

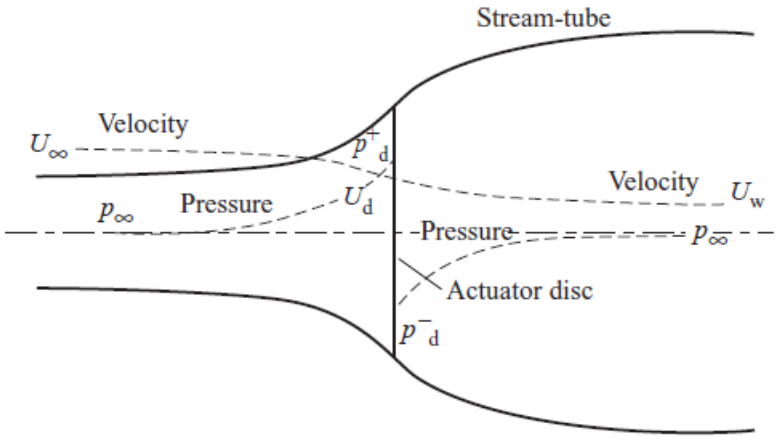

Figure 2.2 Pressures and speeds within the stream-tube (from **Burton 2001**)

The mass of air which passes through a given cross section of the stream-tube in a unit of time is ρAU, where ρ is the air density (1.255 kg/m^3), A is the cross-sectional area and U is the flow velocity. The mass flow must be the same everywhere along the stream-tube,

$$\rho A_\infty U_\infty = \rho A_d U_d = \rho A_w U_w \qquad (2.6)$$

The symbol ∞ refers to conditions upstream, d to conditions at the actuator disc and w to conditions in the wake. However, from now on, the pressures and speeds within the stream-tube will be named as represented in Figure 2.3.

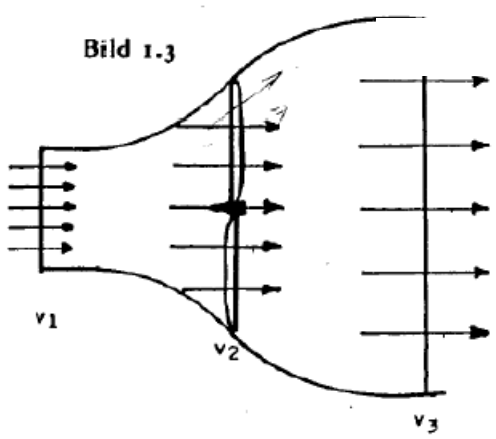

Figure 2.3 Speeds v_1, v_2 and v_3 (from **Wagner**)

Meaning that

$$\rho A_1 v_1 = \rho A_2 v_2 = \rho A_3 v_3 \qquad (2.7)$$

2.1.2.1 Momentum Theory

The power extracted from the rotor is the difference between the wind power before and behind the actuator disc, that according to (2.4) is given by

$$P = P_1 - P_3 = \frac{1}{2}\dot{m}_1 v_1^2 - \frac{1}{2}\dot{m}_3 v_3^2 \qquad (2.8)$$

As it was explained, it is assumed that the affected mass of air remains separated from the air which does not pass through the actuator disc, so $m_1 = m_3 = m$, giving

$$P = \frac{1}{2}\dot{m}(v_1^2 - v_3^2) \qquad (2.9)$$

A second relationship can be formulated over the thrust. The thrust on the actuator disc is

$$F_S = \dot{m}(v_1 - v_3) \quad (2.10)$$

And due to it, the work in the actuator disc is

$$P = F_S v_2 = \dot{m}(v_1 - v_3)v_2 \quad (2.11)$$

This work must be equal to the extracted power according to (2.9)

$$\dot{m}(v_1 - v_3)v_2 = \frac{1}{2}\dot{m}(v_1^2 - v_3^2)$$

$$(v_1 - v_3)v_2 = \frac{1}{2}(v_1^2 - v_3^2)$$

$$(v_1 - v_3)v_2 = \frac{1}{2}(v_1 - v_3)(v_1 + v_3)$$

$$v_2 = \frac{1}{2}(v_1 + v_3) \quad (2.12)$$

That is, v2 is the average value between v1 and v3. Therefore, the extracted power can be adjusted with (2.9), $\dot{m} = \rho A_1 v_1 = \rho A_2 v_2 = \rho A_3 v_3$ and (2.12)

$$P = \frac{1}{2}\rho A_2 v_2 (v_1^2 - v_3^2)$$

$$P = \frac{1}{2}\rho A_2 \frac{v_1 + v_3}{2}(v_1^2 - v_3^2) \quad (2.13)$$

2.1.2.2 Power Coefficient

If it were not accommodated any rotor in the cross section A_2, the air could pass through unhindered. The power which would pass through the undisturbed A_2 is according to (2.4)

$$P_0 = \frac{1}{2}\rho A_2 v_1^3 \quad (2.14)$$

A power coefficient is then defined as

$$C_P = \frac{P}{P_0} = \frac{\frac{1}{2}\rho A_2 \frac{v_1 + v_3}{2} (v_1^2 - v_3^2)}{\frac{1}{2}\rho A_2 v_1^3}$$

$$C_P = \frac{1}{2}(1 + \frac{v_3}{v_1})(1 - \frac{v_3^2}{v_1^2})$$

$$C_P = \frac{1}{2}(1 + \xi)(1 - \xi^2) \qquad (2.15)$$

Thus, it can be defined now an important parameter: the axial flow reduction factor, ξ. This parameter expresses the reduction of speed between before and behind the rotor

$$\xi = \frac{v_3}{v_1} \qquad (2.16)$$

The curve for the aerodynamic efficiency (seen as the power coefficient, C_P) as a function of ξ is shown in Figure 2.4.

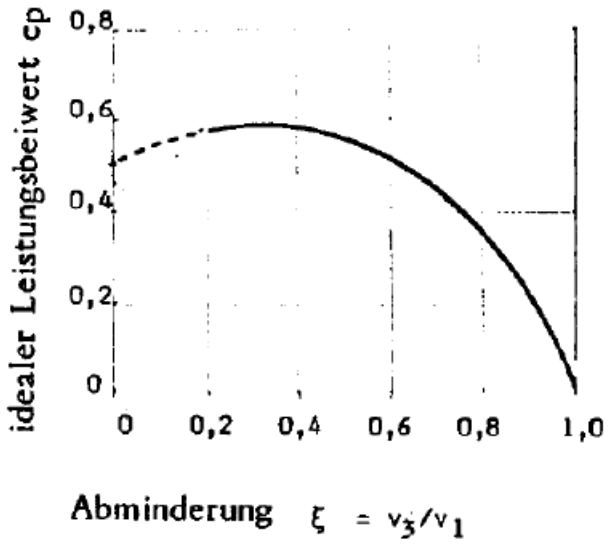

Figure 2.4 Curve for aerodynamic efficiency as a function of the reduction factor (from **Wagner**)

2.1.2.3 The Betz Limit

As it can be inferred from Figure 2.4, the power coefficient has an optimum, which can be obtained by the derivation of (2.14)

$$\frac{dC_P}{d\xi} = \frac{1}{2}(1 - \xi^2) + \frac{1}{2}(1 + \xi)(-2\xi) = 0$$

$$-3\xi^2 + \frac{2}{3}\xi - \frac{1}{3} = 0$$

$$\xi = -\frac{1}{3} \pm \sqrt{\frac{1}{9} + \frac{1}{3}} = -\frac{1}{3} \pm \frac{2}{3}$$

$$\xi_{\text{opt}} = \frac{1}{3} \qquad C_{P_{opt}} = \frac{16}{27} \approx 0.593 \qquad (2.17)$$

This maximum of the power coefficient is known as the Betz limit after Albert Betz, German aerodynamicist (presented in **Betz 1927**), and no current wind turbine is capable of exceeding this limit. The limit is caused not by the design, but because the stream-tube has to expand upstream of the actuator disc and so the cross section of the stream-tube where the air is at the higher, free-stream velocity is smaller than the area of the disc. (**Burton 2001**, Page 45)

In the design of wind turbines it is not necessary to ensure that the correct reduction is always made. This is very reassuring to know because it allows constructions to approximate to the ideal curve and do not require a high production effort to produce an ideal wing. (**Wagner**, Page 5)

2.1.2.4 Thrust Coefficient

The force on the actuator disc caused by the pressure drop, given in (2.10), can be also non-dimensionalized to give the thrust coefficient, C_T.

If it were not accommodated any rotor in the cross section A_2, thrust generated on the actuator disc A_2 would be

$$F_{S_0} = \frac{1}{2}\rho A_2 v_1^2 \qquad (2.18)$$

Then, the thrust coefficient is defined as

$$C_T = \frac{F_S}{F_{S_0}} = \frac{\frac{1}{2}\rho A_2 v_2 (v_1 - v_3)}{\frac{1}{2}\rho A_2 v_1^2}$$

$$C_T = \frac{\frac{1}{2}\rho A_2 \frac{v_1 + v_3}{2}(v_1 - v_3)}{\frac{1}{2}\rho A_2 v_1^2}$$

$$C_T = \frac{1}{2}(1+\xi)(1-\xi) \qquad (2.19)$$

2.1.3 Rotor Disc Theory

How the extracted energy is converted into usable energy depends on the turbine design. Most wind energy converters use a rotor with an angular velocity ω about an axis generally normal to the rotor plane and parallel to the wind direction. The blades of the rotor develop a pressure difference across the disc, which is responsible for the loss of axial momentum downstream (wake). (**Burton 2001**, Page 46)

The loss of axial momentum is associated to a loss of energy which has to be collected by an electrical generator attached to the rotor shaft. The generator exerts a torque equal and opposite to the airflow which keeps the rotational speed constant. The work done by this torque on the generator is converted into electrical energy. (**Burton 2001**, Page 46)

2.1.3.1 Wake Rotation

The work of the torque on the rotor disc by the air passing through it requires an equal and opposite torque imposed on the air. The consequence of the reaction torque is to cause the air to rotate in a direction opposite to that of the rotor; the air gains angular momentum, so it has a velocity component tangential to the rotation as well as an axial component (Figure 2.5).

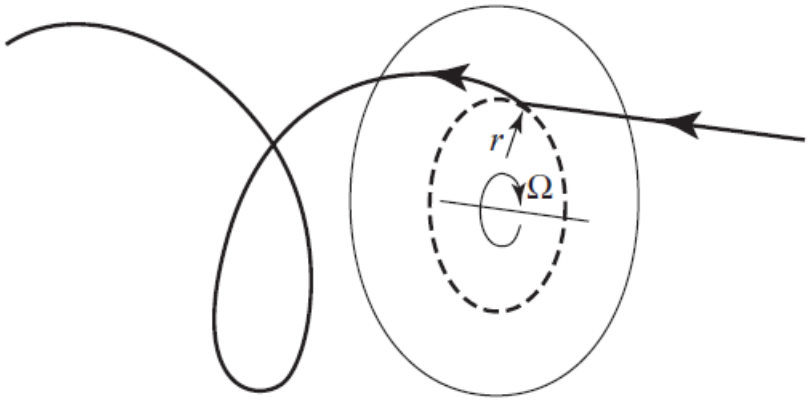

Figure 2.5 Trajectory of an air particle through the rotor disc (from **Burton 2001**)

The acquisition of the tangential component of velocity by the air means an increase in its kinetic energy which is compensated for by a fall in the static pressure of the air in the wake (**Burton 2001**, Page 47).

In a standing system, for example, an air particle would bounce and fly again at the same speed, w_3, which it had previously, w_1 (**Wagner**, Page 12). Only the direction has changed, therefore:

$$|w_1| = |w_3| \qquad (2.20)$$

Figure 2.6 shows a standing system, which can be seen as a very slow rotating speed rotor. On the other hand, a high speed rotor would cause a little spin.

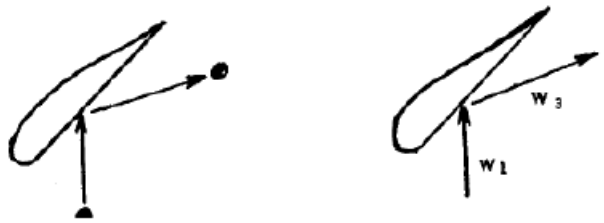

Figure 2.6 Air particle within a slow rotating speed rotor (from **Wagner**)

2.1.3.2 Number of Blades

The influence of the number of blades or the distance between the blades also plays a role within the wind turbine design. Hitherto, it has always been assumed that all the air which flows through the circular surface affected by the blades can be influenced by them. If there were a large number of blades, this assumption would be correct in some respects. If, however, the blades are very distant from each other, there are certain losses, since the whole area is not affected. (**Wagner**, Page 15)

If the blades are represented in a straight line, it is obtained Figure 2.7.

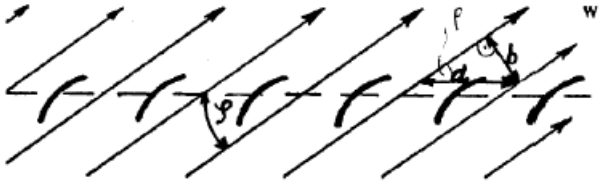

Figure 2.7 Influence of the number of blades (from **Wagner**)

The air flows relative to the blades with an obliquely velocity, due to the rotation of the rotor disc. It can be seen that each blade has to influence a strip of air of width b, which is substantially smaller than the distance between blades, a (**Wagner**, Page 15). The relation between these two distances is given by

$$b = a \sin\varphi \quad (\rho = \varphi \; in \; \mathbf{Figure\ 2.7}) \qquad (2.21)$$

Thus, not the blade distance a, but the considerably smaller air strip width b is decisive.

On the other hand, on the blade tips occurs a considerable effect in which a gradual drop in the air deceleration takes place. This is due to the difference of pressures between up and backwards of the blade which causes the air to flow upwards of the cross section as seen in Figure 2.8. (**Wagner**, Page 15)

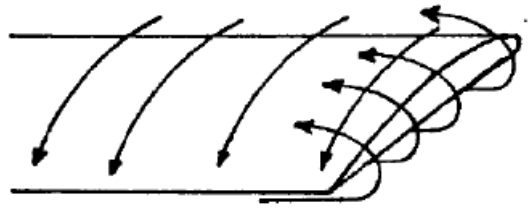

Figure 2.8 Blade tip effect (from **Wagner**)

This effect extends from the tip to inside, the further the inward direction, the larger the air strip width b. Therefore, the outer sections of the blade do not have the same performance as the parts located closer to the root. This can be taken into account assuming, instead of the actual rotor diameter, D, an effective diameter, D_{eff}, which is somewhat smaller, but would produce the same effect as the real diameter with the drop at the edge when the wheel is fully utilized. In propeller calculations, this effective diameter is expressed as $D - D_{eff} = 0{,}44b$, however it can be applied for wind turbines. (**Wagner**, Page 15)

To draw this effects, it is used an efficiency coefficient, η_z, which is obtained from

$$a = \frac{2\pi r}{z}$$

$$b = \frac{2\pi r}{z}\sin\varphi = \frac{2\pi r}{z}\sin\ \varphi$$

$$1 - \frac{D_{eff}}{D} = 0{,}44\frac{b}{D} = 0{,}44\frac{2\pi r}{zD}\sin\ \varphi$$

$$\frac{D_{eff}}{D} = 1 - 0{,}44\frac{2\pi r}{zD}\sin\ \varphi$$

$$\eta \sim \frac{A_{eff}}{A} = \left(\frac{D_{eff}}{D}\right)^2 = \left[1 - 0{,}44\frac{2\pi r}{zD}\sin\ \varphi\right]^2$$

Being η the efficiency of the rotor performance. It should be now integrated over the radius. But if it is set r = R, then

$$\eta = \left[1 - \frac{0{,}44\pi}{z} \sin\ \varphi\right]^2$$

And as it will be explained in 3.1, $\sin\varphi = \frac{v_2}{w} = \frac{v_2}{\sqrt{u_2^2+v_2^2}} = \frac{v_2}{v_2\sqrt{\lambda_0^2+1}} = \frac{1}{\sqrt{\lambda_0^2+1}}$,

$$\eta = \left[1 - \frac{1{,}39}{z}\frac{1}{\sqrt{1+\lambda_0^2}}\right]^2$$

That for r = R ($\lambda_0 = \lambda_t$) gives the equation for η_z from **Hütter 1942**

$$\eta_z = \left[1 - \frac{1{,}39}{z}\frac{1}{\sqrt{1+\lambda_t^2}}\right]^2 \qquad (2.22)$$

2.2 Installation Angles, the Wagner-Rotor

When designing a wind turbine, it is possible to introduce some installation angles that will affect the aerodynamic performance of the rotor. This was developed by Dr. Wagner GmbH (**Wagner**) in the Wagner-Rotor. The wind turbine designed by this company, was to be installed on the platform of a ship to take advance of the high wind forces at sea, and to that point, they were introduced two angles on the structure: the axis angle and the cone angle, Figure 2.9.

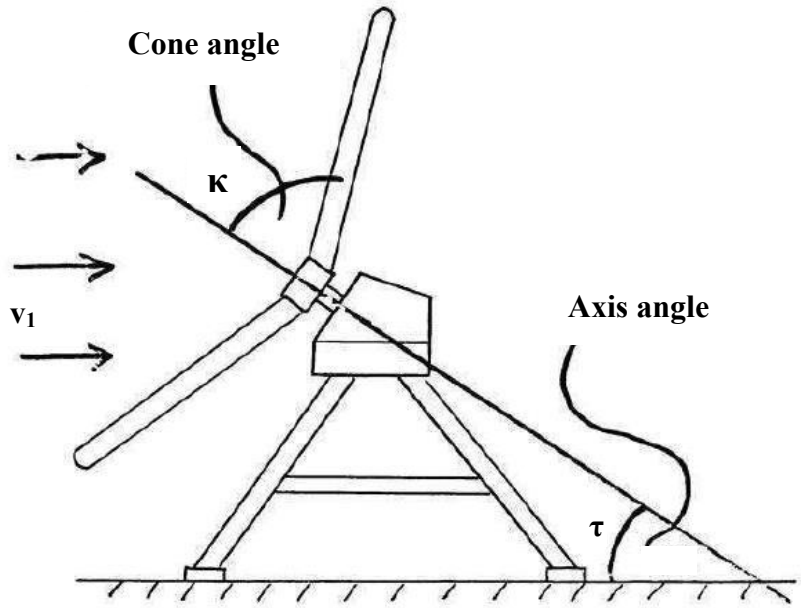

Figure 2.9 Installation angles, κ and τ, of the Wagner-Rotor (from **Lindemann 1985**)

The Wagner-Rotor has an axis angle, τ, which can vary from 0º to 90º and a cone angle, κ, within also a range of 90º and 0º. As a result, the wind flows into the cone formed by the blades set with the given angles. Therefore, the Wagner-Rotor does not need any torque at the appropriate angle, and has a low centre of gravity. (**Lindemann 1985**).

These two angles change the performance of the wind turbine, due to the alteration induced in the direction of the wind which subjects the rotor disc. In Figure 2.10 this effect is shown schematically.

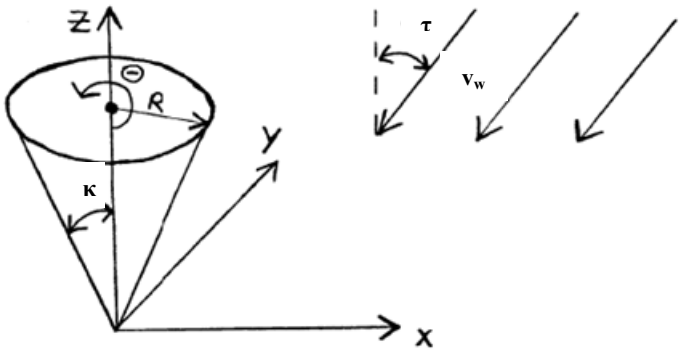

Figure 2.10 Direction of the wind within a Wagner-Rotor-type wind turbine (from **Lindemann 1985**)

The introduction of these angles will be done in section 3.6.

2.3 Review of Codes for Wind Turbine Performance

In this section they will be presented several programs or codes which are focused on wind turbine calculation or similar analysis.

2.3.1 QProp

Qprop is a non-commercial calculation program for the rotor performance map of a propeller engine, developed by **Drela 2004** for the Massachusetts Institute of Technology. For the aerodynamic propeller model, the propeller geometries as well as the profile shapes of the blades must be determined in detail and stored in a file using the syntax. For this purpose, Drela provides a useful guide in 2004 and refers, for example, to the XFoil program for determining the profile properties.

The aerodynamic model for the propeller calculation is a quasinumeric modification of the blade element theory according to **Larrabee 1979**. In detail, the converged local parameters (V; Ω; β; c) are partially differentiated and analytically solvable with the chain rule. The performance data are immediately followed by integration. In the optimal design, two conditions for solubility must be defined. The first is the assumption of differentiated local buoyancy coefficients. The second includes local thrust and moment values. In this way, Drela achieved a high degree of accuracy with the modified method of Larrabee 1979.

2.3.2 QBlade

QBlade is a variant of QProp developed at the Technical University of Berlin in the Department of Experimental Flow Mechanics under the patronage of Oliver Paschereit. The design basis for the determination and determination of local values on the profile is the XFoil program. Using the same container formats, the transition is not only seamless but also graphically embedded in parts. The graphical implementation of XFoil, XFLR5 is used here. The embedding simplifies the design process of the profile because the import and export of the profile data is no longer required. With its graphical interface, QBlade provides a clear overview of the fundamental relationships in the design process of wind turbines. In addition, the interactive graphical interface functions as a simulation tool for various rotor variables.

The main functions of QBlade are as follows:

- an extrapolation of the lift distribution at the defined, or xfoil-generated, profile over the entire area of the work area,

- a graphical three-dimensional representation of the blade geometry, the profile,
- the definition of the wind turbine and its losses,
- the calculation of the rotor power curve in relation to the high speed number,
- the determination of the wind turbine map with respect to the incident velocity,
- determine an annual balance using the Weibull distribution,
- the variability of the sheet element algorithms towards specific linearized solutions,
- the variability of all simulation parameters,
- a graphical representation of the simulation results,
- acquire the results.

The results are divided into four modules: first the sheet design and the optimization of the sheet geometries, secondly the extrapolation of the profil data in the total possible inflow range, thirdly the definition and simulation of the wind turbine and fourthly the simulation of the rotor. All simulations in QBlade are based on the blade element theory with corresponding corrections with respect to the three-dimensional flow field. The basic iterative process and the embedding of XFoil are shown in Figure 2.11 below.

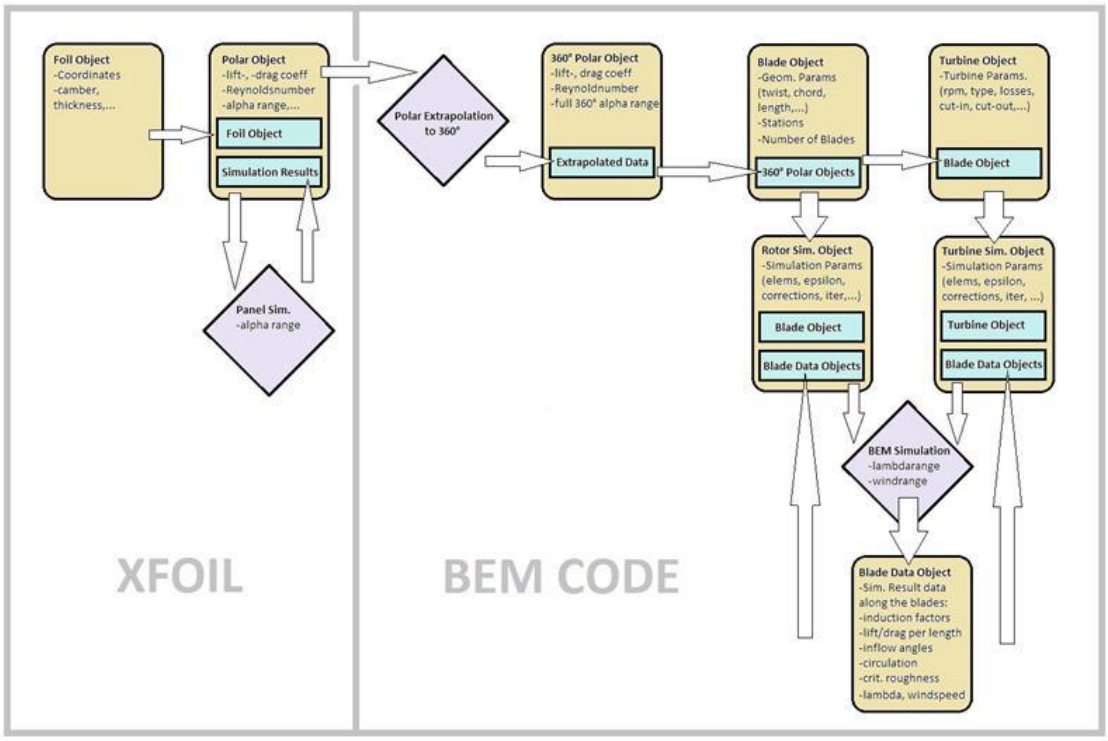

Figure 2.11 Data within the modules in QBlade (from **Marten 2010**)

In the blade design module, the rotor blade is defined sequentially over the parameters chord length, twist, lift and resistance polar as well as the profile. Polars must first be extrapolated in the angle of attack range of 360° with the integrated function of **Montgomerie 2004**. Following the blade design, an optimization of the local leaf geometries can be carried out. The type of the twist is then to be selected with optimum glide ratio, flow cut at all profile

segments or linear. For the optimal chord length, the choice between the method according to **Betz 1926**.

In the module for the rotor simulation, specific rotor blade values can be determined depending on the tip speed ratio. The free inflow is assumed to be homogeneous and the radius of the rotor is normalized. Although this is used to determine microscopic parameters, it does not provide any information about the performance characteristics.

A determination of the blade geometries with subsequent simulation is shown as an example in Figure 2.12.

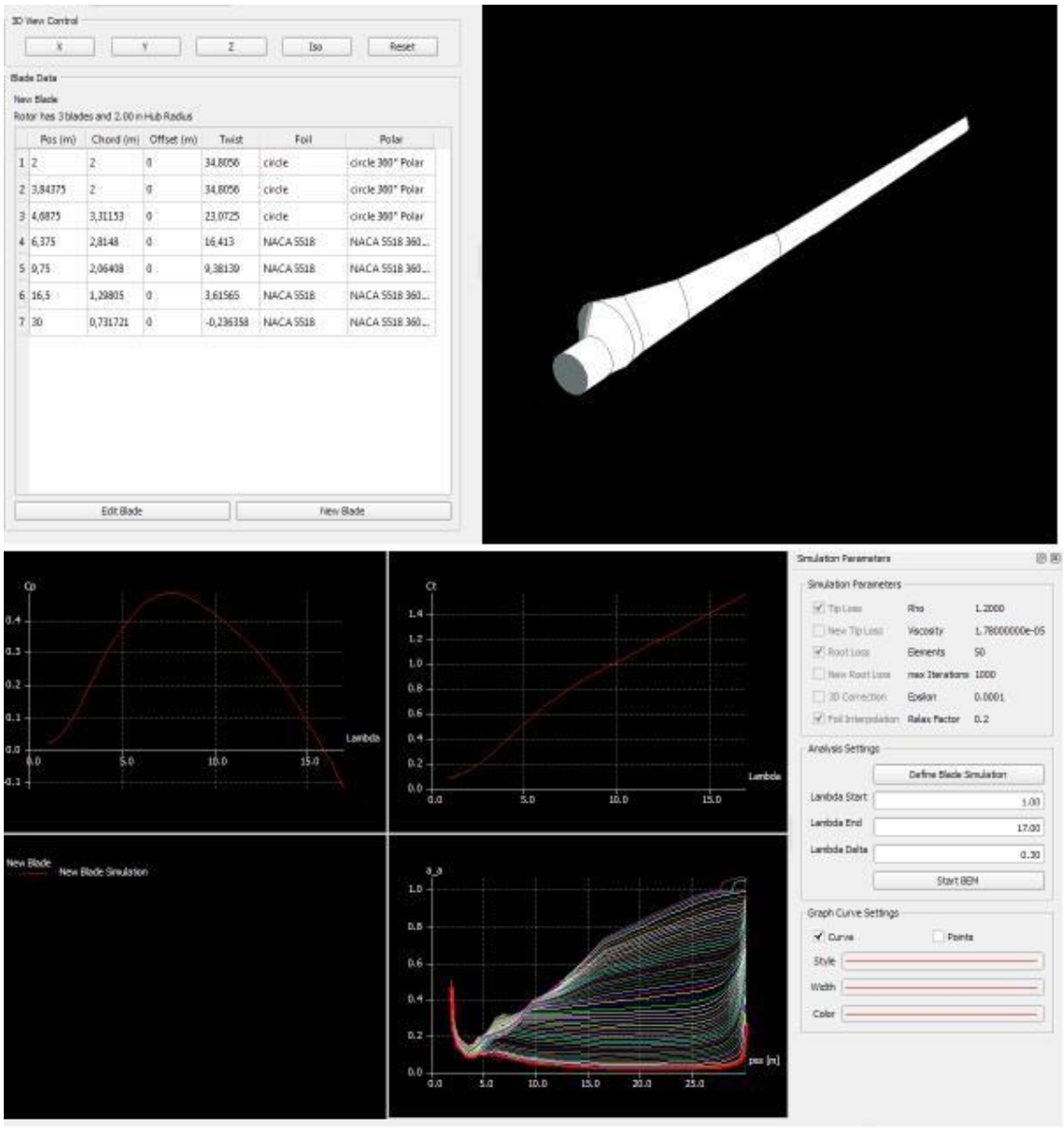

Figure 2.12 Rotor and wind turbine design with blade design and rotor simulation in QBlade (from **Marten 2010**)

The cylindrical shape of the rotor blades near the root is purely structural in wind turbines with large rotor diameters.

The module for simulating the performance characteristics of a wind turbine finally provides the macroscopic examination of its operating state. With it, the optimum performance values and angle of attack corrections can be determined. QBlade offers here basically the choice between different speed-controlled turbines. On the one hand the pitch/stall regulation, on the other hand the regulation of the speed by a corresponding gearbox. For a final dimensioning, the following parameters must also be defined:

- the entire rotor blade,
- the minimum inflow speed,
- the maximum inflow speed,
- systematic losses of the drive train,
- variable losses of the drive train.

The losses in the transmission gear box are caused, for example, by a speed-dependent generator efficiency or by friction in the transmission. It can be calculated in QBlade with the relationship

$$P = (1 - \mathrm{k_v})P_0 - P_{syst} \qquad (2.23)$$

k_v is here the variable loss factor and P_{syst} the systematic loss (from **Marten 2010**).

With the minimum and maximum inflow velocity, calculated by the Weibull distribution, the annual energy supply P_a of the wind turbine can be calculated in QBlade, according to **Marten 2010**.

$$P_a = \sum_{i=1}^{N-1} \frac{1}{2}\left[P(V_{i+1}) + P(V_i)\right] f\{V_i < V_0 < V_{i+1}\} 8760 \qquad (2.24)$$

Figure 2.13 shows the turbine simulation in QBlade.

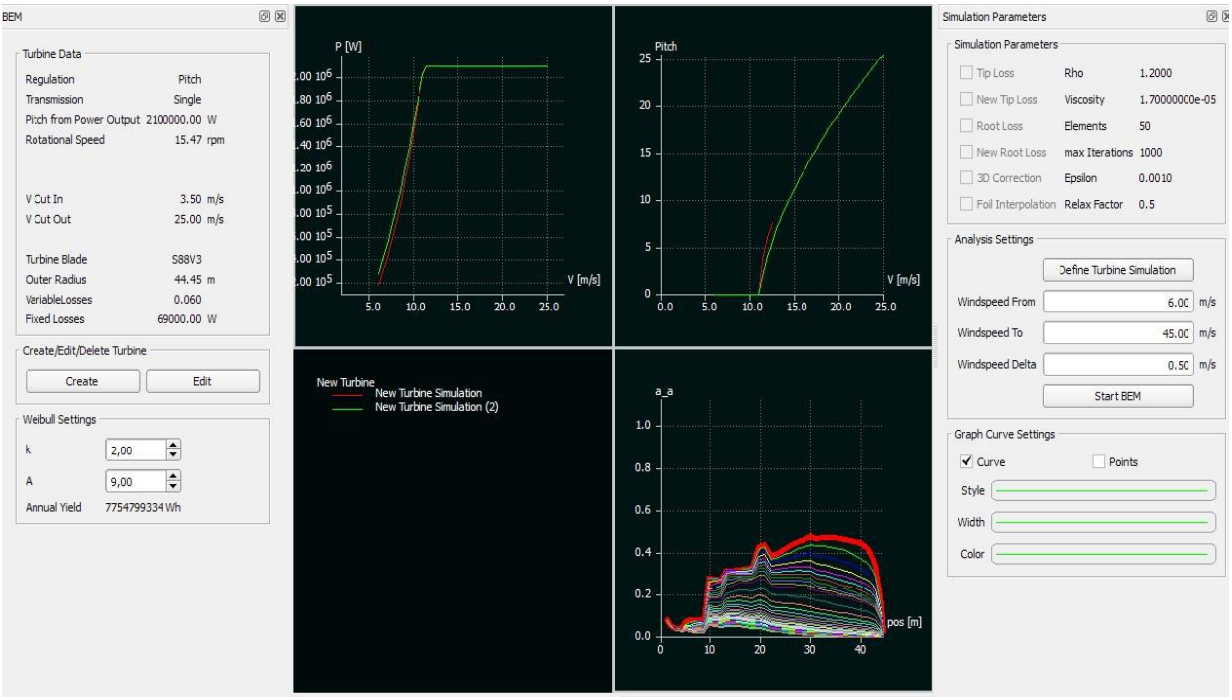

Figure 2.13 Presentation of the turbine simulation with current and annual energy supply in QBlade (from **Marten 2010**)

It should be noted that all simulations in QBlade require the setting of certain parameters as boundary conditions for the calculation with the blade element theory. In addition to the density and the viscosity, the number of blade elements, iteration steps, as well as a convergence criterion and the so-called relaxation factor ω_{relax} according to **Maheri 2006** have to be defined.

In summary, QBlade provides a high degree of accuracy and simulation. Although the calculation basis is the quasinumeric blade element theory, the use of a large number of correction variables is a good example of reality. However, the adjustment parameters must be research. QBlade is therefore based on a broad knowledge.

2.3.3 OpenProp

OpenProp is used for the calculation, design and technical documentation of optimized ship propellers as well as horizontal wind turbines. It was developed at the Massachusetts Institute of Technology under the direction of **Epps 2010** on a Matlab platform. Some important functions are:

- communication with CAD programs for three-dimensional representation and production of propellers
- the propeller optimization using the Lerb criterion (**Lerbs 1952**)

- the optimization of propellers and wind turbines according to **Coney 1989**
- the calculation of the performance curve of propellers and wind turbines based on the preliminary design according to **Epps 2009**
- the design and calculation of jacketed propellers to **Stubblefield 2008**

The operation and input of the data as well as the program structure is clear and well structured thanks to the free accessibility. Optionally, the data sets for the preliminary design or optimization can also be entered via the graphical user interface. A basic schema of the data flow in OpenProp is shown in Figure 2.14.

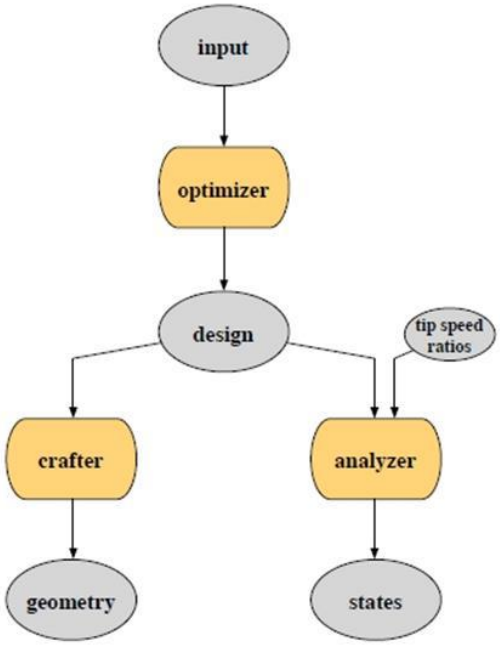

Figure 2.14 Information flow in OpenProp (from **Epps 2010**)

After inputting the data, which can also be parametric, the Lerb criterion is used for design optimization in order to obtain the greatest possible degree of efficiency. Subsequently, the course of the examination is either macroscopic or microscopic. The latter can be used as an example for the production of three-dimensional propeller geometries in the rapid prototyping process.

The underlying calculation method is based on Prandtl's theory with the assumption of a bound induced vortex in the downwind. The induced velocities are determined by means of discrete helical vortex fields according to the vertebrate theory. The rotor is substituted according to the method of **Kerwin 2007** by a representative radial tract, which is divided into a number of N segments. The so-called horseshoe vertebra contains all the vertices of the individual segments with the circulation $\Gamma(i)$. The segments of the turbulent field with the lowest torque are now to be found for the optimization. **Coney 1989** uses the Lagrange multiplier to define an auxiliary function, the minimum of which corresponds to the minimum torque. The resulting non-linear equation system is solved iteratively. The calculation is

basically analogous to the determination of the optimal chord length in OpenProp. However, the relationship of tendon length and parasitic torque can only be conditionally asserted (**Epps 2010**).

$$C_L = \frac{\Gamma}{\frac{1}{2}Vc} \qquad (2.25)$$

A reduction in the chord length leads to an increase in the rotor surface loading and thus to a limitation from a structural viewpoint. **Coney 1989** has consistently set up a non-linear system of equations by introducing the extended area ratio, which makes the chord length indirectly dependent on the torque. However, the solution is complex and time-intensive since both parametrically linearized and iterated.

The macroscopic calculation of the rotor performance field is mathematically complex and time-intensive in OpenProp. In detail, solving a Jacobian matrix of the partial derivatives of relevant parameters, such as velocity, angle of attack, and circulation, provides two state vectors. These are determined iteratively and converge for physically meaningful system states (**Epps 2010**).

For the calculation of the wind turbine characteristics, the circulation is assumed to be a corresponding negative value, but the calculation process remains the same.

In summary, OpenProp is a program with a high level of realism at the expense of computing performance. The implementation of the traglinian theory in Matlab also offers the possibility, to intervene in the program structure more easily. All calculation results are also output in text form. In addition, a CAD design file is created.

2.3.4 Propel

Propel is a relatively rudimentary adaptation of the blade element theory of **Auld 1995**. With it the performance coefficients as well as the efficiency can be calculated conventionally depending on the progress of both propellers and wind turbines. The input parameters are limited to the rotor diameter, the number of blades, the angle of incidence, the taper ratio, the finite chord length of the blade tips, and the twist at the root. If all inputs are selected appropriately, the iteration leads to the discretization of the total thrust, the total torque, the distortion distribution and the efficiency. The type of presentation is clear and the degree of progress can then be varied interactively. Propel offers good comparative studies for the angle

of attack and the fullness of the profile, but does not consider three-dimensional effects such as blade tip vertebra or induced flow effects. The latter has the consequence that the theoretically determined efficiency is five to ten percent higher than the real one. Also the determined thrust is higher and the torque is lower (see **Auld 1995**).

In detail, the blade is divided into ten elements and the local angle of twist is linearized according to

$$\beta = \tan^{-1}\left(\frac{\alpha}{2\pi r}\right) \qquad (2.26)$$

The calculation is based on the Glauert method. Finally, the graphical determination of the optimum efficiency in Propel is shown in Figure 2.15.

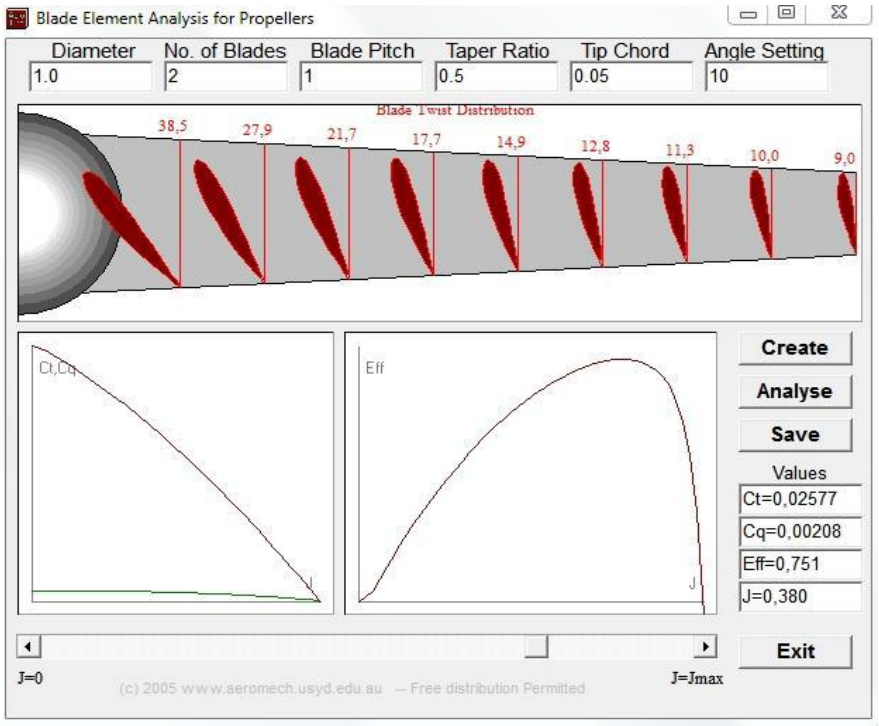

Figure 2.15 Graphical determination of the optimum efficiency in Propel

2.3.5 PropCalc

PropCalc is a program for the representation and for the calculation of propeller coefficients in flight, written by **Schenk 2007**. The representation is limited to the thrust, the power, the efficiency, as well as the power and thrust coefficients. The coefficients are compared with the standard according to the degree of progress. Compared to the already presented programs, PropCalc is based on the experimental determination of the polar specific profiles

in the wind tunnel. These are stored in a corresponding database and can be selected. Because a combination of the profiles is not possible, only a profile shape for the entire propeller is selected and evaluated. With respect to the real propeller, however, the resulting deviations of the results are only in the range of 1-2 percent (**Schenk 2007**). In addition to the fourteen profiles, it can be possible to either add own profiles or modify the existing ones. An overview of the existing database is shown in Figure 2.16.

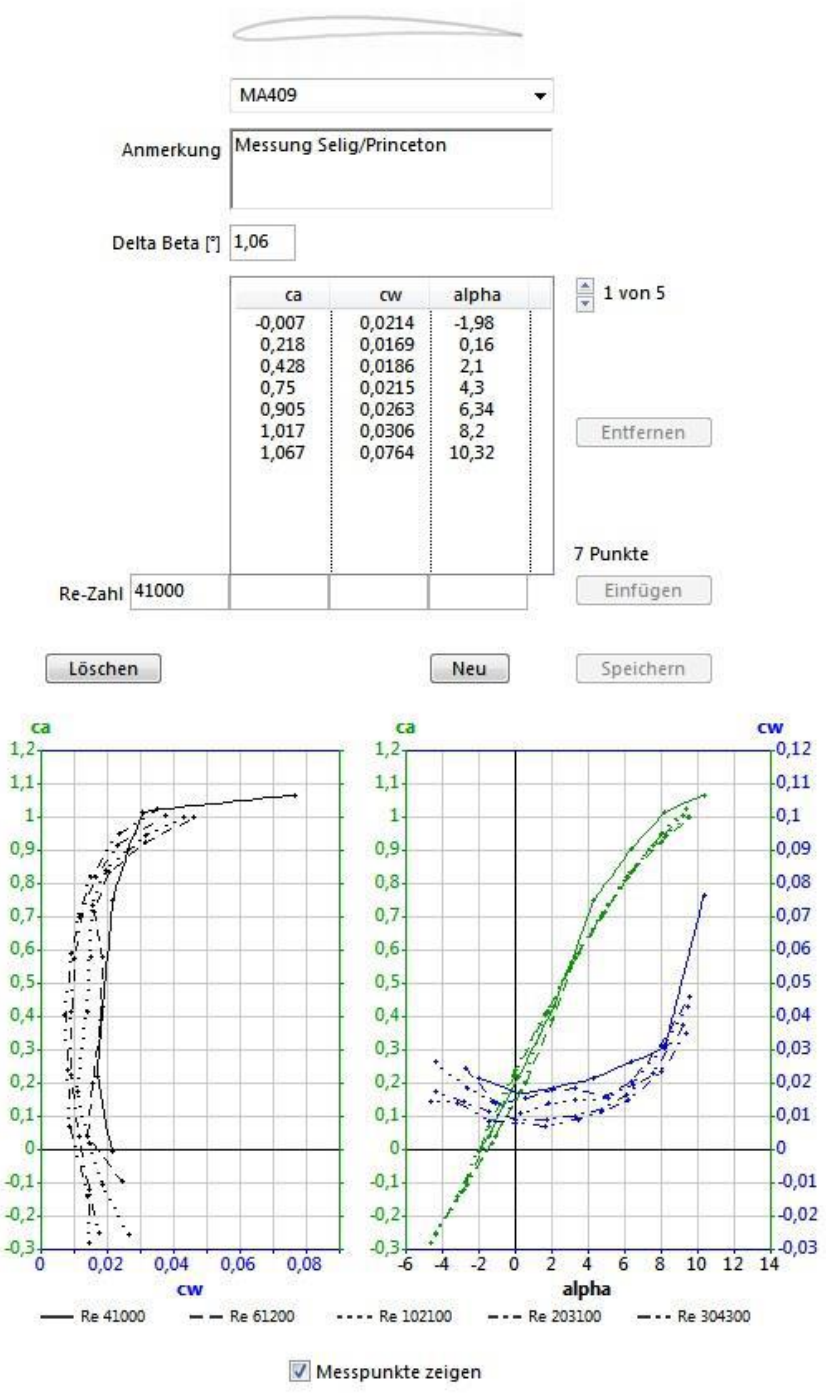

Figure 2.16 Representation of the profile polars integrated in PropCalc for some Reynolds numbers

Another option in PropCalc is the choice of pre-set propeller geometries. Similar to the profiles, there is also an empirical database, which however only includes propellers of the model flying. Analogously, the parameters, such as the diameter or the number of blades, can be changed. Moreover, the blade depth ratio can be varied in the range of 0.5 to 2, the pitch angle in the range of -10° to +10°. If both the profile and the propeller geometries are fixed, the above-mentioned coefficients and characteristic values follow in real-time, as shown in Figure 2.17.

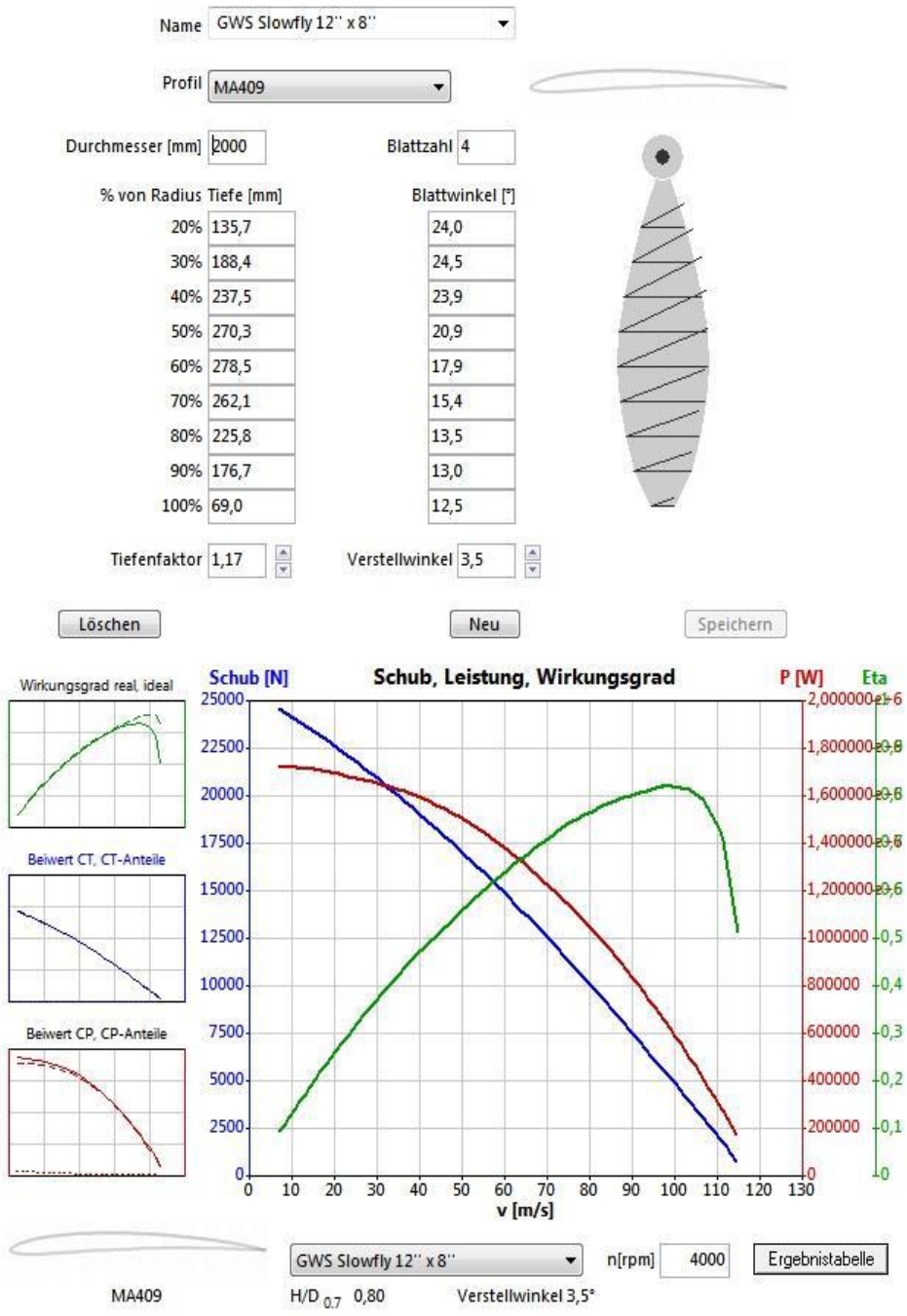

Figure 2.17 Presentation of the performance data of a selected propeller profile combination in PropCalc

The interactive representation in real time offers great advantages in the dimensioning of the propeller. Each parametric set-screw immediately provides a change in values and graphs.

In summary, PropCalc offers the possibility to determine absolute values very quickly. The optimal propeller is not calculable (**Schenk 2007**), but can be approximated quickly. If the propeller to be dimensioned and its profile are not included in the database, discrete values from empirical investigations are required to perform a calculation. Although greatly simplified, PropCalc is a very useful program for the preliminary design because of its operation.

2.3.6 WindKraft

Windkraft is a program for the design of windmills, written by **Herrmann in 2004**. It is used on the one hand to scale small wind turbines on the scale, on the other hand the macroscopic design of conventional wind turbines. The presentation of the results is comprehensive and intuitive to use. In addition to the known performance characteristics, the operating characteristic can also be represented, which is of relevance with respect to the operating state. In addition, the characteristic data of the wind turbine are calculated, for example, the diameter and speed of the wheel, the power factor of the wing, and the Reynolds number on the wing. Any wing sections can be drawn and used as a scale profile template. The profile sections also provide information about the local installation angle as well as the local profile thickness and the depth.

The input parameters are the classical design of wind turbines, respectively the power to be dimensioned, the number of blades, the high speed number the average wind speed and the ideal efficiency. The relationship between the tip speed ratio and the number of blades can be made here for a first approximation. For the selection of the wing profile, it is possible to access the marginal database of the program that takes place numerically in the form of an ASCII file. Existing profiles are plates and three four-digit NACA profiles.

The calculation is performed by means of the blade element theory. The resulting inflow velocity and the angle of incidence are determined under the influence of the fluid by a simplified Schmitz method. For the Reynolds number, an effective radius of the wind turbine according to **Franquesa 1989** of 0.72R is used for the estimation of the dynamic viscosity of air at standard conditions.

Since the wing span and the twist angle along the wing are not constant, either the simplified method of **Schmitz 1956**, adapted by **Franquesa 1989**, is used for calculation or linearized.

The results, , provide a good approximation of the real states. The power output, however, is slightly below expectations despite the neglect of the generator efficiency. The significant difference consists in the numerical optimization of real wing profiles with the variation of the profile shapes along the radius, while the calculations of wind force define a basic profile, which is adjusted only by the local angle of attack on the flow field.

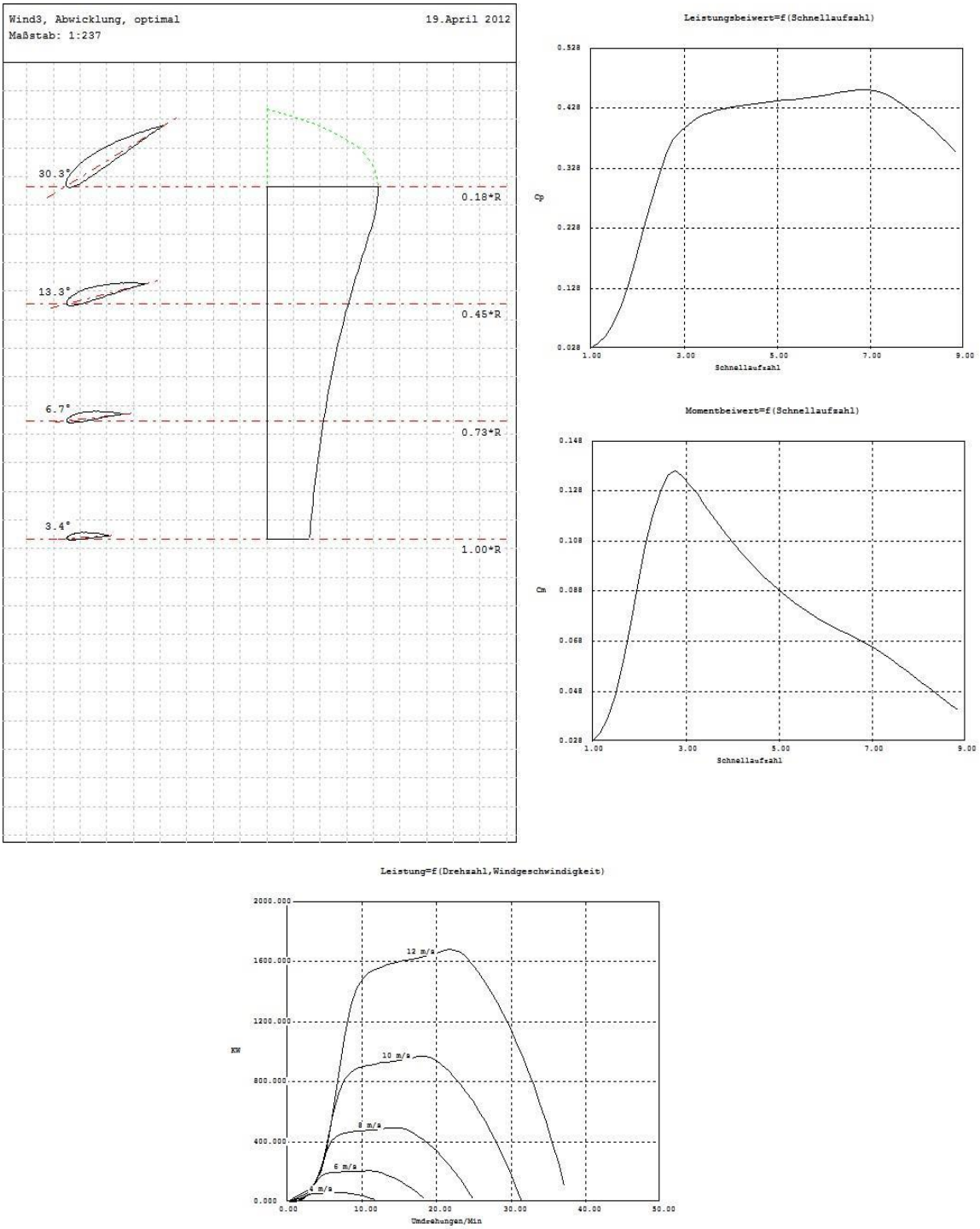

Figure 2.18 Results in WindKraft

3 Blade Element Momentum Theory

In order to analyse the behaviour and the performance of a generic wind turbine, it is going to be used the Blade Element Momentum Theory. This theory consists in dividing a single blade into several elements, so that each element has different characteristics which must be added taking into account the position of the element.

Each element is formed by an airfoil. To that point, it is important to remark that all the coefficients, forces and powers are designed with lowercase letters, in order to distinguish a single element from the whole rotor.

This point explains how is implemented the Blade Element Momentum Theory.

3.1 Speed Ratios, Inflows and Forces on a Blade Element

When a single element is considered, there can be distinguished different relevant parameters and forces. In order to explain them, it is important to highlight the following (**Wagner**, Page 8):

1. The rotation of the blade produces a speed, the "circumferential speed", u, which depends on the rotation of the rotor and the distance of the blade element to the centre of rotation. At the tip of the blade, the largest circumferential speed appears. When the element gets closer to the root, the circumferential speed reduces. This speed is parallel to the rotational speed of the rotor (see picture).

$$u = \omega r \qquad (3.1)$$

2. The “natural wind speed”, v, is perpendicular to the rotation of the rotor. In the rotor plane it is diminished from v_1 to v_2.

$$v_2 = \frac{1}{2}(v_1 + v_3) \qquad (2.13)$$

3. The speed ratio, λ, is defined by the ratio of circumferential speed, u, to natural wind speed, v_1, and the effective speed ratio λ_0 by the circumferential speed, u, to the natural wind speed, v_2, in the rotor plane.

$$\lambda = u/v_1 \quad (3.2)$$

$$\lambda_0 = u/v_2 \quad (3.3)$$

4. The circumferential speed, u, together with the natural wind v, result in the apparent wind speed, w. This resulting wind is the wind, which sees the blade element, Figure 3.1.

$$\alpha = \varphi - \beta \quad (3.4)$$

The resultant w causes the lift force, F_l, perpendicular to w, and the drag force, F_d, in the same direction to w.

5. The angle α is decisive for the lift coefficient. It is made up of the angle of incidence ϕ and the element twist angle β, Figure 3.1.

$$\alpha = \varphi - \beta \quad (3.5)$$

6. The lift force on the element can be projected tangential and perpendicular to the rotor plane

$$F_{l,s} = F_l \cos\varphi \quad (3.6)$$

$$F_{l,t} = F_l \sin\varphi \quad (3.7)$$

In the same way, the drag force on the element

$$F_{d,s} = F_d \sin\varphi \quad (3.8)$$

$$F_{d,t} = F_d \cos\varphi \quad (3.9)$$

7. From Figure 3.1 it can be inferred relations between u, v, w, φ and λ_0

$$\cos\varphi = \frac{u_2}{w_2} = \frac{u_2}{\sqrt{u_2^2 + v_2^2}} = \frac{u_2}{u_2\sqrt{1 + 1/\lambda_0^2}} = \frac{1}{\sqrt{1 + 1/\lambda_0^2}} \quad (3.10)$$

$$\sin\varphi = \frac{v_2}{w_2} = \frac{v_2}{\sqrt{u_2^2 + v_2^2}} = \frac{v_2}{v_2\sqrt{\lambda_0^2 + 1}} = \frac{1}{\sqrt{\lambda_0^2 + 1}} \quad (3.11)$$

$$\tan\varphi = \sqrt{\frac{1+1/\lambda_0^2}{\lambda_0^2+1}} = \frac{1}{\lambda_0}\sqrt{\frac{\lambda_0^2+1}{\lambda_0^2+1}} = \frac{1}{\lambda_0} \qquad (3.12)$$

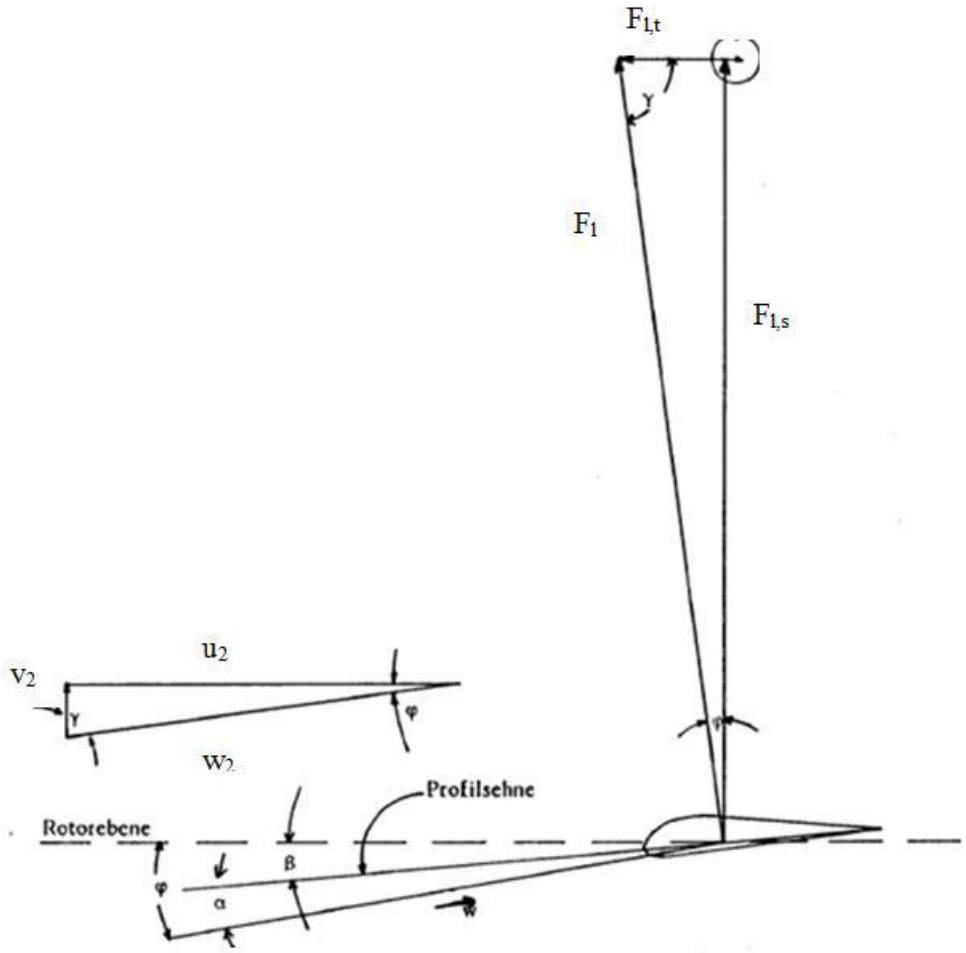

Figure 3.1 Diagram of angles and forces on a blade element (from **Wagner**)

3.2 Wake Rotation Effect on a Blade Element

As it was explained in 2.1.3.1, the consequence of the reaction torque on the rotor disc is to cause the air to rotate in a direction opposite to that of the rotor. That means that, in a slow-speed rotor, the wake behind the rotor disc changes only its direction, (2.20). When this is applied to a single element within a blade,

$$|w_1| = |w_3| \rightarrow \; v_1^2 + u_1^2 = v_3^2 + u_3^2 \rightarrow u_3 = \sqrt{v_1^2 - v_3^2 + u_1^2}$$

$$\frac{u_3}{u_1} = \sqrt{\frac{v_1^2}{u_1^2} - \frac{v_3^2}{u_1^2} + 1}$$

$$\frac{u_3}{u_1} = \sqrt{\frac{v_1^2}{u_1^2} - \frac{v_1^2}{u_1^2}\frac{v_3^2}{v_1^2} + 1} \qquad (3.13)$$

The change in tangential velocity can be expressed in terms of a tangential flow reduction factor σ, that is

$$\sigma = \frac{u_3}{u_1} \qquad (3.14)$$

And substituting $\xi = \frac{v_3}{v_1}$, and $\frac{1}{\lambda} = \frac{v_1}{u_1}$

$$\sigma = \sqrt{\frac{1}{\lambda^2} - \frac{1}{\lambda^2}\xi^2 + 1}$$

$$\sigma = \sqrt{1 + \frac{1 - \xi^2}{\lambda^2}} \qquad (3.15)$$

3.3 Loss of Energy on a Blade Element

In the case of pronounced slow-speed rotors, it is necessary to consider not only the reduction of the wind speed, but also the reduction of the circumferential speed (**Wagner**, Page 11).

In analogy to the calculations given in (2.12), they are obtained the parameters for the flow conditions in the rotor plane

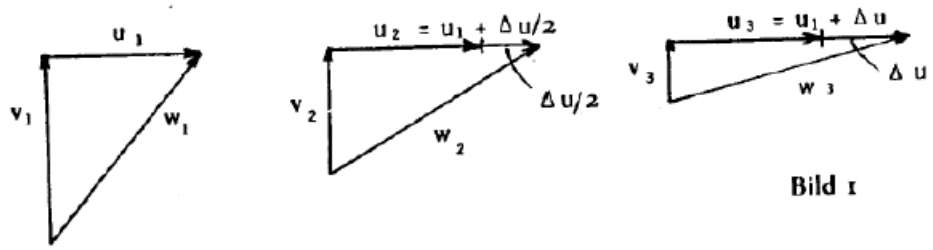

Figure 3.2 Inflows before, in and behind the rotor disc (from **Wagner**)

$$v_2 = v_1 - \Delta v/2 \quad (3.16)$$

$$u_2 = u_1 + \Delta u/2 \quad (3.17)$$

That, with (2.16) and (3.15)(2.20), they can be expressed as

$$v_2 = \frac{1}{2} v_1 (1 + \xi) \quad (3.18)$$

$$u_2 = \frac{1}{2} u_1 (1 + \sigma) \quad (3.19)$$

Which gives

$$\lambda_0 = \frac{u_2}{v_2} = \frac{u_1}{v_1} \frac{1+\sigma}{1+\xi} = \lambda \frac{1+\sigma}{1+\xi} \quad (3.20)$$

3.4 Power Coefficient of a Blade Element

As already noted, the outflowing wind, v_3, still has a spin component, Δu, which still contains energy (**Wagner**, Page 13). The resultant of v_3 and Δu is denoted by v_D,

$$v_D = \sqrt{v_3^2 + \Delta u^2} \quad (3.21)$$

Which applied in (2.9),

$$P_D = \frac{1}{2} \dot{m} (v_1^2 - v_D^2)$$

$$P_D = \frac{1}{2} \dot{m} [v_1^2 - (v_3^2 + \Delta u^2)]$$

$$P_D = \frac{1}{2} \dot{m} [w_1^2 - u_1^2 - w_3^2 + u_3^2 - \Delta u^2]$$

Due to the wake rotation $|w_1| = |w_3|$

$$P_D = \frac{1}{2}\dot{m}[u_3^2 - u_1^2 - \Delta u^2]$$

And as shown in Figure 3.2, $u_3 = u_1 + \Delta u \rightarrow \Delta u = u_3 - u_1$, so

$$P_D = \frac{1}{2}\dot{m}[u_3^2 - u_1^2 - (u_3^2 - 2u_1u_3 + u_1^2)]$$

$$P_D = \frac{1}{2}\dot{m}[2u_1u_3 - 2u_1^2]$$

$$P_D = \dot{m}u_1^2\left(\frac{u_3}{u_1} - 1\right)$$

$$P_D = \dot{m}u_1^2(\sigma - 1)$$

With the same derivation done for (2.15), and denoting the power coefficient with a lowercase letter "i", meaning that is the power generated only by a single element, it is obtained the expression for the power coefficient of a blade element,

$$C_{Pi} = \frac{P_D}{P_0} = \frac{\dot{m}u_1^2(\sigma - 1)}{\frac{1}{2}\rho A_2 v_1^3} = \frac{2\dot{m}u_1^2(\sigma - 1)}{\rho\frac{\dot{m}}{v_2\rho}v_1^3}$$

$$C_{Pi} = \frac{2u_1^2(\sigma - 1)v_2}{v_1^3} = \frac{2u_1^2(\sigma - 1)\frac{1}{2}(v_1 + v_3)}{v_1^3}$$

$$C_{Pi} = \frac{2u_1^2(\sigma - 1)\,{}^1/_2\, v_1(1 + v_3/v_1)}{v_1^3} = \frac{u_1^2}{v_1^2}(\sigma - 1)(1 + \xi)$$

$$C_{Pi} = \lambda^2(1 + \xi)(\sigma - 1) \qquad (3.22)$$

This last expression with (3.15) can be represented as a function of ξ and λ. In Figure 3.3 is shown the evolution of C_{Pi} for different values of speed ratio and for ξ=1/3, noting that with the latter the power coefficient reaches its maximum possible value, 0.59.

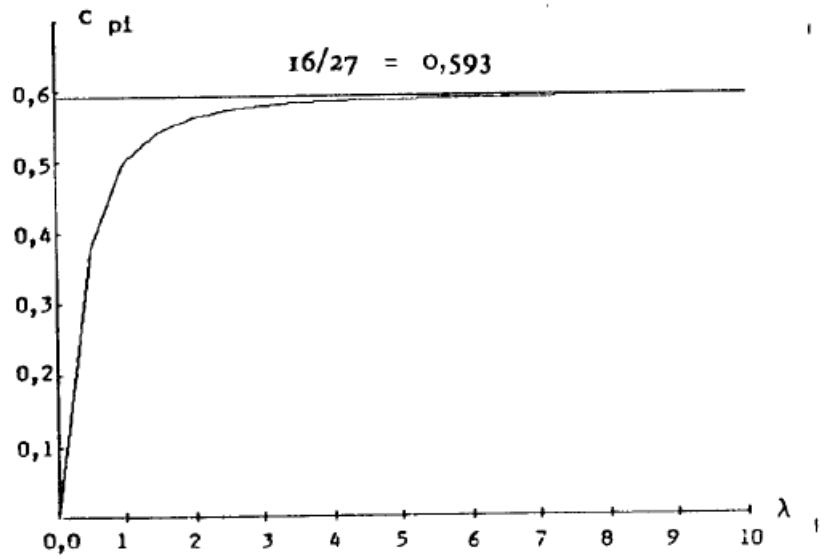

Figure 3.3 Power coefficient on a blade element for ξ=1/3 as a function of λ (from **Wagner**)

3.5 Friction Loss of a Blade Element

Even with the ideal inflow conditions (deceleration to 1/3), the ideal C_P value of 0.59 cannot be achieved. The main cause in high-speed rotors is the friction loss on the blade (in slow-speed rotors losses are caused by flow losses). (**Wagner** , Page 10)

The frictional losses on an element are characterized by its glide ratio, ε, which is the ratio of lift force to drag force on the airfoil. In a blade element, the glide ratio is

$$\varepsilon = \frac{F_l}{F_d} = \frac{\frac{1}{2}\rho w^2 A \cdot C_l}{\frac{1}{2}\rho w^2 A \cdot C_d} = \frac{C_l}{C_d} \qquad (3.23)$$

The resulting forces in the tangential direction, F_T, and in the normal direction, F_S, can be set as shown in Figure 3.1:

$$F_s = F_{l,s} + F_{d,s} = F_l cos\varphi + F_d sin\varphi \qquad (3.24)$$

$$F_t = F_{l,t} - F_{d,t} = F_l sin\varphi - F_d cos\varphi \qquad (3.25)$$

With (3.23) it can be expressed F_d as a function of F_l and ε

$$F_d = \frac{F_l}{\varepsilon} \tag{3.26}$$

Therefore (3.24) and (3.25) with the glide ratio ε are written as follows

$$F_s = F_l \cos\varphi + F_l \frac{1}{\varepsilon} \sin\varphi = F_l \cos\varphi \cdot (1 + \frac{1}{\varepsilon} \tan\varphi) \tag{3.27}$$

$$F_t = F_l \sin\varphi - F_l \frac{1}{\varepsilon} \cos\varphi = F_l \sin\varphi \cdot (1 - \frac{1}{\varepsilon} \cot\varphi) \tag{3.28}$$

The reduction power (power taken from the air), P_S, and propulsive power, P_T, are

$$P_s = F_s \cdot v_2 \tag{3.29}$$

$$P_t = F_t \cdot u_1 \tag{3.30}$$

The ratio of the useful propulsive power P_T of the rotor element to the extracted power from the air P_S is referred to as the blade element friction efficiency, η_P,

$$\eta_P = \frac{P_t}{P_s} = \frac{u_1 F_l \sin\varphi\,(1 - \frac{1}{\varepsilon}\cot\varphi)}{v_2 F_l \cos\varphi\,(1 + \frac{1}{\varepsilon}\tan\varphi)} = \frac{u_1}{v_2}\tan\varphi \frac{1 - \frac{1}{\varepsilon}\cot\varphi}{1 + \frac{1}{\varepsilon}\tan\varphi}$$

Introducing (3.12) and (3.19)

$$\eta_P = \frac{2u_2}{(1+\sigma)} \frac{1}{v_2} \frac{1}{\lambda_0} \frac{1 - \frac{1}{\varepsilon}\lambda_0}{1 + \frac{1}{\varepsilon}\frac{1}{\lambda_0}} = \frac{2\lambda_0}{(1+\sigma)} \frac{1}{\lambda_0} \frac{\lambda_0\left(\frac{1}{\lambda_0} - \frac{1}{\varepsilon}\right)}{\frac{(\varepsilon\lambda_0 + 1)}{\varepsilon\lambda_0}}$$

And from (3.20),

$$\lambda_0 = \lambda \cdot \frac{1+\sigma}{1+\xi} \rightarrow (1+\sigma) = \frac{\lambda_0}{\lambda}(1+\xi) \rightarrow \frac{1}{(1+\sigma)} = \frac{\lambda}{\lambda_0}\frac{1}{(1+\xi)}$$

Finally is obtained the expression for the blade element friction efficiency

$$\eta_P = 2\lambda \frac{\varepsilon - \lambda_0}{(1+\xi)(1+\varepsilon\lambda_0)} \qquad (3.31)$$

If this efficiency is combined with the power coefficient of a blade element, there are obtained more realistic curves from those in Figure 3.3. The result is showed in Figure 3.4 for different values of ξ.

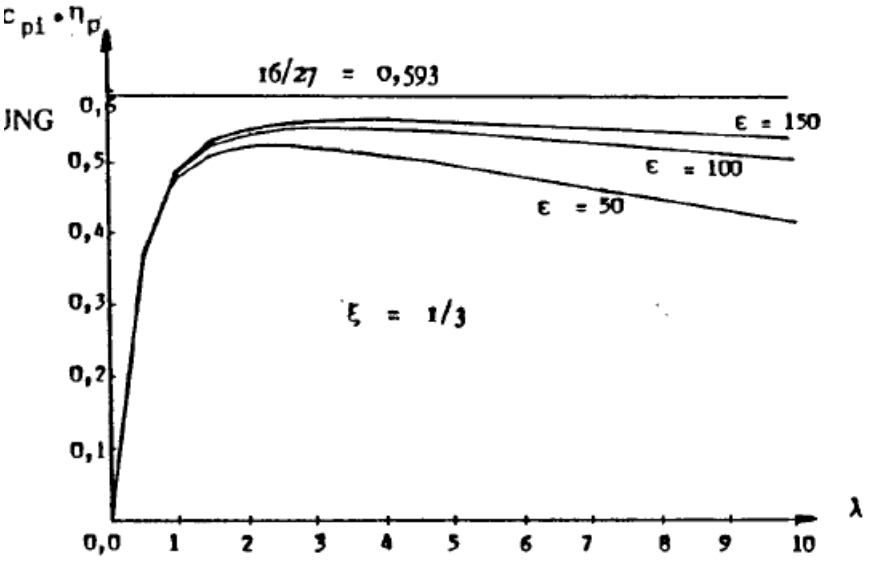

Figure 3.4 Combination of c_{pi} and η_P for different values of ξ as a function of λ (from **Wagner**)

3.6 Blade Element Chord

The blade chord is usually selected by the designer so that the wind is maximized as far as possible at every point of the blade.

A blade element surface is given by

$$\Delta A = t\Delta r \qquad (3.32)$$

The lift force acting on a blade element is, according to (3.24),

$$F_{l,s} = F_l \cos\varphi = \frac{1}{2}\rho w^2 \Delta A \, C_l \, {}^{u}/_{w} = \frac{1}{2}\rho \cdot u \cdot w \cdot t \cdot \Delta r \cdot C_l \qquad (3.33)$$

In order to eliminate the force F_l, a second relation is introduced: the thrust which the airflow exerts on the corresponding ring of the element, (2.10),

$$F_S = \dot{m}(v_1 - v_3) = \rho\dot{V}(v_1 - v_3) = \rho A_{ring} v_2 (v_1 - v_3)$$

$$F_S = \rho \cdot 2\pi \cdot r \cdot \Delta r \cdot v_2 (v_1 - v_3) \qquad (3.34)$$

This force on the given ring must be equal to the sum of forces $F_{l,s}$ on the element for each blade. This relation gives an expression for the blade chord,

$$F_S = z\, F_{l,s}$$

$$\rho \cdot 2\pi \cdot r \cdot \Delta r \cdot v_2 (v_1 - v_3) = z \frac{1}{2} \rho \cdot u \cdot w \cdot t \cdot \Delta r \cdot C_l$$

$$2\pi \cdot r \cdot 2v_2 (v_1 - v_3) = z \cdot u \cdot w \cdot t \cdot C_l$$

$$t = \frac{2\pi r \cdot 2v_2 (v_1 - v_3)}{z \cdot u \cdot w \cdot C_l} \qquad (3.35)$$

Thus, the depth of the blade is now reduced to 4 terms:

1. $(2\pi \cdot r)$: the depth of the blade depends of the geometrical conditions,
2. $1/c_l$: the depth of the blade depends on the reciprocal lift coefficient,
3. $2v_2\ (v_1 - v_2)$: the blade depth depends on the flow conditions,
4. $1/z$: the depth of the blade is inversely proportional to the number of blades.

With (2.12) and (2.16) it is finally obtained the chord distribution

$$t = \frac{2\pi r (v_1 + v_3)(v_1 - v_3)}{z \cdot u \cdot w \cdot C_l} = \frac{2\pi r v_1^2 \left(1 - \frac{v_3^2}{v_1^2}\right)}{z \cdot u \cdot w \cdot C_l} = \frac{2\pi r \cdot (1 - \xi^2)}{uw} \cdot \frac{1}{z} \cdot \frac{1}{C_l} \qquad (3.36)$$

For each radius, a different blade depth is obtained, the larger as the root of the rotor is approached. To make this clear, (3.36) is transformed, so that the quantities u and w are eliminated.

These previous quantities, u and w, are now more precisely expressed as u_2 and w_2 when the influence of the vortexes are included. So, with (3.3) and (3.18) ($v_2 = \frac{1}{2} v_1 (1 + \xi) \rightarrow v_1^2 = \frac{4v_2^2}{(1+\xi)^2}$), it follows the expression that is going to be useful in the next chapters for the chord distribution

$$t = \frac{8\pi r}{C_l \cdot z} \cdot \frac{1}{\lambda_0^2} \cdot \frac{1}{\sqrt{1 + {}^1/_{\lambda_0^2}}} \cdot \frac{1-\xi}{1+\xi} \qquad (3.37)$$

With $\lambda_0 = \lambda \cdot \frac{1+\sigma}{1+\xi}$ and $\sigma = \sqrt{1 + \frac{1-\xi^2}{\lambda^2}}$, it is possible to draw curves for the blade chord for each blade element position, as shown in Figure 3.5.

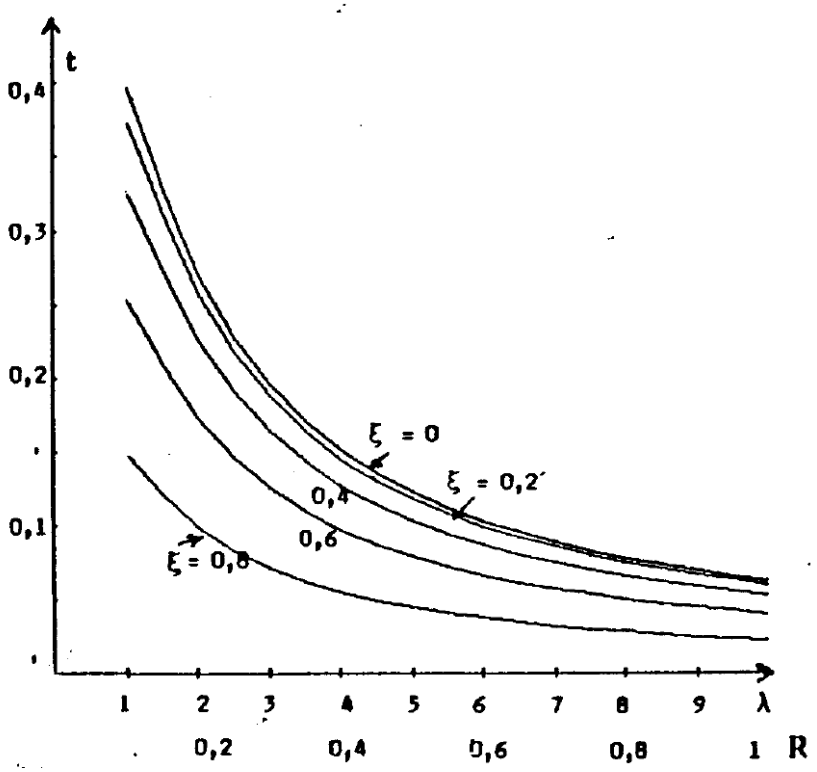

Figure 3.5 Element chord distribution as a function of λ and ξ (from **Wagner**)

Although this expression is going to be used, the chord distribution is given by the designer. On the one hand, the ideal blade, Figure 3.6 a, produces an ideal reduction at every point, cannot be constructed constructively, since in the vicinity of the root it grows to enormous widths and requires unnecessarily material. (**Wagner**)

On the other hand, a trapezoid profile, Figure 3.6 b, which is very simple to construct, is only about 1% worse than the ideal blade. Even cheaper would be a pure rectangle unity taper ratio, Figure 3.6 c. In this case, it takes place a 5% of efficiency losses. (**Wagner**).

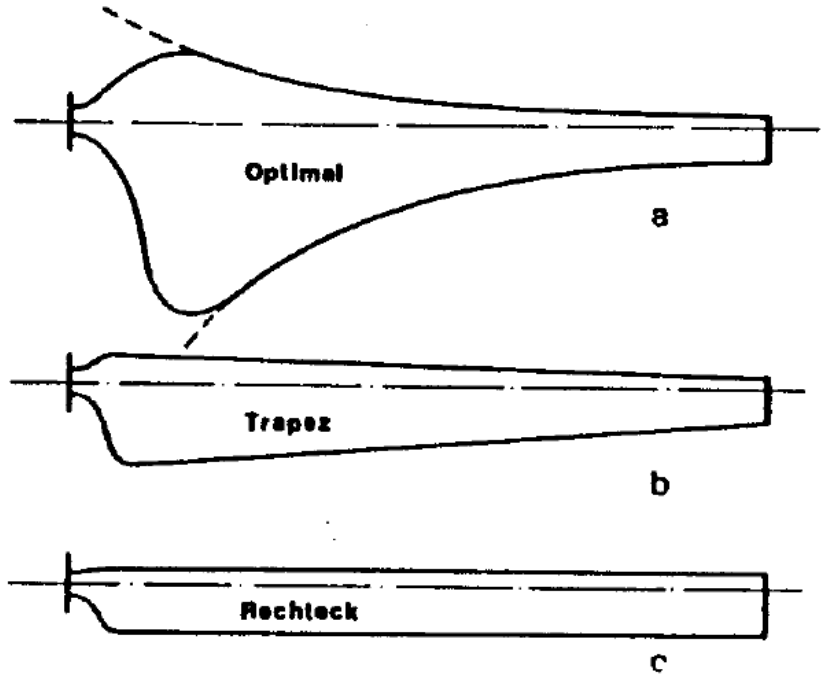

Figure 3.6 Blade types (from **Wagner**)

For these reasons, in what follows, the chord distribution will be a linear one, as expressed in (3.38), which forms a trapezoid profile.

$$\frac{t}{R} = \frac{t_0 - t_t}{R} \frac{(1 - R'_m)}{(1 - R'_0)} + \frac{t_t}{R} \qquad (3.38)$$

Where t_t is the chord at the tip, t_0 the chord at the root, L the length of the blade, R the effective radius of the rotor and R'_m will be defined in section 5.1.

3.7 Power Coefficient Calculation

All these explained influences must be weighted according to the position of the blade element. This is seen when observing that the single efficiency of a blade element at the tip has a greater effect on the overall efficiency than the same element efficiency when located at the root of the blade.

It must take place, therefore, an integration of the efficiency (C_P) along annular surfaces to take into account the position of the blade element and its angle of rotation. This integration will be developed through the ring surface corresponding to the given blade element. Thus, the ring surface is

$$A_r = r \cdot \Delta r \Delta\theta \qquad (3.39)$$

The power coefficient is then, the sum of all the ring surfaces each multiplied by the degrees of efficiency present there, divided by the entire circular area. This can be expressed as

$$C_P = \eta_z \cdot \frac{1}{\pi R^2} \int_0^R \int_0^{2\pi} r \cdot C_{Pi}(r,\theta) \cdot \eta_P(r,\theta) \cdot dr \cdot d\theta \qquad (3.40)$$

This last expression will be the base of the following program presented in chapter 5. Figure 3.7 is an example of the sought curve derived from (3.40) for C_P as a function of λ_t for a given rotor.

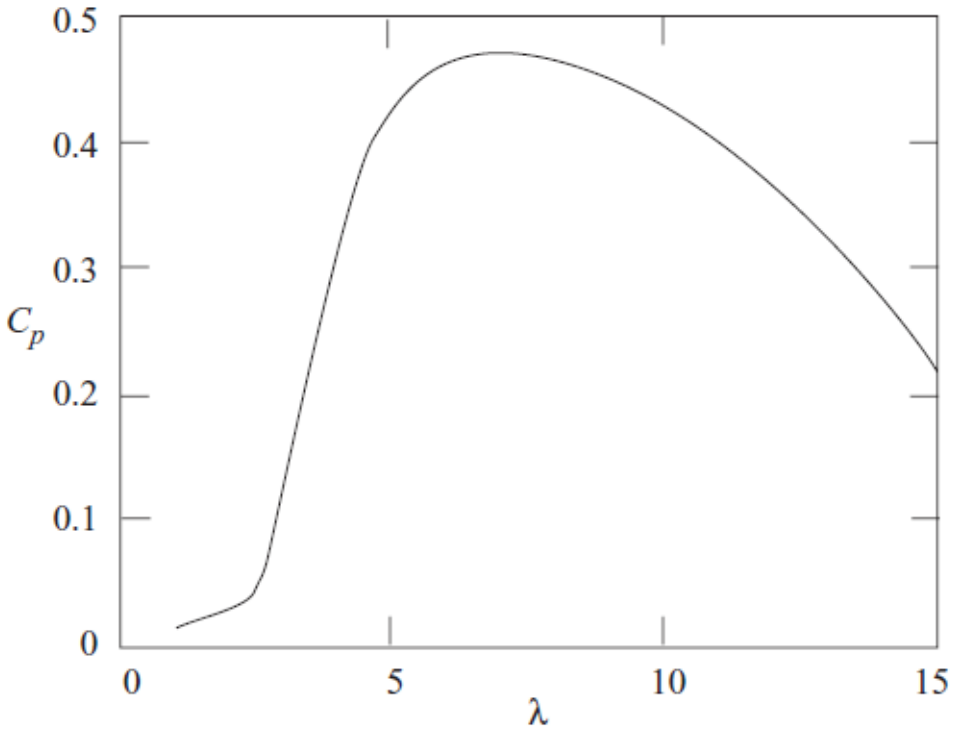

Figure 3.7 Power coefficient - tip speed ratio curve (from **Wagner**)

3.8 Effect of the Installation Angles into the Blade Momentum Theory

In section 2.2 it was presented the Wagner-Rotor wind turbine. This type of rotor has two installation angles which apply an effect into its performance, due to the fact that they alter the incidence angle of the wind. This change affects the speed ratio, base of the Blade Momentum Theory.

Subsequently, it is developed how the installation angles are introduced into the speed ratio according to **Lindemann 1985**. As shown in **Lindemann 1985**, it is demanded that the wind only flows outwards through the conical surface. This requirement is fulfilled if,

$$\tau \leq \kappa \qquad (3.41)$$

The calculation of the speed number is divided into three parts:

1. calculation of the speed v_1,
2. calculation of speed u_1,
3. calculation of λ from $\lambda = u_1 / v_1$.

Using the differential geometry and Figure 2.10, it is going to be calculated the component of v_w perpendicular to the cone surface. All data are given in Cartesian coordinates. The cone surface is described by

$$\vec{x} = (r \cdot cos\theta\,, \quad r \cdot sin\theta\,, \quad r \cdot cot\kappa) \qquad (3.42)$$

In that way, the wind speed is described by

$$\overrightarrow{v_w} = (-v_w \cdot sin\tau\,, \quad 0\,, \quad -v_w \cdot cos\tau) \qquad (3.43)$$

The normal vector is perpendicular to the surface of the cone shell

$$\vec{n} = \overrightarrow{x_r} \text{ x } \overrightarrow{x_\theta}$$

$$\vec{n} = \begin{Bmatrix} cos\theta \\ sin\theta \\ cot\kappa \end{Bmatrix} \text{ x } \begin{Bmatrix} -r \cdot sin\theta \\ r \cdot cos\theta \\ 0 \end{Bmatrix} = r \begin{Bmatrix} -cot\kappa \cdot cos\theta \\ -cot\kappa \cdot sin\theta \\ 1 \end{Bmatrix} \qquad (3.44)$$

So the projection of v_w on the direction of -n is

$$v_{w\vec{n}} = \frac{-\overrightarrow{v_w} \bullet \vec{n}}{|\vec{n}|}$$

This speed perpendicular to the cone is the needed velocity v_1. The direction -n must be chosen since n is directed inwards into the cone, but in v_w the component is sought outwards out of the cone,

$$v_1 = v_{w\vec{n}} = v_w \frac{cos\tau - sin\tau \cdot cot\kappa \cdot cos\theta}{\sqrt{\cot^2 \kappa + 1}} \qquad (3.45)$$

The circumferential speed u_1 is also dependent of the wind speed in a Wagner-Rotor-type rotor, as shown in Figure 3.8.

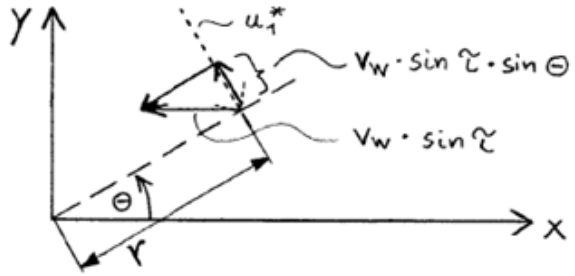

Figure 3.8 **C**ircumferential speed dependence of the wind speed in a Wagner-Rotor-type rotor (from **Lindemann 1985**)

$$u_1^* = \dot{\theta} \cdot r = \omega \cdot r \qquad (3.46)$$

$$u_1 = \omega r - v_w sin\tau \cdot sin\theta \qquad (3.47)$$

The speed ratio, λ, can now be determined from the calculated speeds as

$$\lambda = \frac{u_1}{v_1} = \frac{(\omega r - v_w sin\tau \cdot sin\theta)\sqrt{\cot^2\kappa + 1}}{v_w(cos\tau - sin\tau \cdot cot\kappa \cdot cos\theta)}$$

The speed ratio at the tip is therefore defined as follows

$$\lambda_t = \frac{u_1}{v_1} = \frac{\omega R}{v_w} \qquad (3.48)$$

Introducing (3.48) in the λ expression, it is finally obtained the speed ratio for the given installation angles,

$$\lambda = \frac{(\lambda_t \frac{r}{R} - sin\tau \cdot sin\theta)\sqrt{\cot^2\kappa + 1}}{cos\tau - sin\tau \cdot cot\kappa \cdot cos\theta} \qquad (3.49)$$

4 Wind Turbine Configurations

4.1 Direct Speed Drive versus Gearbox Generators

When talking about the inner generator of a wind turbine, there are different types of operation, in order to withdraw energy. In particular, they have been developed two types of operation based in synchronous and induction (asynchronous) generators, which are a consequence of how the rotation of the blades is transmitted to the grid.

In gearbox-operated wind turbines the blades rotate around a shaft connected through a gearbox to the generator. This gearbox converts the rotational speed of the shaft of about tens of rotations per minute into about thousands of rotations per minute, which the generator needs to generate electricity. The inner wheels and bearings of the gearbox suffer great stress because of wind turbulence (changing wind conditions) and any component defect can bring the turbine to a halt. This is the reason why the gearbox is the highest-maintenance part of a wind turbine. “Gearboxes in offshore turbines, which face faster wind speeds, are even more vulnerable than those in onshore turbines.” (**Morris 2011**).

Figure 4.1 Flex-drive planetary gearbox (from **Tong 2010**)

For economy and reliability, gearbox generators increase the speed of rotation to drive an induction generator that is connected directly to the utility grid. Induction machines are also known as asynchronous machines, that is, they rotate below synchronous speed when used as a motor, and above synchronous speed when used as a generator. So when rotate faster than its normal operating or no-load speed, an induction generator produces AC electricity.

Because an induction generator synchronises directly with the main utility grid (produces electricity at the same frequency and voltage) no rectifiers or inverters are required. (**Rama 2016**)

A typical design of an induction generator is the squirrel-cage structure, where bars are embedded within the body of the rotor and connected together at their ends by shorting rings as shown in Figure 4.2. As the conducting bars are short-circuited together, a large current flows around them and a magnetic field is created inside the rotor causing the machine to rotate.

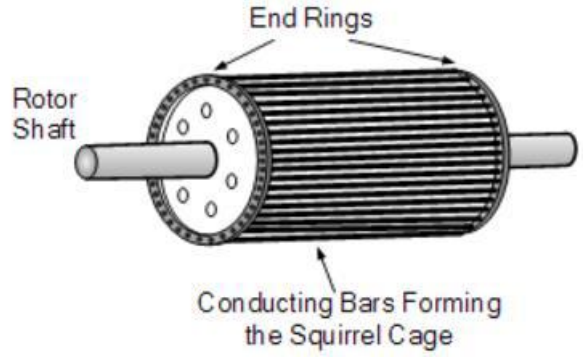

Figure 4.2 Squirrel-cage structure (from **Rama 2016**)

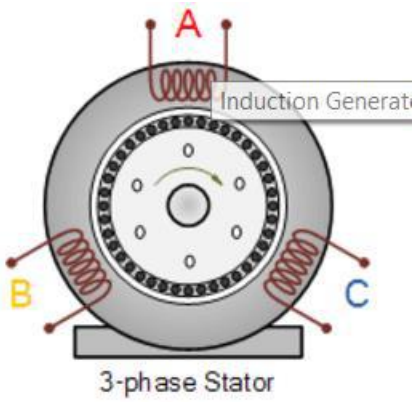

Figure 4.3 Induction (asynchronous) generator (from **Rama 2016**)

Since the magnetic field of the rotor follows the one of the stator, the rotor accelerates up to synchronous speed set by the frequency of the grid supply. The faster the rotor rotates, the lower is the resulting relative speed difference between the rotor cage and the rotating stator field and thus the voltage induced is winding. As the rotor approaches to synchronous speed, it slows down as the weakening rotor magnetic field is insufficient to overcome the friction losses. The result is that the rotor is now rotating slower than synchronous speed. Then, an induction machine can never reach its synchronous speed, as to reach it, there would be no current induced into the squirrel cage, no magnetic field and thus no torque. (**Rama 2016**)

The difference in rotational speed between the rotating magnetic field of the stator, n_S, and the rotor speed, n_R, is referred to in induction machines as “slip”, expressed as a percentage. This slip means that the operation is thus “asynchronous” and the heavier the load attached to an asynchronous generator, the higher is the resulting slip, as higher loads require stronger magnetic fields. More slip is associated with more induced voltage, more current and a stronger magnetic field. Then, for an induction generator, its operating speed has to be above the rated synchronous speed. (**Rama 2016**)

Because of the problems attached to gearbox maintenance and performance, it was developed a new way of taking power from a wind turbine, through the direct drive operation. With this operation, maintenance and service costs are lower (fewer wearing parts, no gear oil change, etc.) and operating expenses are reduced.

The direct drive operates as described in **Enercon** web page: "The rotor hub and annular generator are directly connected to each other as a fixed unit without gears. The rotor unit is mounted on a fixed axle, the so-called axle pin. (…) The direct drive system has only two slow-moving roller bearings. The reason for this is the low speed of the direct drive. The annular generator is of primary importance in the gearless system design. Combined with the rotor hub it provides an almost frictionless flow of energy, while the gentle running of fewer moving components guarantees minimal material wear. Unlike conventional induction generators, the annular generator is subjected to minimal mechanical wear, which makes it ideal for particularly heavy loads and a long service life." (**Enercon**). In Figure 4.4 is shown the arrangement of a direct-drive hub of a wind turbine.

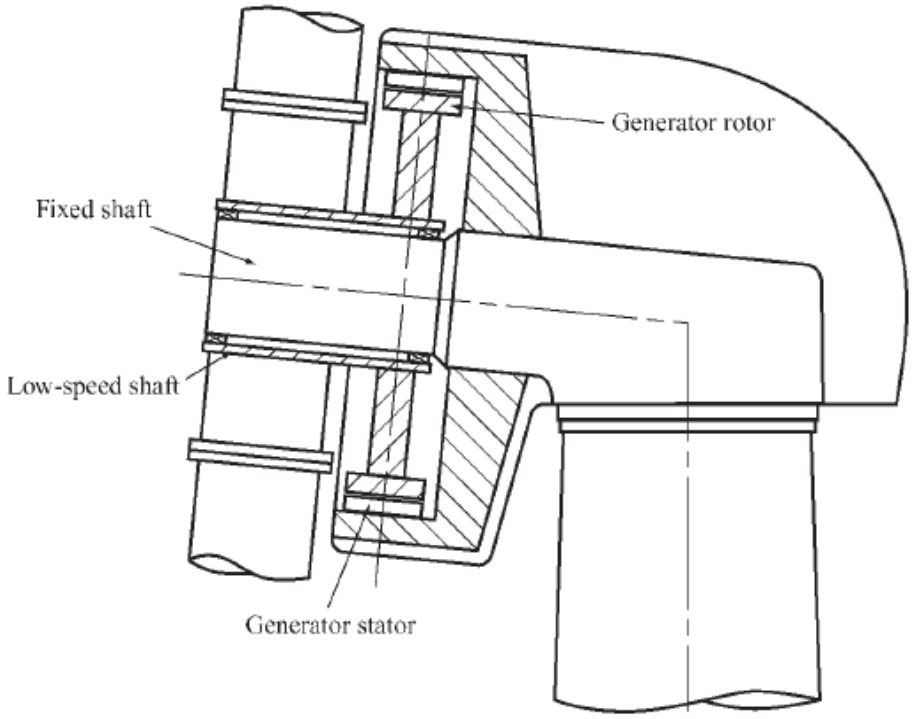

Figure 4.4 Direct-drive generator section (from **Burton 2001**)

The power output of any rotating electrical machine may be generally described by (**Freris 1990**):

$$P = \frac{1}{4} K D^2 L n \qquad (4.1)$$

where D is the rotor diameter, L is the length, n is the rotational speed, and K is a constant.

So if the rotational speed is reduced, then it is necessary either to lengthen the generator or to increase the diameter. Finally, it is cheaper to increase the diameter as this raises the power by the square. Thus, direct-drive generators for wind turbines tend to have larger diameters but with limited length.

"Induction generators require a rather small radial distance between the surface of the rotor and the stator (known as the air-gap). This is necessary to ensure an adequate magnetic flux density as all the excitation is provided from the stator. Contrast, synchronous generators have excitation systems on the rotor and so, can operate with larger air-gaps. It is difficult to manufacture large diameter electrical machines with small air gaps for mechanical and thermal reasons. Hence direct-drive wind turbines use synchronous generators (…). The use of a synchronous generator, in turn, leads to the requirement for solid-state frequency conversion equipment to de-couple the generator from the network and permit variable-speed operation." (**Burton 2001**).

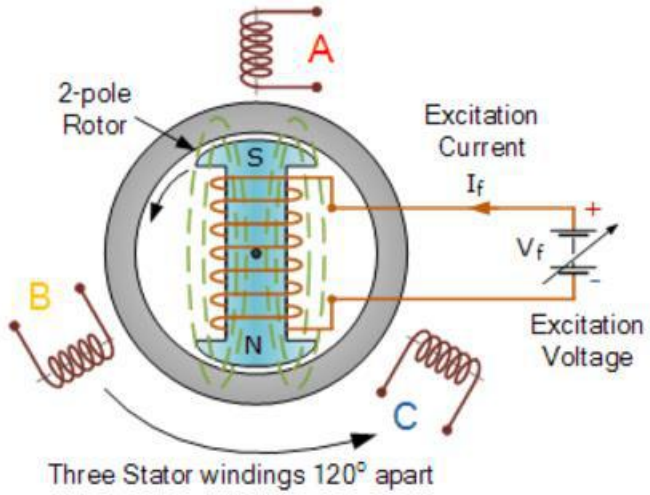

Figure 4.5 Synchronous generator (from **Rama 2016**)

A synchronous generator within a direct-drive turbine has a wound salient two-pole rotor, which is connected to a DC supply voltage, and three coils in the stator, Figure 4.5. The external DC excitation voltage produces an electromagnetic field around the coil with north and south poles. When the rotor shaft is turned by the turbines blades, the rotor poles will also

move at the same angular velocity producing a rotating magnetic field. As the rotor rotates, its magnetic flux cuts the individual stator coils one by one, and by Faraday's law, a current is induced in each stator coil. (**Rama 2016**)

The magnitude of the voltage induced in the stator winding is a function of the magnetic field intensity which is determined by the field current, the rotating speed of the rotor, and the number of turns in the stator winding. As the synchronous machine has three stator coils separated 120° each one, a 3-phase voltage supply is generated in the stator windings. This 3-phase stator winding is connected directly to the load, and as the current generating coils are stationary, they make it easier to wind and insulate the windings, as they are not subjected to rotational and centrifugal forces allowing for greater voltages to be generated. (**Rama 2016)**

As explained, wound-field synchronous machines require DC current excitation in the rotor winding, which is done through the use of brushes and slip rings on the generator shaft. However, there are several disadvantages such as requiring regular maintenance, cleaning of the carbon dust, etc. An alternative approach is to use brushless excitation which uses permanent magnets, called permanent magnet synchronous generator. The permanent magnets can be mounted on the surface of the rotor, embedded into the surface or installed inside the rotor and the air gap between the stator and rotor is reduced for maximum efficiency. (**Rama 2016)**

4.2 Fixed Speed versus Variable Speed; Pitch Control versus Stall Control

Up to this time, it has not been mentioned how the wind turbine operates for different wind speeds. Wind turbines are subjected to a range of wind speeds, and not only to one single value of it. To this point, nowadays they exist two types of operation which have been applied to actual rotors: fixed speed and variable speed operations.

Firstly, it is important to explain what rate wind speed is. This wind speed is the minimum wind speed at which the wind turbine can produce its rated output power.

The first design was to make the wind turbines to operate at fixed speed when producing power. "In a start-up sequence the rotor may be parked (…), and on release of the brakes would be accelerated by the wind until the required fixed speed was reached. At this point, a connection to the electricity grid would be made and then the grid (through the generator) would hold the speed constant. When the wind speed increased beyond the level at which rated power was generated, power would be regulated (…) by stall or by pitching the blades." (**Özdemir 2013**).

- Stall-operated fixed-speed wind turbine (pitching to stall): "The wind turbine is started as an induction motor as the wind speed reaches cut-in. The rotor speed is driven by the available wind and is driven above synchronous speed at a very small slip (1% at most). As the wind speed increases at constant rotational speed, the tip speed ratio decreases and the operating C_P travels along ABCD, Figure 4.6, when the rated power is reached at the wind speed designed for the wind turbine. As the wind speed increases further, the operating C_P decreases further and the tip speed ratio gets even smaller" (**Muljadi 2013**).

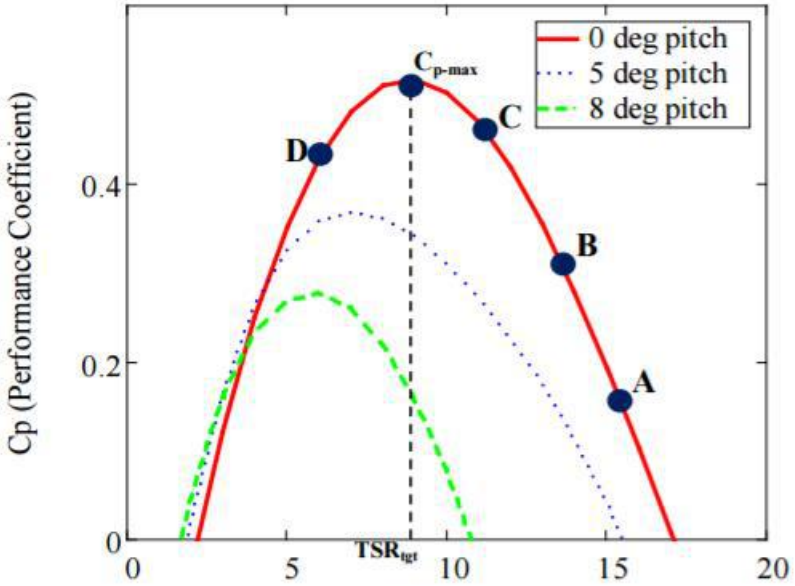

Figure 4.6 C_P-λt curve for the operation of a stall-operated fixed-speed wind turbine (from **Muljadi 2013**)

- Pitch-controlled fixed-speed wind turbine (pitching to feather): "The blade pitch control is activated in the high wind speed region to limit the stresses imposed on the mechanical components, to limit the output power generated, and to avoid a runaway condition if the wind turbine loses connection to the grid. Limiting the aerodynamic torque (…) is important to ensure that the mechanical components of the turbine (gearbox, generator shaft, low-speed shaft, etc.) will not be stressed due to overloads caused by wind fluctuations and turbulence." (**Muljadi 2013**). Figure 4.7 shows the power curve of an example of a pitch-controlled fixed-speed wind turbine at 15 rpm with and without pitch. With pitch, the output of the wind turbine is limited to 1.5 MW. Moreover, Figure 4.6 shows the effect of changing the pitch angle on the C_P-λ_t curve, indicating that, when increasing the pitch angle, the C_P-λ_t curve moves to lower C_P and λ_t values.

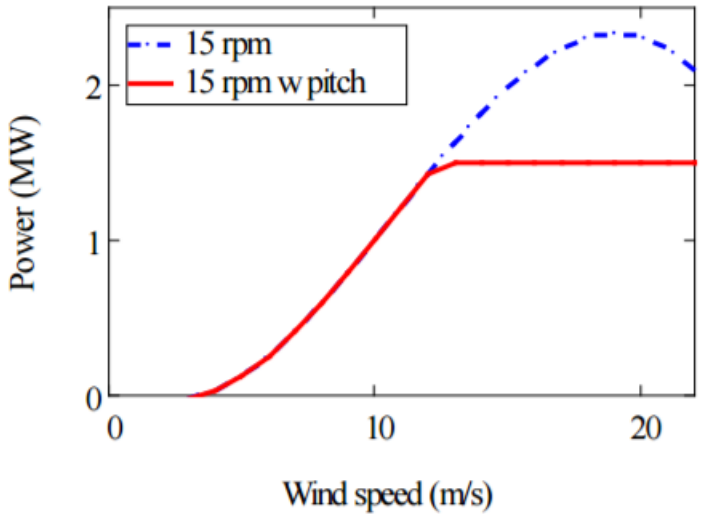

Figure 4.7 Power-Wind speed curve for the operation of a pitch-controlled fixed-speed wind turbine (from **Muljadi 2013**)

Years later, variable speed operation was introduced into wind turbines. "This allowed the rotor and wind speed to be matched, and the rotor could maintain the best flow geometry for maximum efficiency. The rotor could be connected to the grid at low speeds for very light winds and would speed up in proportion to wind speed. As rated power was approached, and certainly after rated power is being produced, the rotor would revert to nearly constant speed operation, with the blades being pitched as necessary to regulate power." (**Özdemir 2013**).

The main differences between variable speed operation and the fixed speed operation are:

- variable speed in operation below rated power can enable energy capture,
- variable speed above rated power relieves loads, ease pitch system duty and reduce output power variability.

"Superficially, it seemed to offer better control than stall regulation, but it emerged through experience that pitch control in a fixed speed wind turbine at operational wind speeds higher than the rated wind speed could be quite problematic. The most notable reason is that, since in constantly changing wind conditions it is necessary to adjust pitch to the most appropriate angle and under high loads, excessive power variations could result, and the control system could be set with the blades in the wrong position. In view of such difficulties, which were most acute in high operational wind speeds, pitch control in combination to a rigidly fixed speed became a 'challenging' operation." (**Özdemir 2013**).

On the one hand, according to **Özdemir 2013**, variable speed increases cost and reliability concerns. There was never a clear case for variable speed on economic grounds, with small energy gains being offset by extra costs and also additional losses in the variable speed drive.

On the other hand, the stall-operated fixed-speed design remains viable, but the direction towards variable speed in new large wind turbines relates to better output power quality to the grid, naturally combined with pitch regulation. However, together with pitch regulation and advanced control strategies in variable-speed wind turbines, stall offers ways to limit loads and fatigue within the system and is almost universally employed in new large wind turbine designs.

4.3 Pitch Set Angle

Another parameter which affects the power output is the pitch set angle of the blades, β_S. The design of a blade uses to involve a twist distribution; however, the blade can be also set at the root with an overall pitch angle affecting its performance.

Little changes in pitch angle can have a great effect on the power output. For example, positive pitch angle settings, Figure 4.8, increase the design pitch angle and so decrease the angle of attack. Conversely, negative pitch angle settings increase the angle of attack and may cause stalling on some blade elements. The effects of a few degrees of pitch are shown in Figure 4.9.

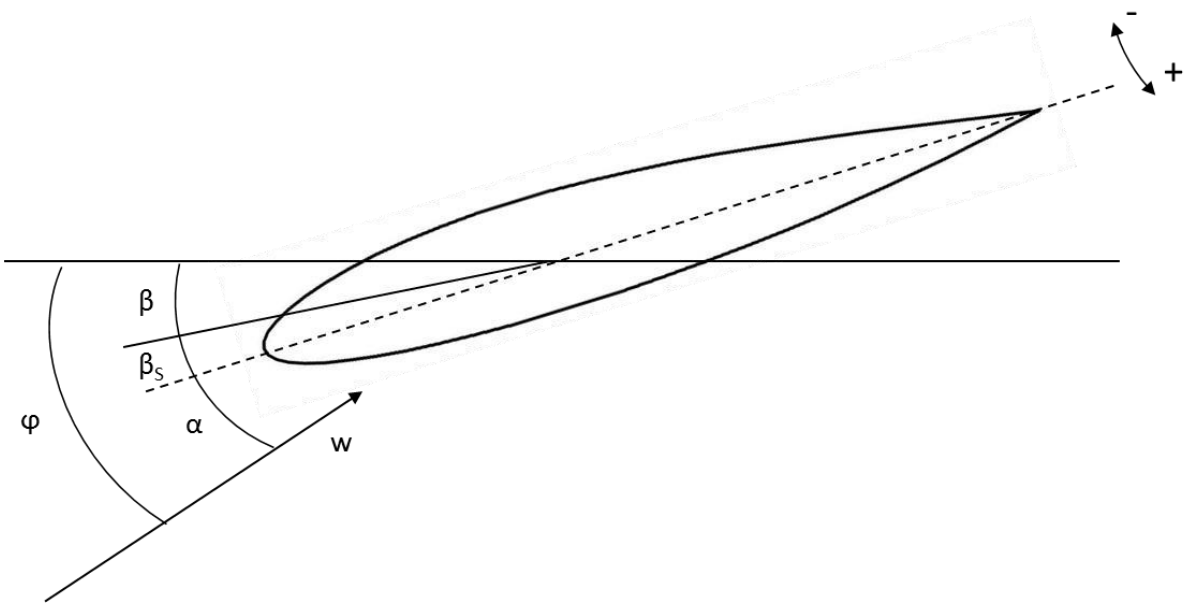

Figure 4.8 Pitch and twist angles on a blade element (own design)

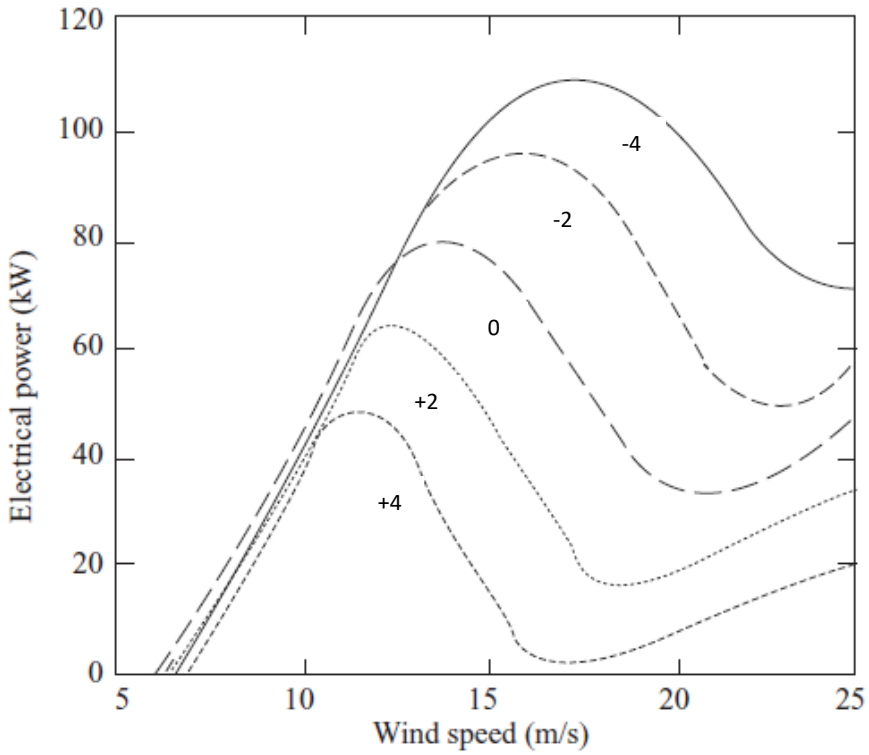

Figure 4.9 Effect on extracted power of blade pitch set angle (from **Burton 2001**)

"A turbine rotor designed to operate optimally at a given set of wind conditions can be suited to other conditions by appropriate adjustments of blade pitch angle and rotational speed." (**Burton 2001**, Page 180).

The most important application of pitch control is for power regulation generally in fixed speed operation, but pitch control has other advantages. For example, by adopting a large positive pitch angle, a large starting torque can be generated as a rotor begins to turn. Moreover, a 90° pitch angle is used when shutting down because this minimises the rotor speed at which the parking brake is applied. When this happens, the blade is said to be "feathered".

Power regulation in fixed speed operation can be achieved either by pitching to promote stalling or pitching to feather to reduce the lift force on the blades (by reducing the angle of attack) (**Burton 2001**, Page 181).

4.3.1 Pitching to Stall

At wind speeds below the rated one, the blade pitch angle is kept at 0°. As rated power is reached, only a small negative pitch angle about 2°, is necessary to promote stalling and so to limit the power to the rated level. As the wind speed increases, they are needed small adjustments in both the positive and negative direction to maintain constant power by stalling.

The small sizes of these pitch angle adjustments make pitching to stall very attractive. (**Burton 2001**, Page 181).

4.3.2 Pitching to Feather

By increasing the pitch angle as rated power is reached, the angle of attack can be reduced. A reduced angle of attack will reduce the lift force and the torque while the flow around the blade remains attached.

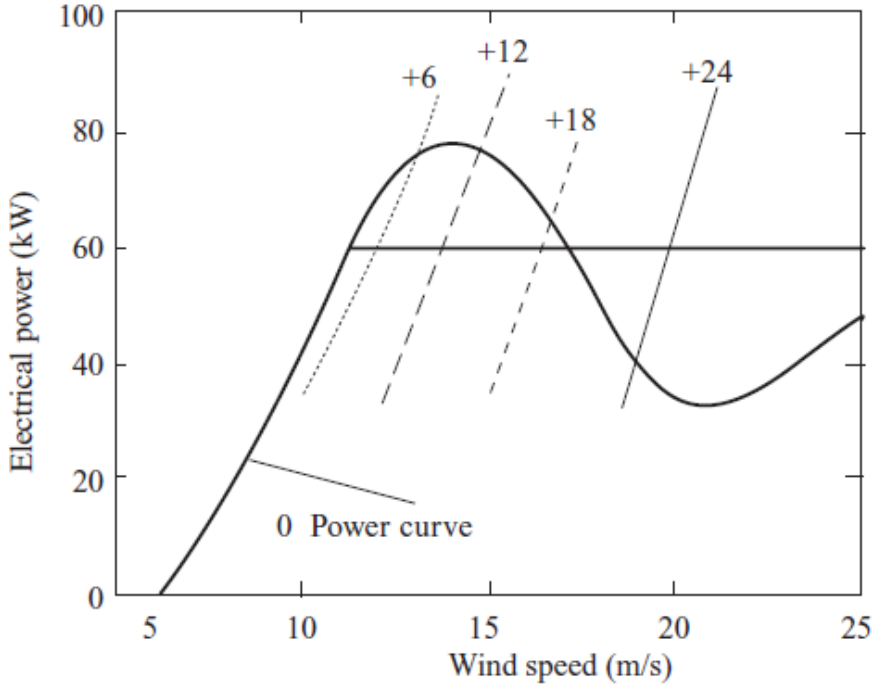

Figure 4.10 Pitching to feather power regulation requires large changes of pitch angle (from **Burton 2001**)

In Figure 4.10 is shown a zero degree pitch angle power curve. They are also shown fragments of other power curves for higher pitch angles as they cross the rated power level, so that the crossing points give the necessary pitch angles to maintain rated power at the corresponding wind speeds.

As it can be seen in Figure 4.10, the required pitch angles increase progressively with wind speed and are generally much larger than is needed for the pitching to stall method. In turbulent conditions, large pitch angles are needed to maintain constant power and the inertia of the blades will limit the response speed of the control system. (**Burton 2001**, Page 182)

As the blades remain non-stalled, if large gusts occur (wind speeds above the rated level), they take place great changes of angle of attack, associated to grate changes in lift. Therefore,

gust loads can be more severe than for stalled blades. The advantages of the pitching to feather method are that the flow around the blade remains attached, and so well-understood, and provides good, positive damping. Also, feathered blade parking and assisted starting are possible. Thus, pitching to feather has been the preferred pitch control option mainly because blade loads can be predicted with more confidence than for stalled blades (**Burton 2001**, Page 182).

5 Blade Element Momentum Spread Sheet

To fulfil the aim of this thesis, it has been developed an Excel tool, called Blade Element Momentum Spread Sheet, which helps to calculate the required data. This program is based on the one developed in Fortran 95 by **Lindemann 1985** and **Lindemann 1988**.

5.1 Basic Calculation Procedure

Once the performance and criteria has been presented and explained, the basis for a wind turbine calculation program is settled. In this program they are introduced all the information and equations developed in previous sections, as well as all the different geometrical cases in order to make a realistic support for a wind turbine design.

The aim of the program is to calculate the average efficiency over the wind rotor area; in particular the total power factor C_P. In addition, the tool calculates all possible wind turbine rotors corresponding to the input parameters and its limit positions. As to achieve this objective, the program has been based on the Fortran tool from **Lindemann 1985**.

As it was mentioned in section 3.7, the core of the program is equation (3.40). This expression is the necessary one to obtain the total efficiency of a given wind turbine. In order to carry out its calculation, the integration is turned into a summation as

$$C_P = \eta_z \frac{1}{A} \sum_{i}^{A} C_{Pi} \cdot \eta_P \cdot \Delta A \qquad (5.1)$$

The operation of the spread sheet is as follows:

1. The user introduces the desired basic geometry, wind speed and rotational speed.

2. A value for the tip speed ratio, λ_t, is given from 1 to 20 and the efficiency coefficient, $\eta_z(\lambda_t)$, is calculated.

3. A value for the angle of rotation, θ, is given from 0 to 2π.

4. A value for non-dimensional blade distance from the root, R' = r/R, is given from R'_0 to 1.

5. The speed ratio at the element, $\lambda(R', \theta, \lambda_t, \tau, \kappa)$, and its axial reduction factor, $\xi(R', \theta, \lambda_t, \tau, \kappa)$, are calculated.

6. The power coefficient of the blade element, $C_{Pi}(\lambda, \xi)$, and its friction efficiency, $\eta_P(\lambda, \xi)$, are calculated.

7. The integration is carried out by the sum of each power coefficient multiplied by the friction efficiency and the surface of each element ring sector, $\Delta A(R', \theta, \tau, \kappa)$.

8. The summation is divided by the total surface area of the rotor, A, and multiplied by the efficiency coefficient, $\eta_z(\lambda_t)$.

To make it easier to understand, the coarse structure of the program is shown as a scheme in Figure 5.1.

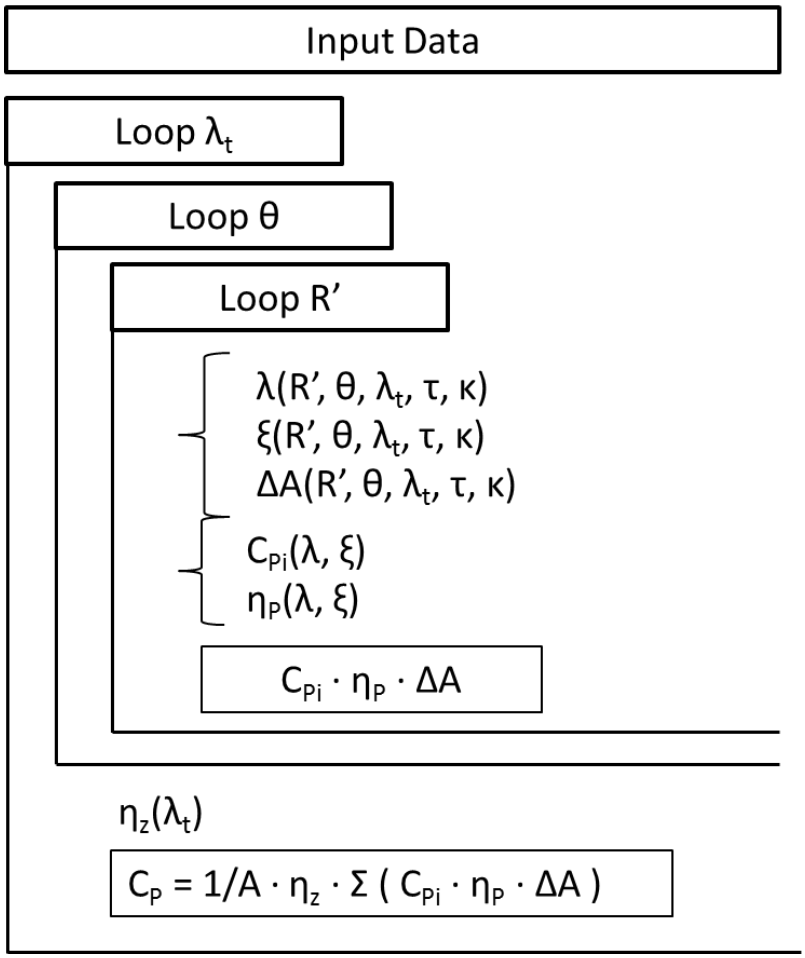

Figure 5.1 Structure of the Blade Element Momentum Spread Sheet (from **Lindemann 1985**)

Where the steps for θ and R' are set as $\Delta\theta = 20°$ and $\Delta R' = 0.05$.

5.1.1 Input Data

To start the rotor calculation, they are necessary several parameters which are set by the user. These parameters will define the performance principles of the wind turbine, its external conditions and minimum geometrical requirements.

As it was explained in sections 2.2 and 3.8, this tool seeks different objectives, and one of those is to compare diverse wind turbine configurations for the same conditions variating its installation angles. So, two of the principal input data are the axis angle, τ, and the cone angle, κ.

They are also required the length of the blade, L, and the length from the root until the circular airfoil sections end (circular root), L_0. Also, it is an important parameter the number of blades, z, which will determine several performance characteristics of the rotor and its rotation speed, ω.

As geometrical blade parameters, they are needed the taper ratio, t_t/t_0, the chord at the root with respect to the blade length, t_0/L (element just after the circular root), and the relation of chords between the circular root and the element at root, t_r/t_0.

Regarding twist, when a linear twist angle distribution is selected, they are needed the twist angle at the tip, β_t, and at the root, β_0. Finally, for later calculations, it will be introduced a pitch angle, β_S, which will affect all blades equally.

Moreover, they can be varied the steps of tip speed ratio, angle of rotation and non-dimensional radius ($\Delta\lambda$, $\Delta\theta$, $\Delta R'$) involved in the loop calculation.

Lastly, they are introduced two types of blade: a blade composed entirely by the same airfoil and a blade composed by a transition of airfoils. When the first option is selected, it must be inserted the name of an airfoil (in what follows, there are only available three NACA airfoils: NACA 0012, NACA 0015, and NACA 0018). On the other hand, when the second option is selected, it is assumed the following airfoil distribution along the blade:

$$\begin{cases} \frac{L_0}{L} \leq R' < \frac{1}{3} \;\; ; \;\; NACA\ 0018 \\ \frac{1}{3} \leq R' < \frac{2}{3} \;\; ; \;\; NACA\ 0015 \\ \frac{2}{3} \leq R' \leq 1 \;\; ; \;\; NACA\ 0012 \end{cases}$$

In Figure 5.2 is shown how is the interface of the input data section in Element Momentum Spread Sheet.

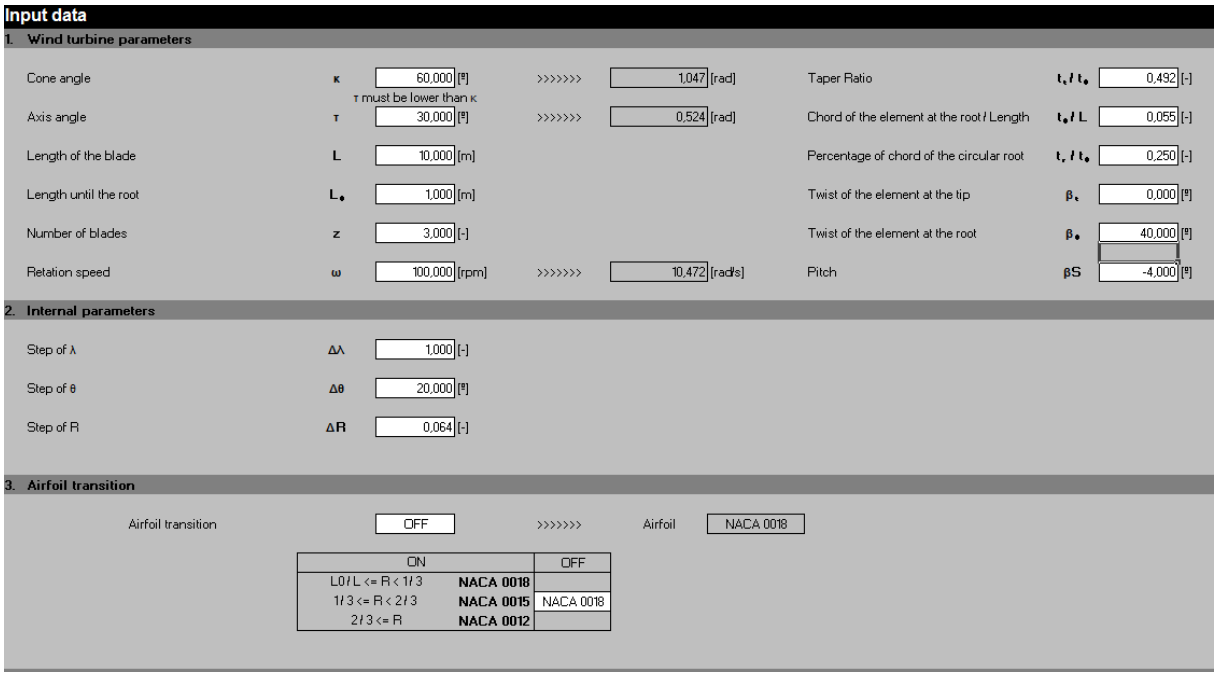

Figure 5.2 Input data in Blade Element Momentum Spread Sheet

With all these parameters, they are calculated some others that are necessary for the rest of the program, Figure 5.3. These are.

- chord at the tip with respect to the blade length: t_t/l
- chord of the circular root: t_r
- percentage of root (circular airfoil sections): $r_t = l_0/l$
- change of twist along the blade: $Q = \frac{\beta_0 - \beta_t}{R_t - 1}$
- effective radius: $R = L \sin \kappa$
- chord at the tip with respect to the effective radius: $t_t' = t_t/R$
- change of chord along the blade: $U = \frac{(t_0 - t_t)}{R(1 - R_t)}$
- non-dimensional effective rotor area (explained later on in 5.1.2): $A = \pi\sqrt{cotg^2\kappa + 1}$

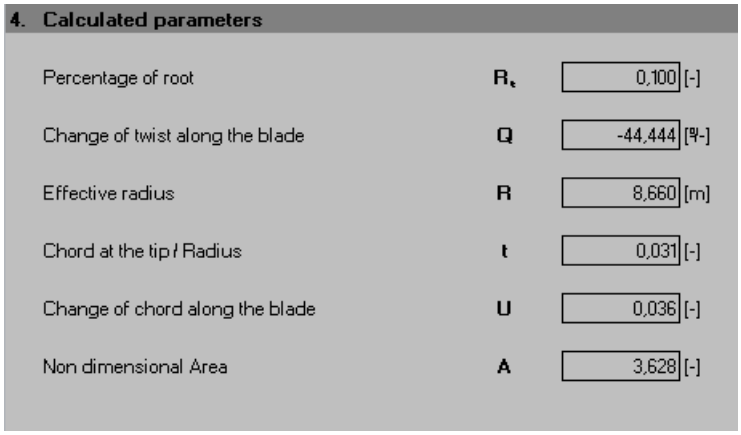

Figure 5.3 Calculated parameters in Blade Element Momentum Spread Sheet

5.1.2 Main Program

The main program is where all the relevant variables are obtained and put together in order to obtain the aerodynamic efficiency. This part of the program is settled in a single spread sheet within the Excel tool, called "C_P".

To carry out the calculations, variables are set in the middle of each element, that is

$$\theta_m = \theta + \frac{\Delta\theta}{2}$$

$$R'_m = R' + \frac{\Delta R'}{2}$$

With the geometrical data and the given installation angles, the surface of a single ring element sector corresponding to its location and angle of rotation is

$$\Delta A(R', \theta, \lambda_t, \tau, \kappa) = \frac{1}{2}\sqrt{cotg^2\kappa + 1} \cdot \left[(R' + \Delta R')^2 - R'^2\right] \cdot \Delta\theta \qquad (5.2)$$

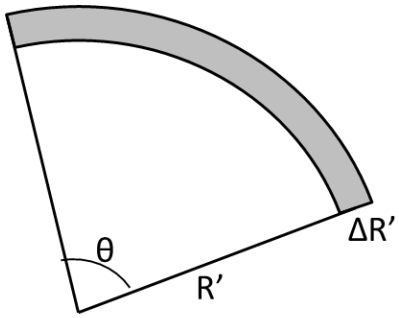

Figure 5.4 Ring sector (own design)

The calculation of $\lambda(r, \theta, \lambda_t, \tau, \kappa)$ and $\xi(r, \theta, \lambda_t, \tau, \kappa)$ involves the obtaining of other intermediate parameters. Thus, with all this established, now expression (3.49) is introduced as follows to obtain λ

$$\lambda(R', \theta, \lambda_t, \tau, \kappa) = \frac{(\lambda_t R'_m - sin\tau \cdot \sin\theta_m)\sqrt{\cot^2\kappa + 1}}{cos\tau - sin\tau \cdot cot\kappa \cdot \cos\theta_m} \qquad (5.3)$$

The next step is to obtain $\xi(R', \theta, \lambda_t, \tau, \kappa)$, however, it needs to be calculated separately through a subroutine. This step and the mentioned subroutine will be developed in section 5.1.2. After carrying out the subroutine, they are given to the main program the axial reduction factor, ξ, the effective speed ratio, λ_0 and the glide ratio of the analysed element, ε_m.

When the speed ratio and the axial reduction factor for the position of the element are finally obtained, it is possible to calculate the tangential reduction factor, σ,

$$\sigma = \sqrt{1 + \frac{1 - \xi^2}{\lambda^2}} \qquad (3.15)$$

which helps to achieve the power coefficient for the blade element,

$$C_{Pi}(\lambda, \xi) = \lambda^2 (1 + \xi)(\sigma - 1) \qquad (3.22)$$

This value has not to be higher than 0.593 (theoretical maximum) nor lower than 0. When the element gives a value of $C_{Pi} < 0$, it is assumed that this element has a void efficiency.

Consecutively, it is obtained the friction efficiency of the analysed element thanks to expression (3.31)

$$\eta_P(\lambda, \xi) = 2\lambda \frac{\varepsilon - \lambda_0}{(1 + \xi)(1 + \varepsilon\lambda_0)} \qquad (3.31)(3.15)$$

After that, it is possible to multiply these values, so $\Sigma(C_{Pi} \cdot \eta_P \cdot \Delta A) = C_{Pi}(\lambda, \xi) \cdot \eta_P(\lambda, \xi) \cdot \Delta A(R', \theta, \lambda_t, \tau, \kappa)$. Once done that, within the λ_t loop, they are calculated the efficiency coefficient, $\eta_z(\lambda_t)$, and the total effective surface area of the rotor

$$\eta_z = \left[1 - \frac{1{,}39}{z} \frac{1}{\sqrt{1 + \lambda_t^2}}\right]^2 \qquad (2.22)$$

$$A = \sqrt{cotg^2\kappa + 1} \cdot \pi \left(\frac{r = R}{R}\right)^2 = \sqrt{cotg^2\kappa + 1} \cdot \pi \qquad (5.4)$$

So it is finally possible to obtain $C_P = \frac{1}{A} \cdot \eta_z \cdot \Sigma(C_{Pi} \cdot \eta_P \cdot \Delta A)$.

5.1.3 Subroutine for Axial Reduction Factor

As it has been mentioned, the axial reduction factor requires an individual subroutine within the program. This subroutine is found in a separate spread sheet in the Excel tool called “Subroutine Xi”.

The calculation of the reduction factor needs to be done by iteration, following the next steps. The equation from ξ is going to be determined for each blade element, which comes from (3.37).(3.47)

$$t = \frac{8\pi r}{C_l \cdot z} \cdot \frac{1}{\lambda_0^2} \cdot \frac{1}{\sqrt{1 + {}^1/_{\lambda_0^2}}} \cdot \frac{1-\xi}{1+\xi} \qquad (3.36)$$

Thus, the values of ξ can be obtained as zeros, for example, using the Regula Falsi method from (3.37):

$$f(\xi) = \frac{8\pi r}{C_l \cdot z} \cdot \frac{1}{\lambda_0^2} \cdot \frac{1}{\sqrt{1 + {}^1/_{\lambda_0^2}}} \cdot \frac{1-\xi}{1+\xi} - t = 0$$

Or simplifying as

$$\frac{1+\xi}{1-\xi} = \frac{8\pi r}{C_l \cdot z \cdot t} \cdot \frac{1}{\lambda_0^2} \cdot \frac{1}{\sqrt{1 + {}^1/_{\lambda_0^2}}} = B \qquad (5.5)$$

$$\xi = \frac{B-1}{B+1} \qquad (5.6)$$

Here, B is a placeholder and the following must be considered:

- the lift coefficient C_l is dependent on the profile angle of attack, α,
- the profile angle is dependent on the effective speed and the twist angle, β,

$$\alpha = \arctan(\frac{1}{\lambda_0} - \beta) \qquad (5.7)$$

- the effective speed ratio λ_0 depends on the speed ratio, λ, and, again, on the reduction factor: $\lambda_0 = \lambda \frac{1+\sigma}{1+\xi}$.

Therefore, a solution for the reduction factor is only possible iteratively.

As a first approximation, it is set $\lambda_0 = \lambda$ and $\xi_a = 0$ (reference value), and with the twist angle for the element analysed (the distribution of twist along the blade, β(R'), will be given and described in section 5.3.) it is computed α as $\alpha = \arctan(\frac{1}{\lambda_0} - \beta)$ with the following conditions:

- if $\lambda_0 < 0$, $\alpha = \alpha + 180°$
- if $\alpha < \alpha_{min}$ or $\alpha > 90°$ and $\lambda_0 < 0$, $\lambda_0 = -\lambda_0$
- if $\alpha < \alpha_{min}$, $\alpha = 2\alpha_{min} - \alpha$
- if $90° < \alpha < 180° - \alpha_{min}$, $\alpha = 180° - \alpha$

In this case, the airfoils that are going to be used are symmetric ones (i.e. NACA 00XX), and as their Cl - α curves are symmetric in relation to the ordinate axis, all the information will be collected for positive angles of attack, so it will be established $\alpha_{min} = 0$, as the symmetric point.

The next step is to calculate C_{lm} (lift coefficient for the analysed element) and ε_m (glide ratio for the analysed element), according to the corresponding airfoil C_l - α curve. This is done once the angle of attack is obtained, in order to interpolate between two entire values of α (due to the fact that the collected information is given in entire values of angles of attack, see **Sheldahl 1981**). Expressions (5.8) and (5.9) show it:

$$C_{lm} = C_l(i_\alpha) + (\alpha - \mathrm{i}_\alpha)[C_l(i_\alpha + 1) - C_l(i_\alpha)] \qquad (5.8)$$

$$\varepsilon_m = \varepsilon(i_\alpha) + (\alpha - \mathrm{i}_\alpha)[\varepsilon(i_\alpha + 1) - \varepsilon(i_\alpha)] \qquad (5.9)$$

With the condition that C_{lm} cannot be lower than 0, and that if $C_{lm} < 1 \cdot 10^{-3}$, the axial reduction factor for that element is $\xi = 1$.

With the values of C_{lm} and $\lambda_0 = \lambda$, it is possible to obtain the placeholder B, for each θ_m and R'_m and the input data. Once B in obtained, ξ is calculated by $\xi = \frac{B-1}{B+1}$.

The reduction factor cannot be lower than zero, and if that happens, it becomes $\xi = 0$ for that element. Moreover, it is going to be established that ξ must fulfil a stop condition, that is:

$$\left|\frac{\xi_a - \xi}{\xi}\right| > 0.01$$

When this condition is accomplished, the calculated value of ξ is considered valid and is transferred to the main program as the value for that blade element, as well as λ_0 and ε_m. However, when this condition is not fulfilled, it will be established $\xi_a = \xi$ (previous value which did not fulfil) and for λ_0

$$\lambda_0 = \sqrt{\frac{4(\lambda^2 + 1)}{(1 + \xi)^2} - 1} \qquad (5.10)$$

The rest of the steps are followed in the same way as explained and the iteration is repeated until the stop condition is accomplished.

5.2 Set of Airfoil Distribution

As it has been mentioned in 5.1.1, there are two possible ways of operation with respect to the blade airfoils. The first one is to introduce the same NACA airfoil along the whole blade, and the second one is to apply a distribution of NACA airfoils. When the user selects the desired option, data from the sheet "Airfoils" is used according to it for the rest of calculations.

In this sheet they are presented the three NACAs with their respect lift and drag coefficients for each angle of attack from -20° to 180°. As these are all symmetric airfoils, angles between -20° to -1° have void data, due to the fact that their C_l – α curves are symmetric, and therefore, values for negative angles of attack can be obtained from the positive ones. The values of all C_l and C_d coefficients have been taken from **Sheldahl 1981**.

What is important in the sheet "Airfoils" is the influence of the Reynolds number. In this sheet this number can be changed for each airfoil, choosing between $4 \cdot 10^4$ and $3{,}6 \cdot 10^5$, which are the orders of magnitude involved in the rotor aerodynamics carried out in this thesis.

5.3 Set of a Blade Twist Angle Distribution

As it has been seen, the twist angle distribution along the blade is important for the different calculations, mostly involved in the ξ subroutine. It has been mentioned that this distribution can be linear or nonlinear. Linear distributions are used as a simplified case of study. However, realistic models should include nonlinear ones as it will be seen.

Twist angles are applied in expression (5.7) to obtain angles of attack for each element, and with those, the corresponding lift coefficients. It is shown then, that these twist angles must be given previously, due to the fact that they cannot be calculated unless the angle of attack is a given parameter.

$$\alpha = \arctan\left(\frac{1}{\lambda_0} - \beta\right) \qquad (5.7)$$

For users, in Blade Element Momentum Spread Sheet, all the subsequent values of twist and pitch angles explained within the next sections are presented in the spread sheet called “Twist, Pitch & Chord”.

5.3.1 Linear Twist Angle Distribution

This section describes how to implement a linear twist angle distribution, although it is only a simplified case. This type of distribution was the one used in **Lindemann 1985**, and as this has been the base program for the actual development, it is necessary to be explained as a guiding point

In order to introduce this distribution, the user will give as parameters the previous mentioned twist angle at the tip, β_t, and twist angle at the root, β_0. With these two selected values, the twist linear distribution is:

$$\beta = Q(R'_m - 1) + \beta_t \qquad (5.11)$$

Being $Q = \frac{\beta_0 - \beta_t}{R_t - 1}$, as mentioned in 5.1.1.

This returns a linear distribution, which, for example, with $\beta_0 = 40°$ and $\beta_t = 0°$ gives the twist angles shown in Figure 5.5.

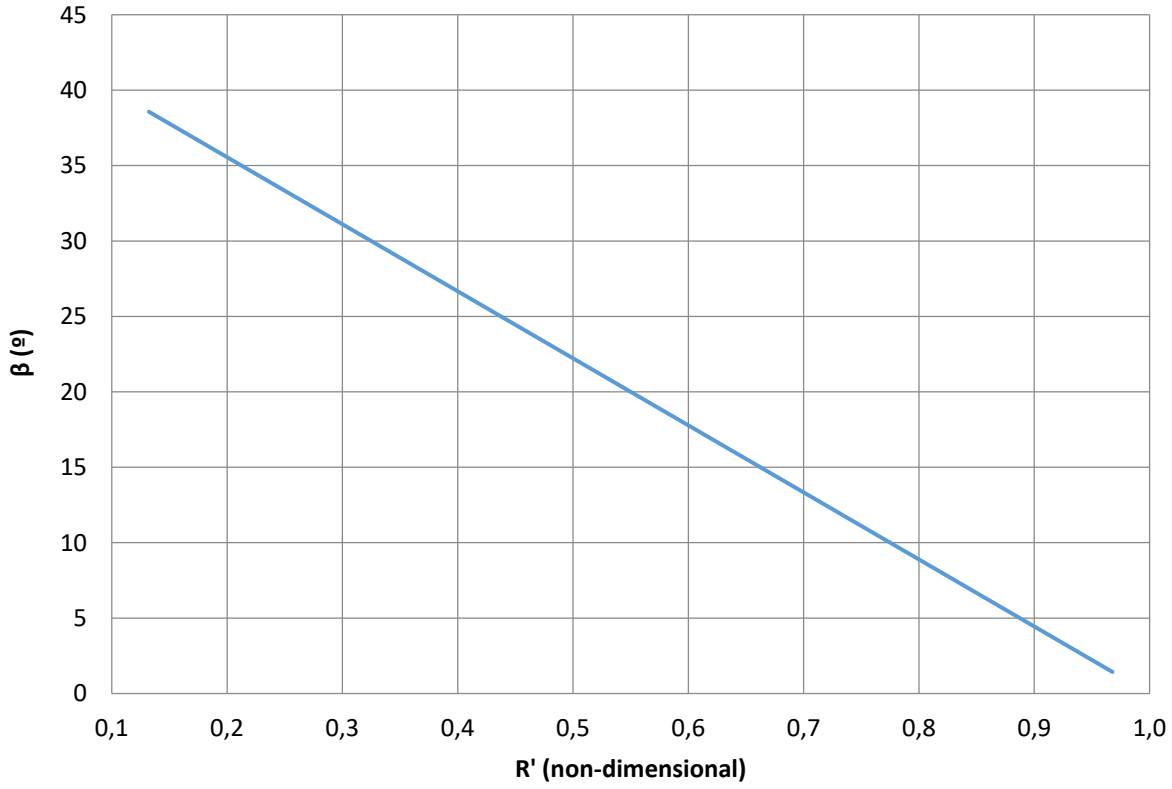

Figure 5.5 Lineal twist angle distribution along the blade length for $\beta_0 = 40°$ and $\beta_t = 0°$ (from Blade Element Momentum Spread Sheet)

This distribution generates different angles of attack along the blade, and also, these angles are different for each position around the rotor plane and each tip speed ratio. In order to show this, for example, for $\lambda_t = 1$ and $\theta_m = 10°$ and $\theta_m = 310°$ the respective angles of attack along the blade are the ones showed in Figure 5.6. Moreover, another comparison between angles of attack for the same angular position but different tip speed ratios is shown in Figure 5.7.

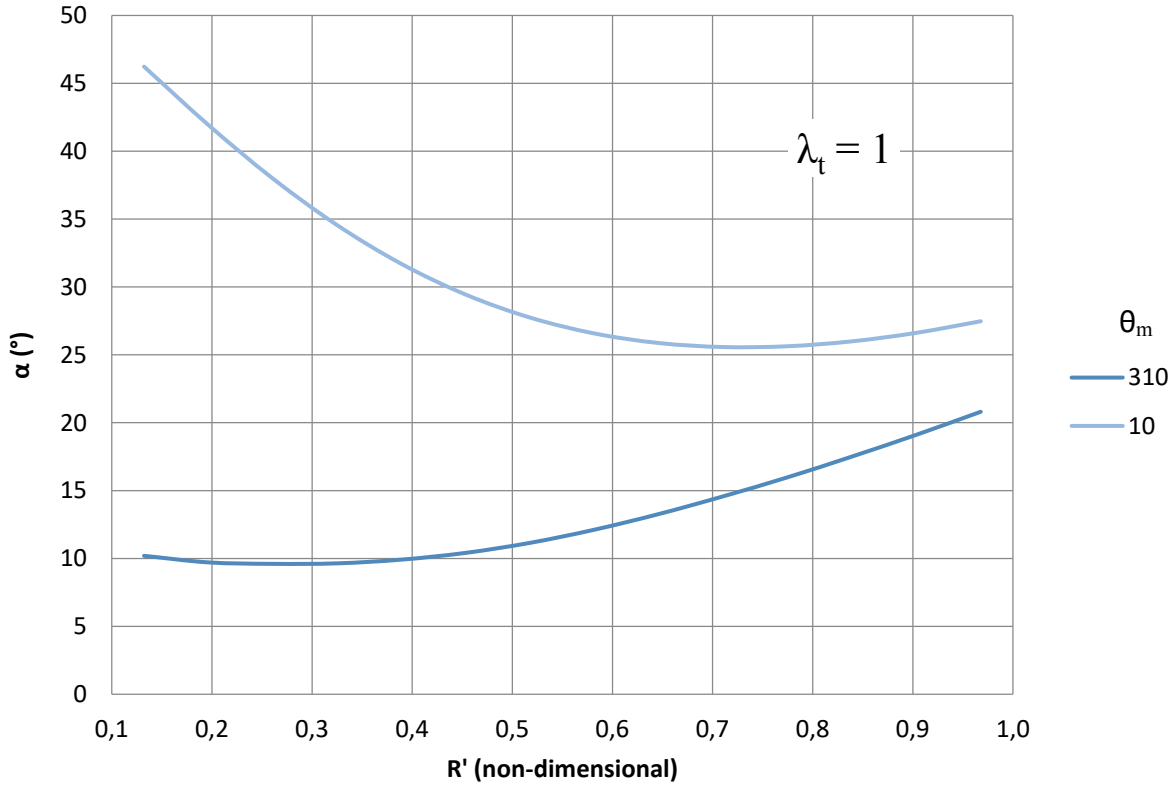

Figure 5.6 Angles of attack for $\lambda_t = 1$ and $\theta_m = 10°$, $\theta_m = 310°$ (from Blade Element Momentum Spread Sheet)

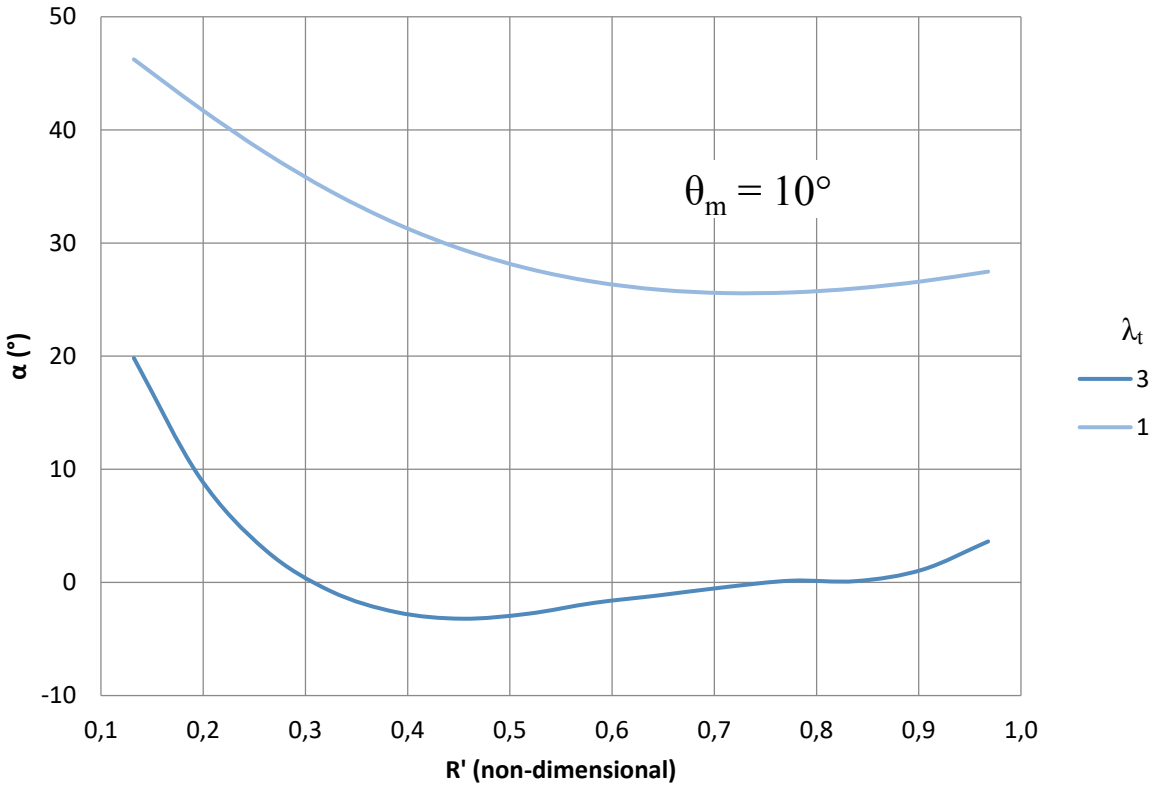

Figure 5.7 Angles of attack for $\theta_m = 10°$ and $\lambda_t = 1$, $\lambda_t = 3$ (from Blade Element Momentum Spread Sheet)

5.3.2 Variable Nonlinear Twist Angle Distribution

In order to introduce a nonlinear twist angle distribution, a condition for the angle of attack is needed. One possible condition is to impose that each blade element has to operate always with its maximum glide ratio (maximum aerodynamic efficiency).

This condition has to take into account the airfoil distribution along the blade, once has been set, it is necessary to look for the angle of attack which maximizes the ratio $\varepsilon_m = C_l/C_d$ for each airfoil element. This will minimize drag losses, even though drag has been ignored in the determination of the optimum flow induction factors and blade geometry it should not be ignored in the calculation of torque and power.

The imposed geometry implicates that all elements must change their twist differently and separately for each angular position, as shown in Figure 5.8.

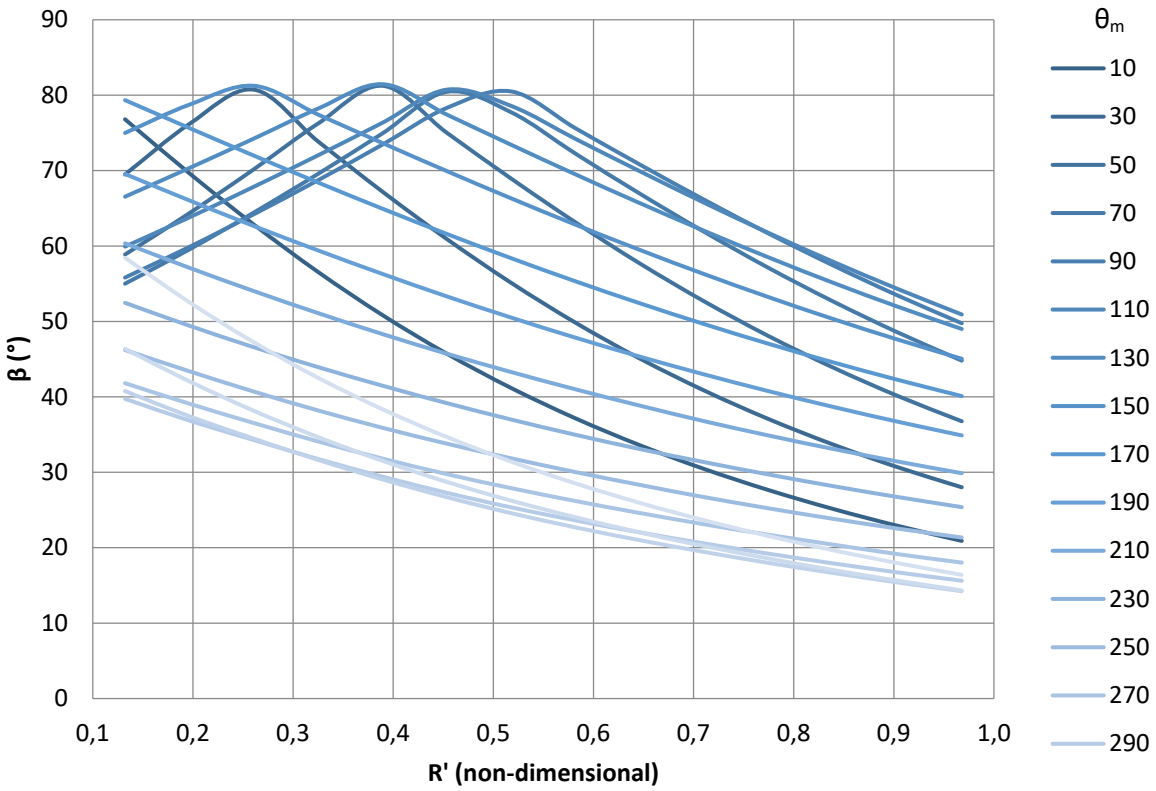

Figure 5.8 Change of twist angle distribution with the anguar position (from Blade Element Momentum Spread Sheet)

5.3.3 Constant Nonlinear Twist Angle Distribution

The variable twist angle distribution sets an extreme complicated performance of the blades, and, therefore, involves a difficult manufacturing, establishment and control. For that reason, a new dealing has to be implemented, in order to be a compromise solution between the linear distribution and the variable nonlinear one.

For this work, it has been taken a solution based on the previous nonlinear distribution. With that aim, as it can be observed in Figure 5.8, most of the twist distributions for different angular positions are as polynomial curves (except for some curves that have a peak), which sets that the new distribution has to follow that trend.

There are multiple possible options, and from now on, it will be applied as a base, the resultant curve for $\lambda_t = 1$ and $\theta_m = 10º$ offset upwards or downwards, so that at the tip it reaches $\beta_t = 0°$. This curve is recalculated every time a parameter from the input data is changed, so it is particular for each different blade. In Figure 5.9 and Figure 5.10 is shown an example of this distribution which results from $\kappa = 60°$, $\tau = 30°$, $L = 10$ m, $L_0 = 1$ m, $z = 3$, $t_t/t_0 = 0.49$, $\beta_S = 0°$, $\omega = 100$ rpm, among others.

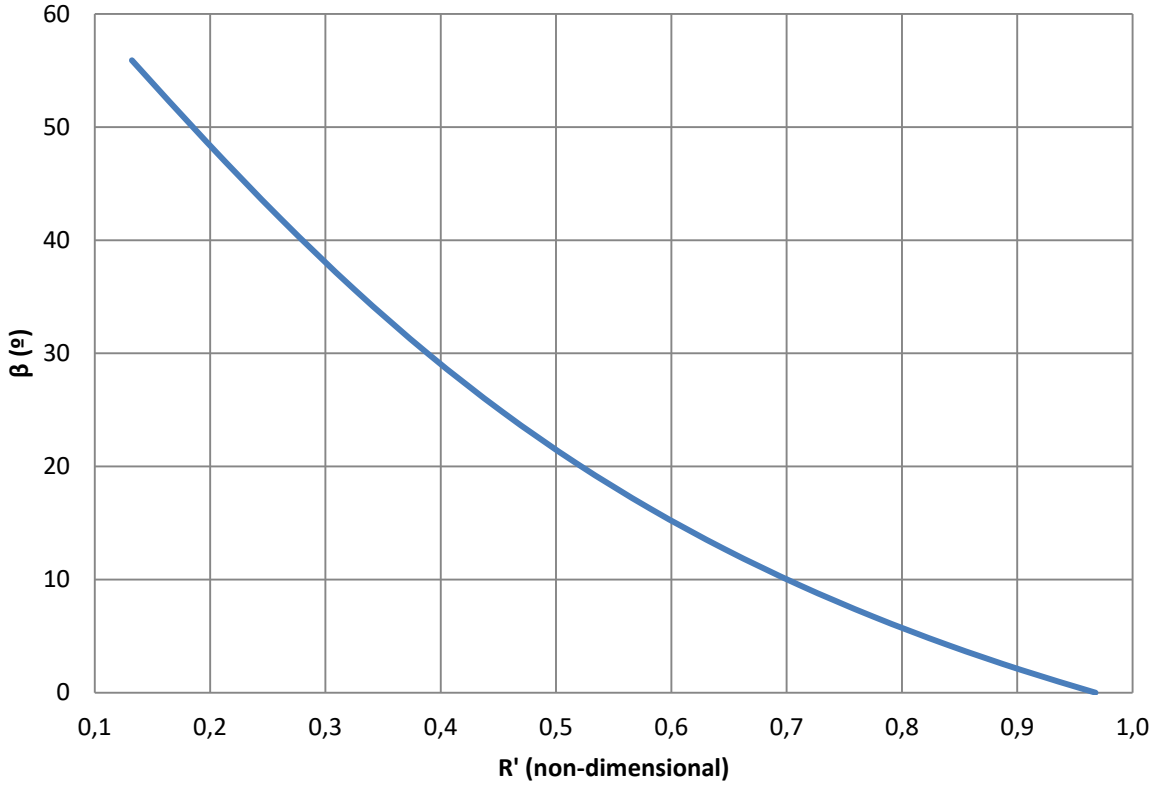

Figure 5.9 Twist angle base distribution correspnding to λ_t = 1 and θ_m = 10º (from Blade Element Momentum Spread Sheet)

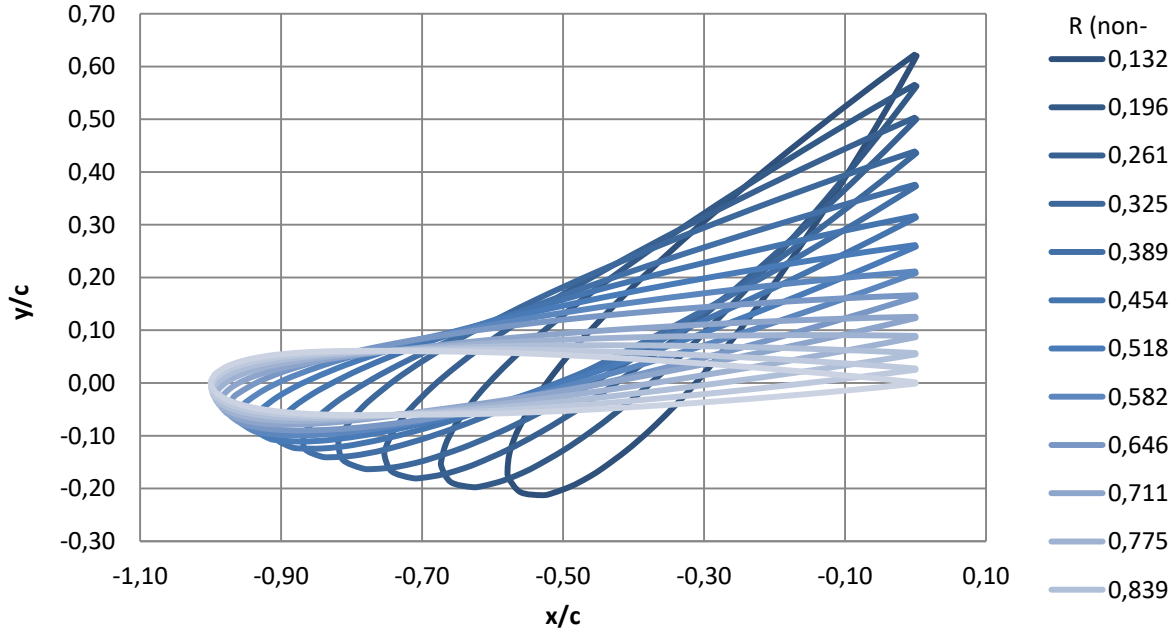

Figure 5.10 Airfoil twist angle base distribution correspnding to λ_t = 1 and θ_m = 10º (from Blade Element Momentum Spread Sheet)

In this thesis, this has been selected as an option for nonlinear twist angle distribution, due to that it gives good results and it can be considered as a compromise solution. However, the distribution can be changed as the user desires between all nonlinear resultant distributions for each combination of λ_t and θ_m.

5.4 Set of a Blade Pitch Angle

In order to introduce a pitch set angle within the rotor blades, the user can set this angle in the input data page. This angle will be added to the twist angle distribution for all blades, showing the results of introducing a positive or negative pitch angles. Figure 5.11 shows where the constant pitch angle is introduced in the Blade Element Momentum Spread Sheet.

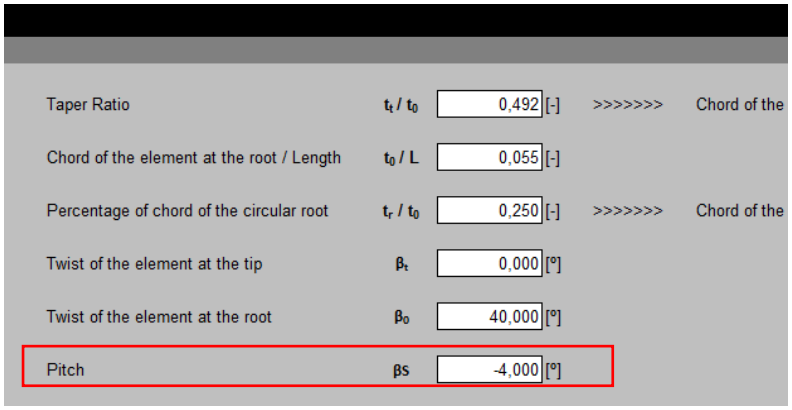

Figure 5.11 Introduction of a constant pitch set angle in the Blade Element Momentum Spread Sheet

On the other hand, it can be set another pitch operation. This option is based on what it was explained in 5.3.2 about twist angle distributions to reach the maximum glide ratio on every blade element. As it was explained, to finally achieve a constant nonlinear twist distribution, the base curve (in this case, the curve for $\lambda_t = 1$ and $\theta_m = 10º$) is offset in order that, at the tip, $\beta_t = 0°$ is obtained. What it is proposed in this thesis is that blades in each angular position can be pitched a variable quantity to bring closer the constant twist distribution curve to the variable twist distribution curve calculated in section 5.3.2. This pitch operation generates angles of attack of for maximum $\varepsilon = C_l/C_d$ on every element and in every angular position, so it minimises drag losses on the blades.

The value of this variable pitch angle is calculated for each angular position, θ_m, as the difference between the twist angle values at R' ≈ 0.8 of the distribution required for ε_{max} and the distribution selected as base ($\lambda_t = 1$ and $\theta_m = 10º$).

$$\beta_{S,variable}(\theta_m) = \beta_{\varepsilon_{max}}(R' = 0.8) - \beta_{base}(R' = 0.8) \qquad (5.12)$$

As the result of this, the different evolutions of β_S along the rotating plane for each λ_t are presented in Figure 5.12. It is important to remark that this curves have been obtained for $\kappa = 60°$, $\tau = 30°$, $L = 10$ m, $L_0 = 1$ m, $z = 3$, $t_t/t_0 = 0.49$, $\omega = 100$ rpm, among others, and they depend on the input data.

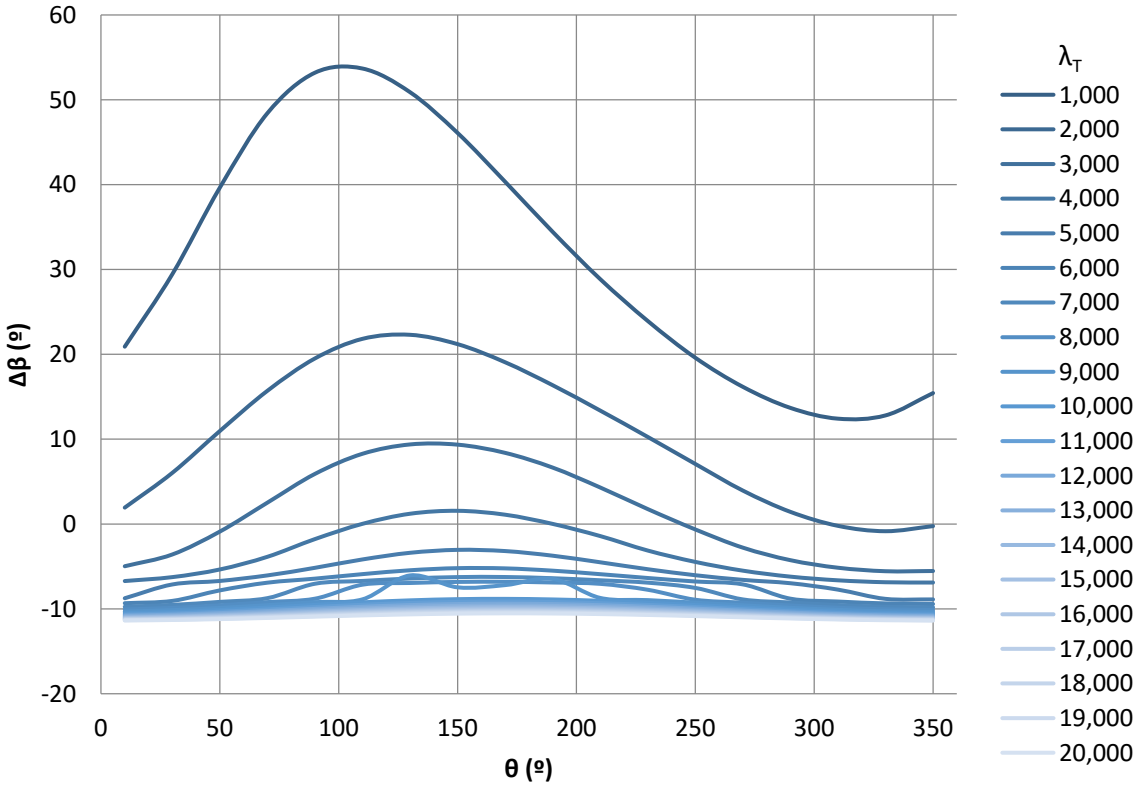

Figure 5.12 Variable pitch angle distributions for λ_t from 1 to 20 (from Blade Element Momentum Spread Sheet)

As it can be seen, for low tip speed ratios, the needed pitches are larger and more variable along the rotating plane than the ones needed for higher tip speed ratios.

6 Investigation of Generic $C_P - \lambda_t$ Curves

The previous chapters have shown the calculation basis and the procedure. Once this has been completely set, in the following sections they will be seen and described the obtained results taking into account different parameters.

6.1 $C_P - \lambda_t$ Curves

As it was explained, the main objective of a wind turbine is to withdraw power from the wind. Therefore, the principal parameter of a wind turbine rotor is the extracted power. This is represented through the power coefficient, C_P, or, so called, aerodynamic efficiency. An example of this type of curve is the one showed in Figure 3.7.

After expression (3.40), in Blade Element Spread Sheet they are obtained values of C_P for each tip speed ratio from 1 to 20. For example, a wind turbine with $\kappa = 60°$, $\tau = 60°$, $L = 10$ m, $L_0 = 1$ m, $z = 3$, $t_t/t_0 = 0.49$, $\beta_S = 0°$ etc. gives the curve in Figure 6.1.

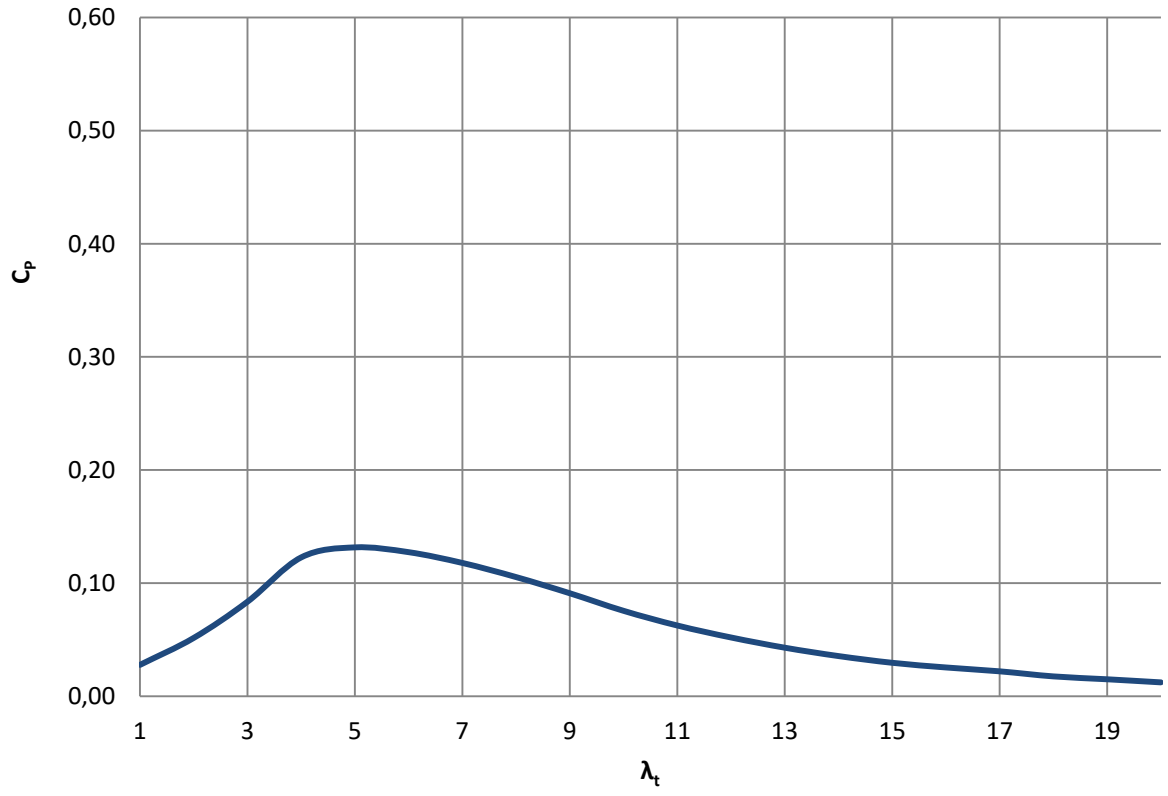

Figure 6.1 Example of power coefficient curve (from Blade Element Momentum Spread Sheet)

In what follows, it will be presented the effects of the several parameters on the $C_P - \lambda_t$ in order to compare the different operations of each wind turbine. To that point, they will be fixed several parameters, which set a "base" rotor:

Table 6.1 Fixed parameters for C_P calculation. Base rotor

Parameter	Name	Value	Units
κ	Cone Angle	85	[°]
τ	Axis Angle	0	[°]
L	Blade Length	10	[m]
L_0	Circular Root Length	1	[m]
z	Number of Blades	3	[-]
ω	Rotation Speed	100	[rpm]
t_t / t_0	Taper Ratio	0.5	[-]
t_0 / L	Chord at the Root With Respect to the Blade Length	0.06	[-]
β_S	Pitch Angle	0	[°]
Airfoil	No transition: NACA 0015	-	-

This base rotor will be the base to compare the following effects related to each parameter. This rotor gives the following power curve,

Figure **6.2** Power coefficient curve for the base wind turbine (from Blade Element Momentum Spread Sheet)

, and as it can be inferred from it, the maximum C_P is 0.222, obtained for $\lambda_t = 8$.

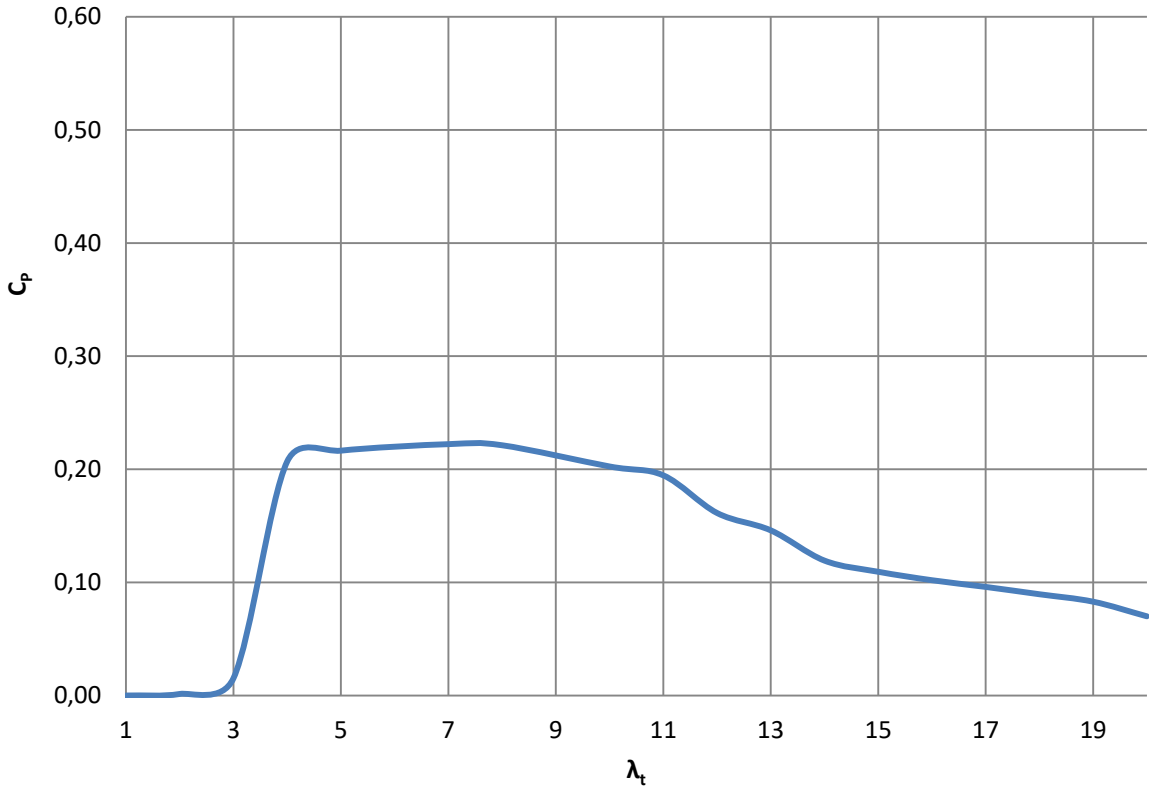

Figure 6.2 Power coefficient curve for the base wind turbine (from Blade Element Momentum Spread Sheet)

6.1.1 Axis Angle and Cone Angle

These angles were presented in section 2.2 as an application of the Wagner-Rotor on this thesis. In section 3.8 it was explained how those affect the aerodynamic performance, showing that its main contribution affects the derivation of the speed ratio, expression (3.49), and the effective rotor areas, expressions (5.2) and (5.4):

$$\lambda = \frac{(\lambda_t \frac{r}{R} - sin\tau \cdot sin\theta)\sqrt{\cot^2 \kappa + 1}}{cos\tau - sin\tau \cdot cot\kappa \cdot cos\theta} \qquad (3.49)$$

$$\Delta A = \frac{1}{2}\sqrt{cotg^2\kappa + 1} \cdot \left[(R' + \Delta R')^2 - R'^2\right] \cdot \Delta\theta \qquad (5.2)$$

$$A = \sqrt{cotg^2\kappa + 1} \cdot \pi \qquad (5.4)$$

To compare with the base rotor, the axis angle is fixed in $\tau = 0°$ while the cone angle variates from 85° to 0°. In Figure 6.3 they are shown the different resultant curves. It can be observed

that this variation influences the power curve by setting it closer to the origin (the maximum C_P appears for lower tip speed ratios) when the cone angle decreases.

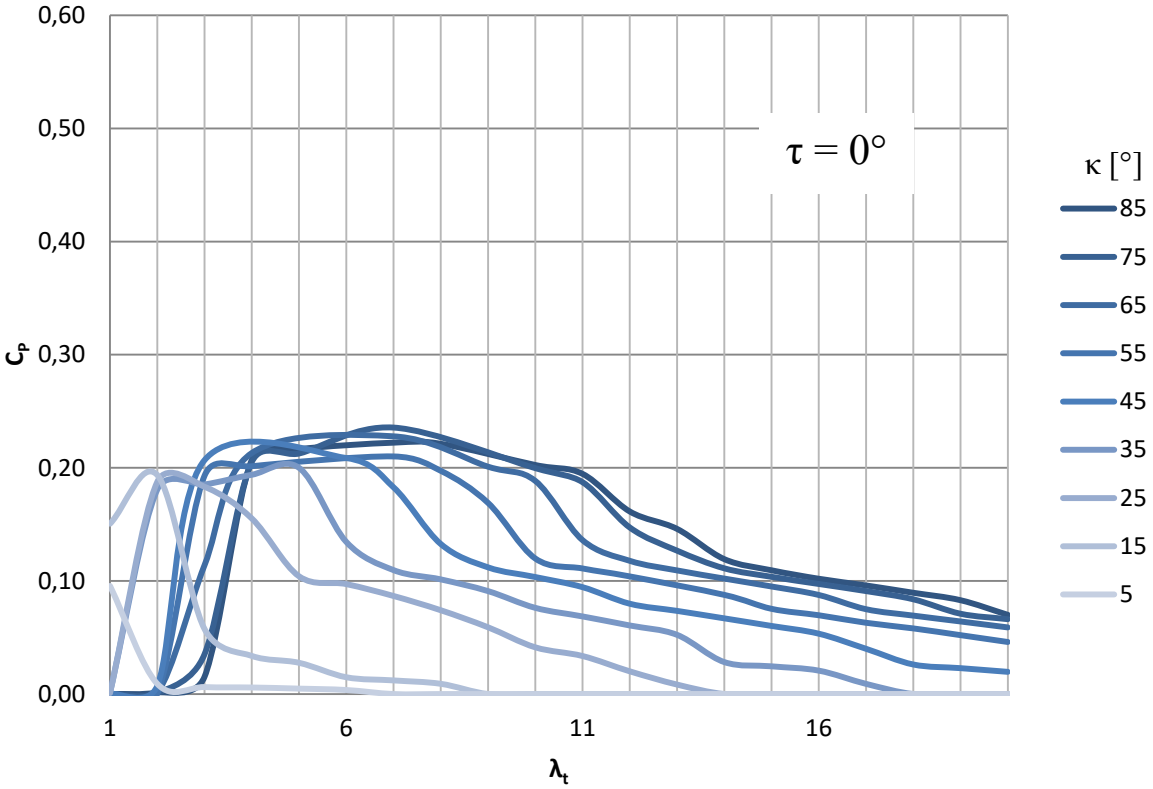

Figure 6.3 Power coefficient curves for τ = 0° and κ between 85° and 5° (from Blade Element Momentum Spread Sheet)

On the other hand, when fixing the cone angle as κ = 85° and variating the axis angle between 0° and 85°, results Figure 6.4. The effect of incrementing the axis angle is to reduce the curve maximum, as well as setting it for lower speed ratios.

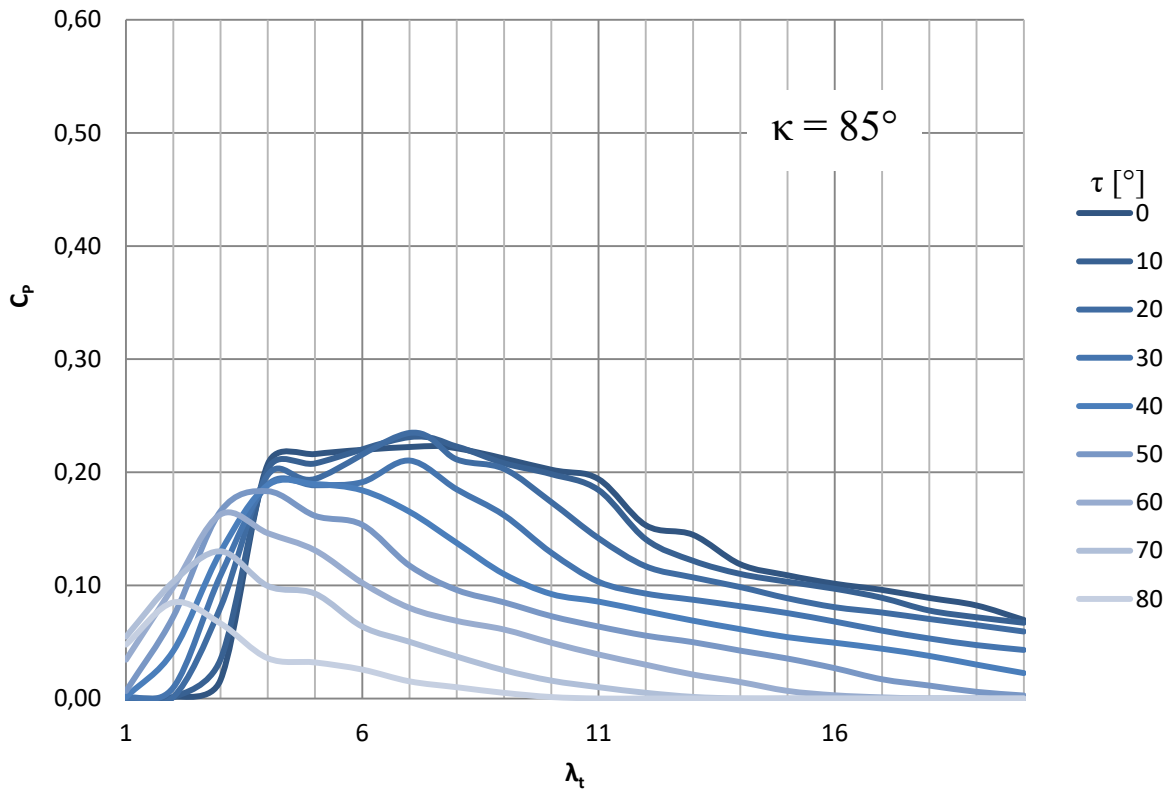

Figure 6.4 Power coefficient curves for κ = 85° and τ between 0° and 80° (from Blade Element Momentum Spread Sheet)

Finally, combining the variation of both angles, they are obtained, for example, curves as shown in Figure 6.5. There are several conclusions to remark; on the one hand, it can be observed that the curve with higher power coefficients is the one of the base rotor, and, on the other hand, the lower κ is, the more abrupt the curve is (less round), and the lower τ is, a bigger maximum is obtained.

Therefore, it can be demonstrated that the most effective rotor is the base rotor, with a high cone angle and a low axis angle.

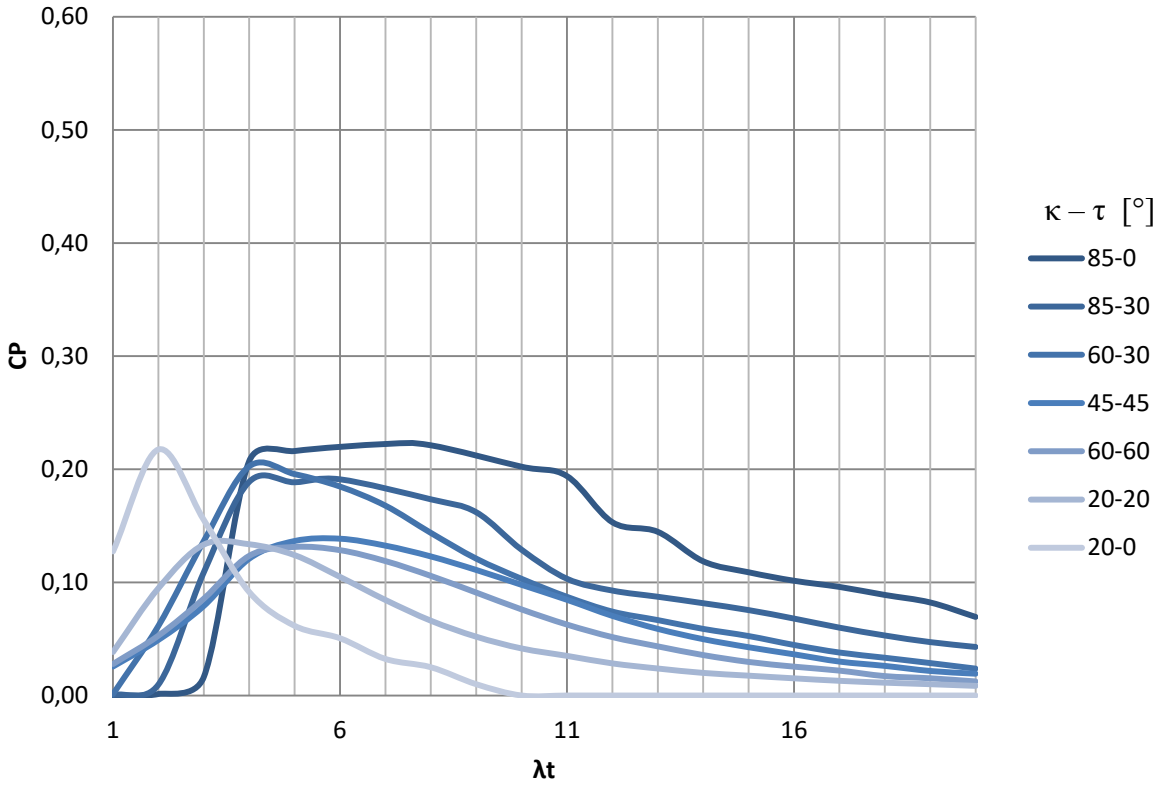

Figure 6.5 Power coefficient curves for different values of κ and τ (from Blade Element Momentum Spread Sheet)

6.1.2 Blade Pitch Angle

Blade pitch angle settings affect the design pitch angles for each element, and therefore, their angles of attack. As explained in 4.3, positive pitch angle settings increase the design pitch angle and so decrease the angle of attack. Negative pitch angle settings increase the angle of attack.

In order to visualize this effect, (6.1) shows how the introduction of a pitch angle setting acts within the Blade Element Momentum Spread Sheet.

$$\alpha = \operatorname{atan}\frac{1}{\lambda_0} - (\beta + \beta_S) \qquad (6.1)$$

As it was mentioned in 4.3, blades can be pitched to stall or to feather. Subsequently, in Figure 6.6 and Figure 6.7 they are shown different curves for several pitch angles with typical values of stall-operated wind turbines. It can be seen that positive pitch angle settings reduce the overall power output and negative ones increase it.

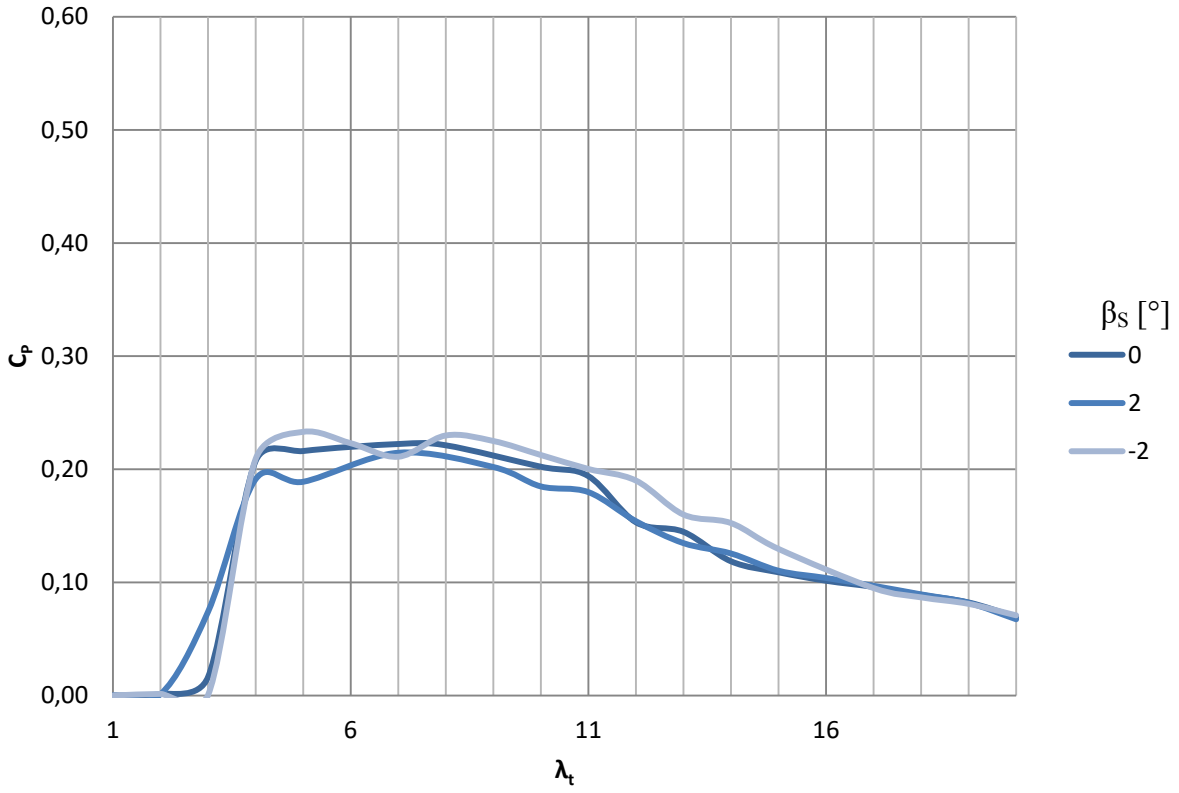

Figure 6.6 Comparison of power coefficient curves between the base rotor and pitch angle settings of 2° and -2° (from Blade Element Momentum Spread Sheet)

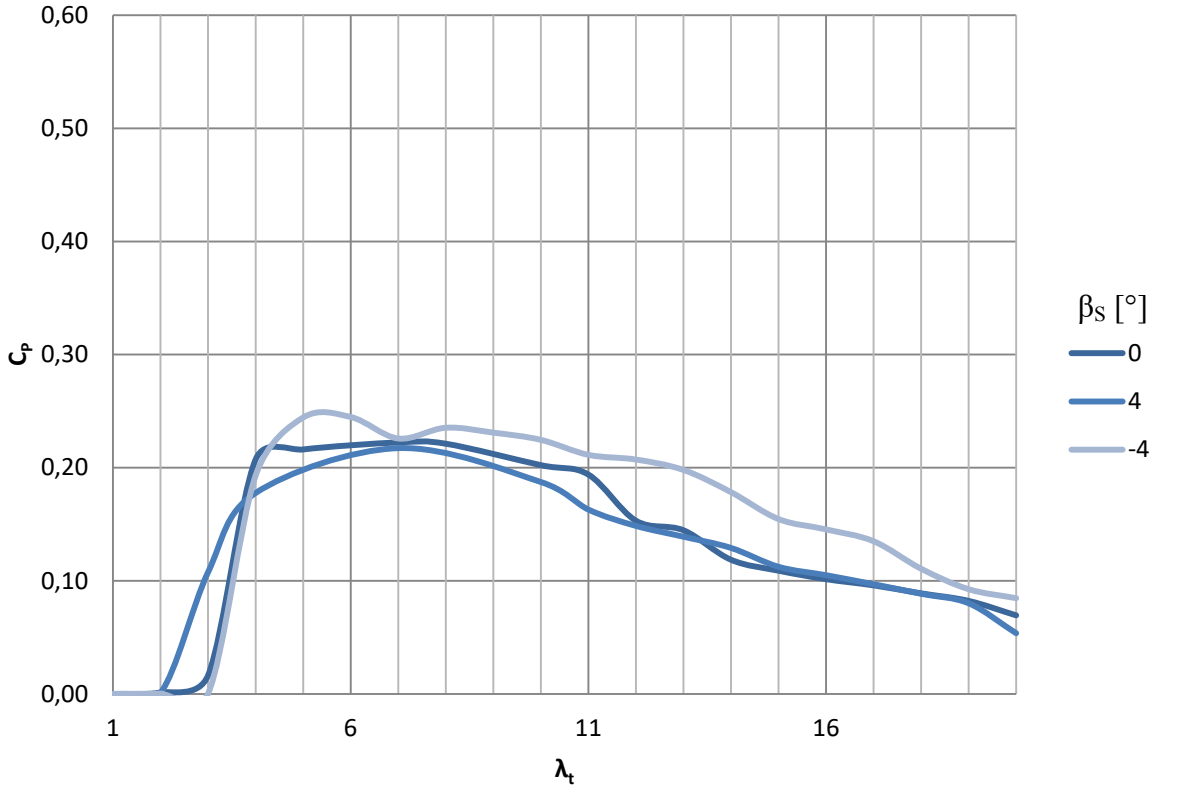

Figure 6.7 Comparison of power coefficient curves between the base rotor and pitch angle settings of 4° and -4° (from Blade Element Momentum Spread Sheet)

6.1.3 Number of Blades

The number of blades is an important parameter in a rotor design. This parameter affects directly the efficiency of the wind turbine as it was explained in 2.1.3.2. The more blades, the higher the efficiency is, expression (2.22).

$$\eta_z = \left[1 - \frac{1{,}39}{z}\frac{1}{\sqrt{1+\lambda_t^2}}\right]^2 \qquad (2.22)$$

However, this parameter is dependent on the manufacturing cost, so they are installed a number of blades reaching a compromise between efficiency and cost.

To show the influence of the number of blades in the power coefficient, it is presented Figure 6.8 with some curves of efficiency of the rotor performance, η_z, corresponding to different blade numbers, from 1 to 6. As this parameter is proportional to the power coefficient, it can be presented separately.

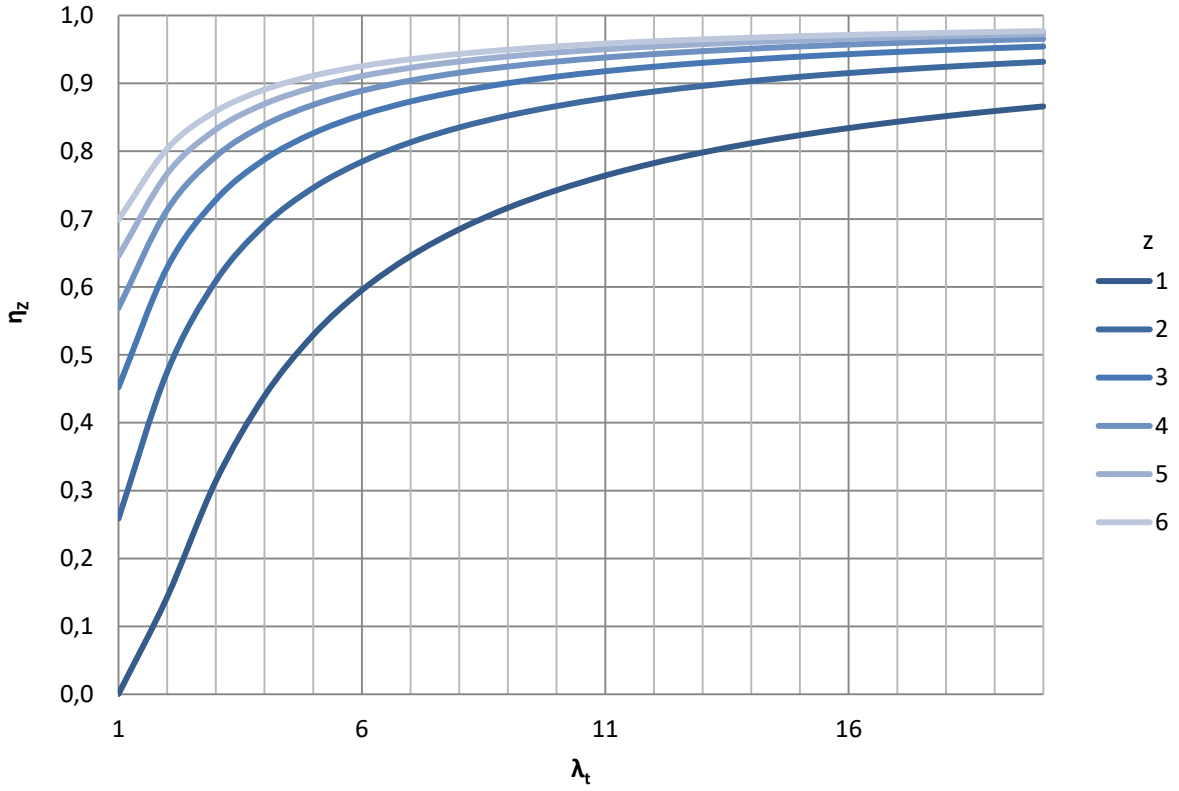

Figure 6.8 Efficiency of the rotor performance for different number of blades (from Blade Element Momentum Spread Sheet)

As it can be seen, the lowest efficiency is given for one blade and it increases for the same tip speed ratio when introducing more blades in the rotor. Ideally, $\eta_z = 1$ would be obtained for an infinite number of blades.

6.1.4 Blade Taper Ratio

The taper ratio, t_0/t_t, has also a great influence in the aerodynamic efficiency. This parameter plays in the calculation of the axial reduction factor, ξ, through the chord distribution, t, as expression (5.5) shows,

$$\frac{1+\xi}{1-\xi} = \frac{8\pi r}{C_l \cdot z \cdot t} \cdot \frac{1}{\lambda_0^2} \cdot \frac{1}{\sqrt{1 + {}^{1}/_{\lambda_0^2}}} = B \qquad \begin{matrix} (\ 5.5\ ) \\ (\ 2.22\ ) \end{matrix}$$

Where, setting a lineal chord distribution, t can be expressed as it was shown in expression (3.38)

$$\frac{t}{R} = \frac{t_0 - t_t}{R} \frac{(1 - R'_m)}{(\ 1\ -\ R'_0\ )} + \frac{t_t}{R} \qquad (\ 3.38\ )$$

This can be simplified with some of the previously explained parameters: change of chord along the blade, U, and chord at the tip with respect to the effective radius, t'_t

$$t = U\ (1\ -\ R'_m)\ +\ t'_t \qquad \begin{matrix} (\ 6.2\ ) \\ (\ 2.22\ ) \end{matrix}$$

Thus, given a chord at the root with respect to the blade length, t_0/L and a blade length, the taper ratio will influence U and t'_t as

$$U = \frac{t_t}{t_0} \cdot \frac{t_0}{L} \cdot L \cdot \frac{(t_0/t_t - 1)}{R(1 - R_t)}$$

$$t'_t = \frac{\frac{t_t}{t_0} \cdot \frac{t_0}{L} \cdot L}{R}$$

Therefore, the bigger the taper ratio is, the higher B will be.

Some examples of the final result on C_P are the curves represented in Figure 6.9. It can be seen that when the taper ratio reduces, the curves distance from the origin. Their maximums remain the approximately the same but the rotor generates less power for low tip speed ratios.

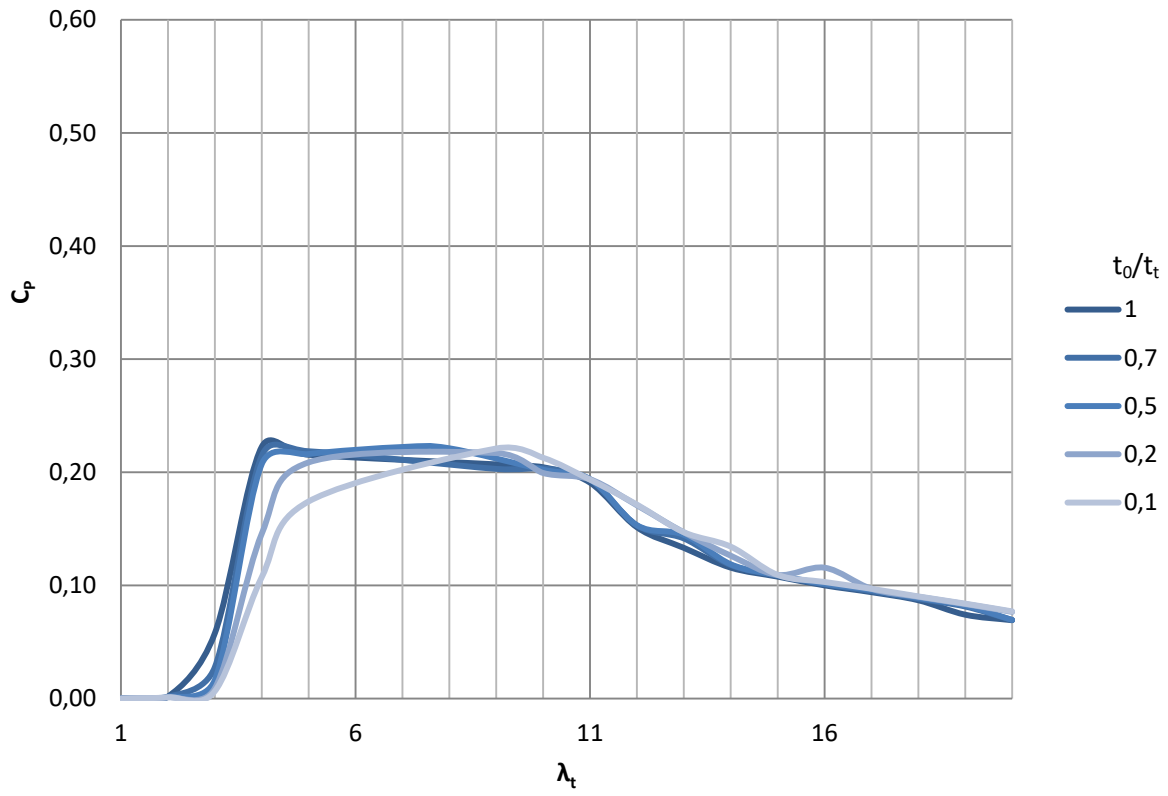

Figure 6.9 Power coefficient curves for different values of taper ratio (from Blade Element Momentum Spread Sheet)

6.2 $C_P - V_w$ Curves

It is important to know how the performance of the rotor is when some other parameters are fixed. In that case, it is relevant to have an idea of how the wind turbine extracts power for each wind speed, which is the main variable within the design of a rotor, giving the power curve $C_P - V_w$.

To this objective, it will be fixed the speed rotation in order to know which speed is the ideal one for each rotor for given conditions. Then, once the rotation speed is set, it will be shown the influence of different pitch angle settings, so the user can have an idea of the preliminary design of the analysed rotor.

6.2.1 Rotation Speed

For this analysis they are going to be taken three different rotor configurations based on the base rotor but variating their installation angles. The first one is the initial base rotor: $\kappa = 85°$ and $\tau = 0°$, the second one the base rotor with $\kappa = 60°$ and $\tau = 30°$, and the third one the base rotor with $\kappa = 45°$ and $\tau = 45°$. In Figure 6.10 they are shown the power curves ($C_P - V_w$) of these three rotors and for a rotation speed of $\omega = 100$rpm.

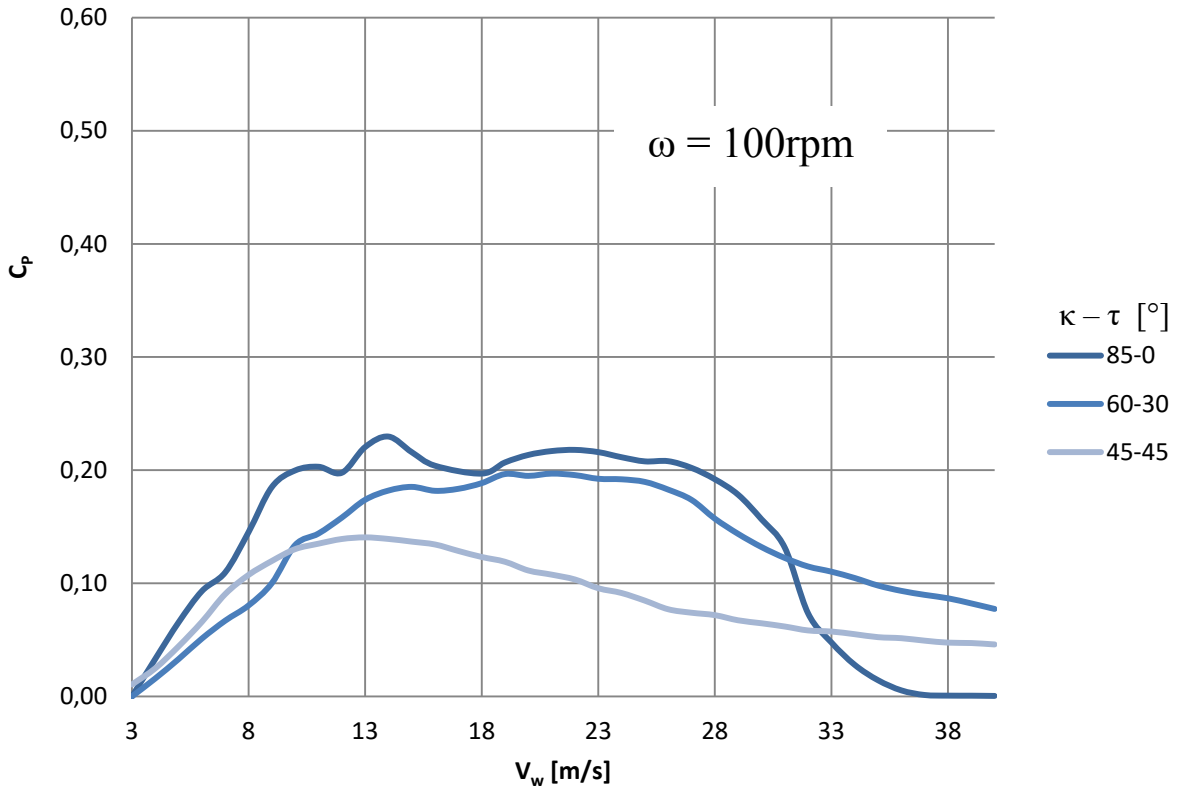

Figure 6.10 Power curves for the three different rotor configurations and rotation speed ω = 100 rpm (from Blade Element Momentum Spread Sheet)

It can be noticed that the base rotor results in a more abrupt curve compared to the other two configurations, having that, for high wind speeds, power falls quickly. Moreover, with the same conditions, the base rotor ($\kappa = 85°$, $\tau = 0°$) extracts more power at every wind speed, although it is ineffective for higher speeds. However, when reducing the cone angle and incrementing the axis angle, the rotor can operate for higher speeds, extracting power from it.

In order to show the effect of the rotation speed, in Figure 6.11, Figure 6.12 and Figure 6.13 they are represented some power curves variating this speed.

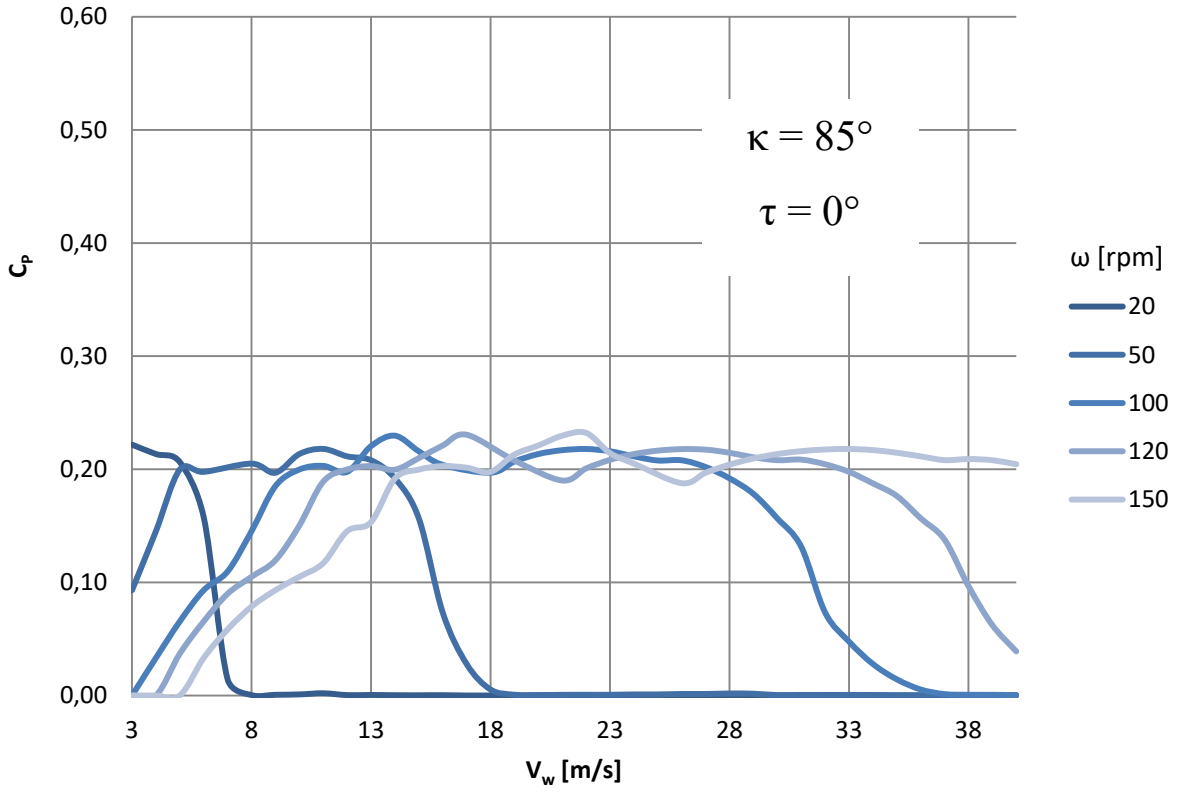

Figure 6.11 Power curves for the base rotor regarding different rotation speeds (from Blade Element Momentum Spread Sheet)

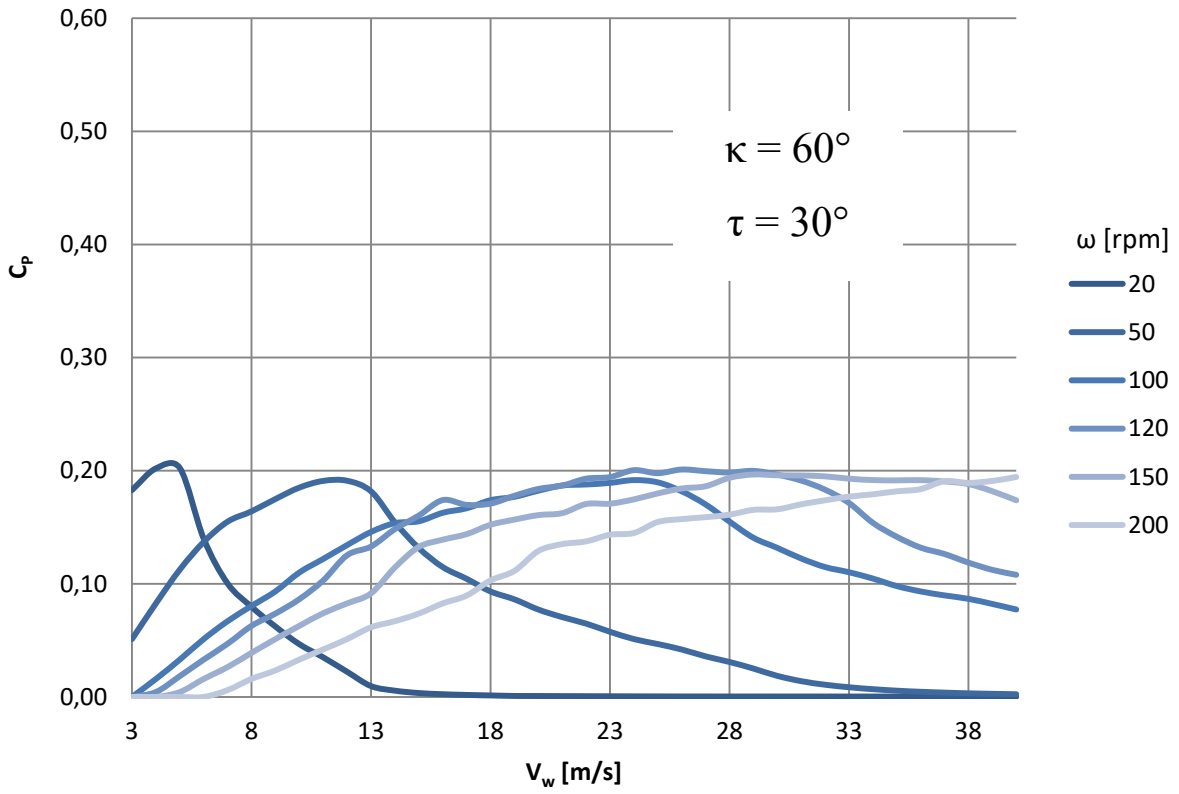

Figure 6.12 Power curves for the base rotor with κ = 60° and τ = 30° regarding different rotation speeds (from Blade Element Momentum Spread Sheet)

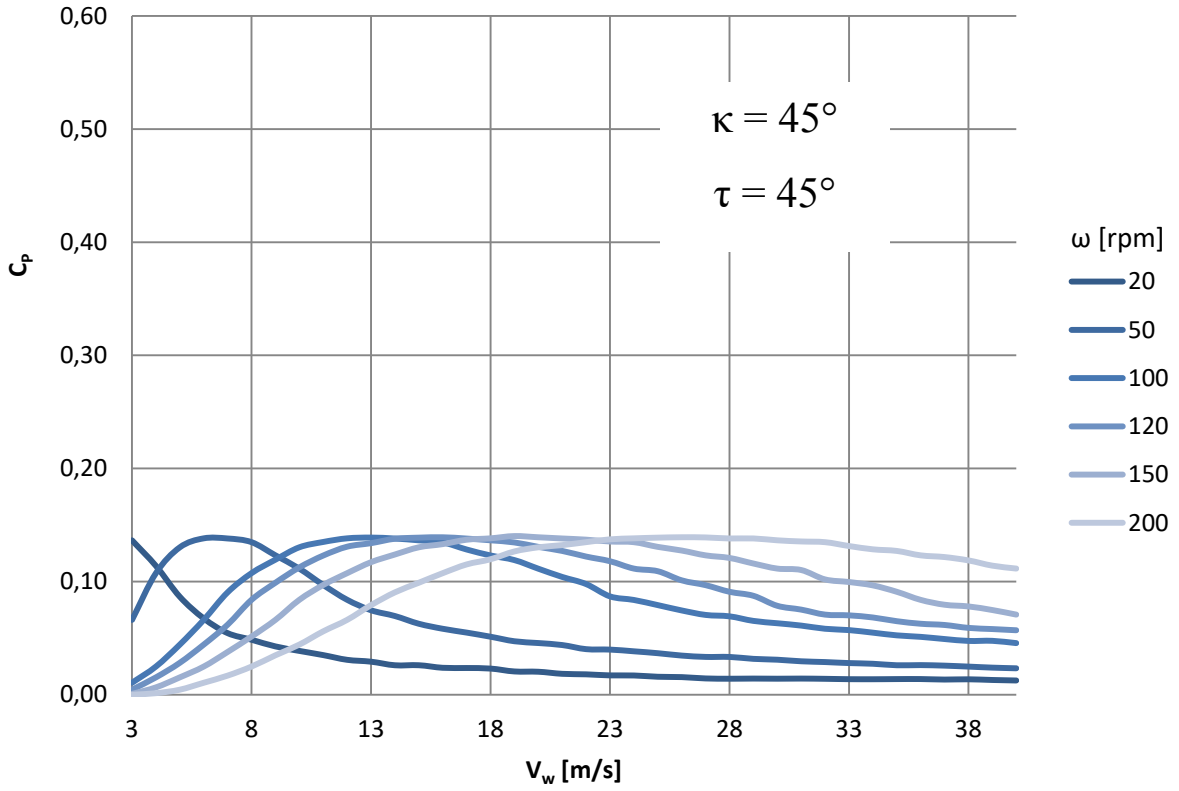

Figure 6.13 Power curves for the base rotor with κ = 45° and τ =45° regarding different rotation speeds (from Blade Element Momentum Spread Sheet)

Regarding the previous curves, the introduction of installation angles helps the rotor to operate with higher wind speeds but limits the maximum power. However, by incrementing the rotation speed, the rotor can be operated in faster winds. Therefore, in order to set a rotor speed it is necessary to study the wind profile that will subject the wind turbine.

6.2.2 Pitch Angle Setting

Below it is presented how the pitch angle affects the power curve of a given rotor. In this case, they will be also taken the three different rotors described before. The rotation speed will be set again as 100 rpm.

In Figure 6.14, Figure 6.15 and Figure 6.16 they are represented power curves for each of the three rotors variating their pitch configuration. It can be noticed in all rotors that when the pitch is incremented, they generate less power for the same wind speed, confirming the effect of pitching for power limitation.

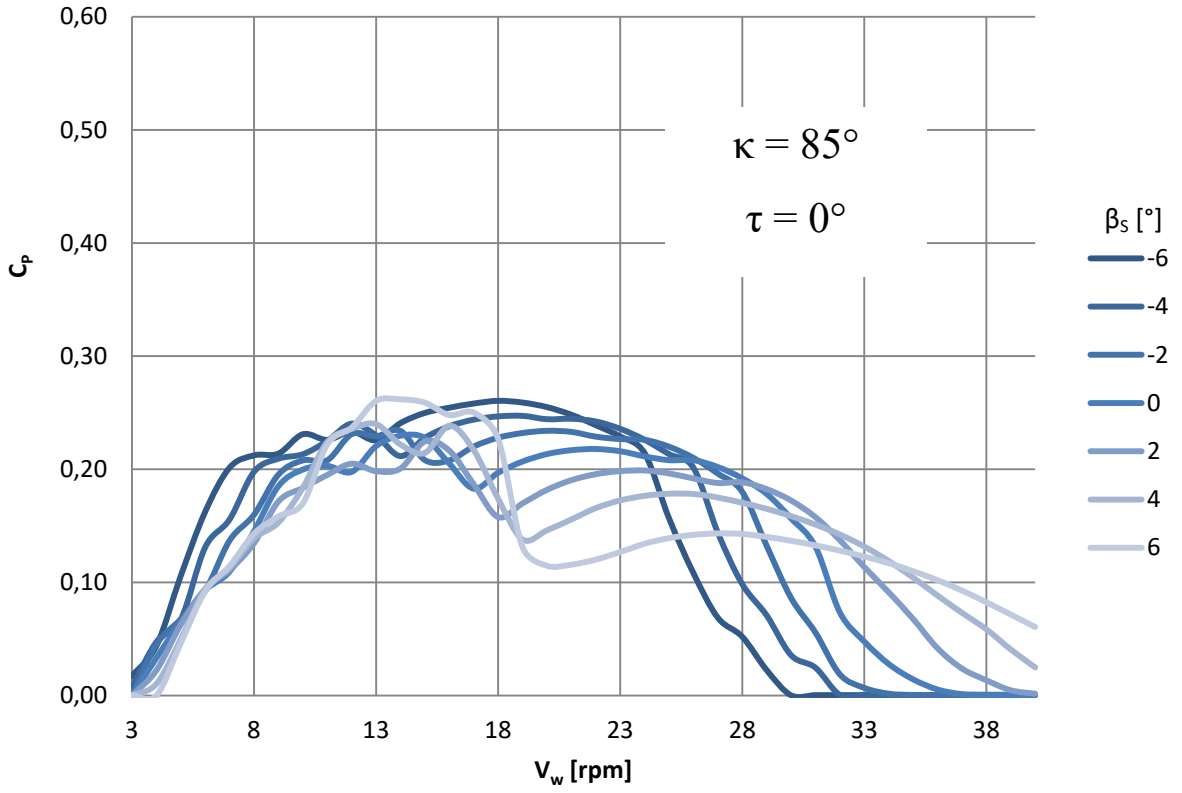

Figure 6.14 Power curves for the base rotor regarding different pitch angle settings (from Blade Element Momentum Spread Sheet)

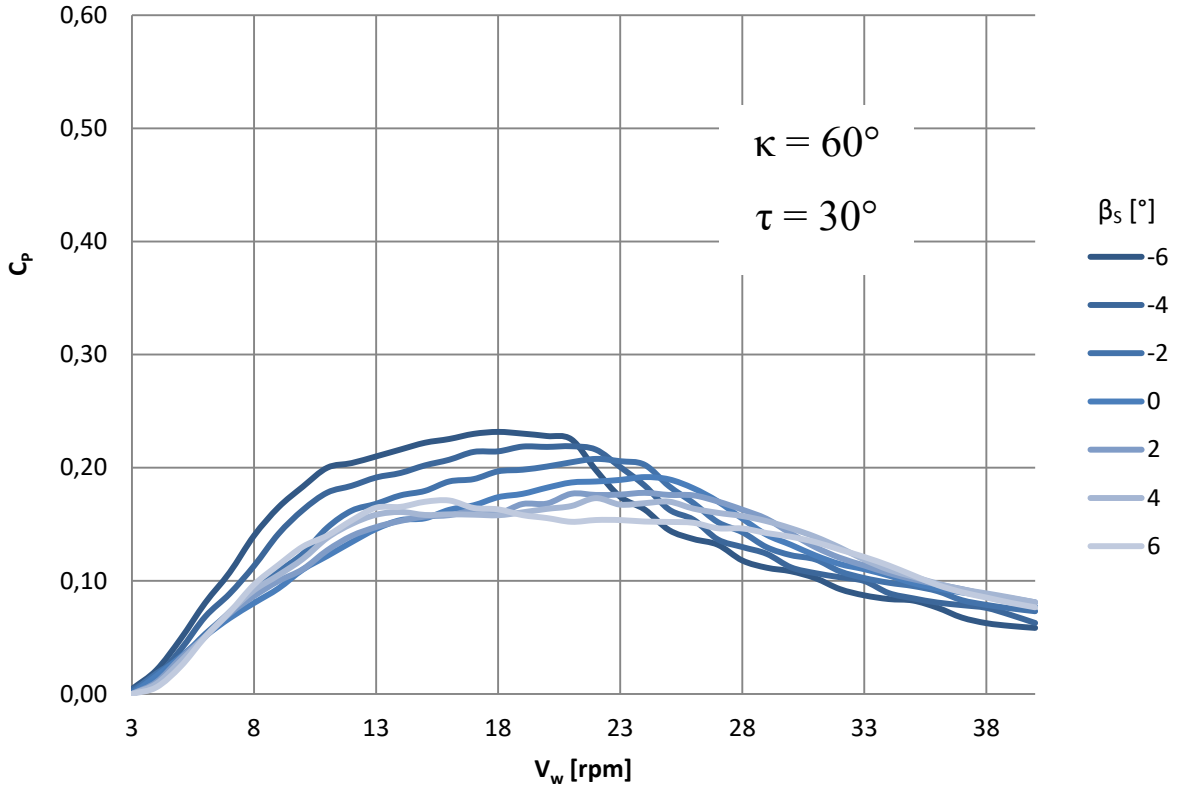

Figure 6.15 Power curves for the base rotor with κ = 60° and τ = 30° regarding different pitch angle settings (from Blade Element Momentum Spread Sheet)

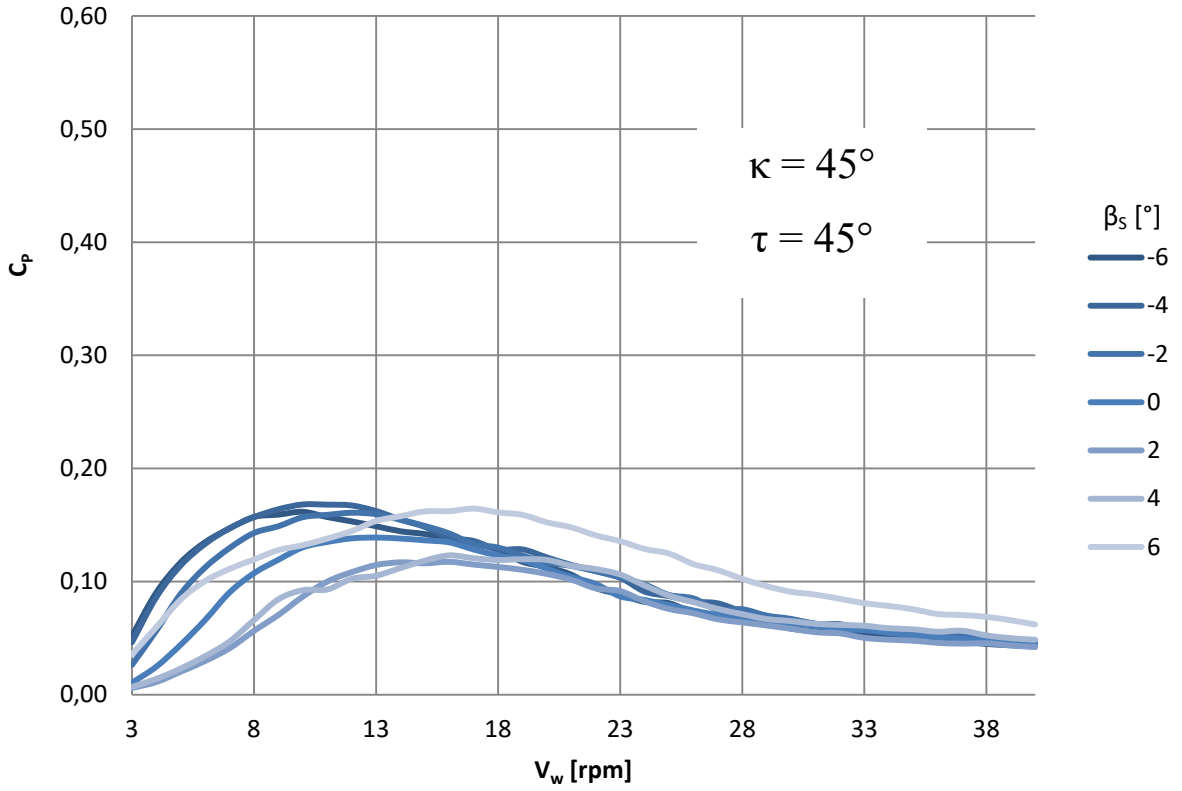

Figure 6.16 Power curves for the base rotor with κ = 45° and τ = 45° regarding different pitch angle settings (from Blade Element Momentum Spread Sheet)

There is another conclusion to obtain after these curves. As shown in Figure 6.16, when pitch increases, the extracted power reduces for the same wind speed. However after β_S = 2°, the power curve gives higher C_P.

This effect is related to the cone angle; when this angle has a high value, pitch angle settings return negative angles of attack, which, having symmetric airfoils, give again higher power coefficients. However, the extracted power will be obtained in the opposite direction.

7 Optimization

It has already been set the basic preliminary design guideline to take into account. The user could analyse a given rotor with them, variating different parameters and observing their effects. However, it is interesting to have an idea of how this rotor could be optimized under some conditions.

There are multiple options and criterion to take into account when optimizing a rotor. For example, the rotor can be optimized in order to obtain the highest maximum possible, or to obtain the highest C_P for a given wind speed. Nevertheless, these criterions work only for one wind speed, when a real rotor is subjected to a range of winds.

For that reason, the criterion that has been followed in this thesis and in Blade Element Momentum Spread Sheet is to optimize a given rotor so that the whole $C_P - \lambda_t$ curve returns the highest power values. This means that the area of the curve has to be the maximum for some given conditions.

They are going to be used two parameters to optimize the curve, although they can be used other ones, depending on the users requirements. In this thesis they will be used the taper ratio, t_0/t_t, and the number of blades, z.

7.1 Optimum Taper

To observe how the taper ratio can optimize a given rotor, they are going to be compared the three rotors presented in chapter 6:

- base rotor: $\kappa = 85°$ and $\tau = 0°$,
- base rotor with $\kappa = 60°$ and $\tau = 30°$,
- base rotor with $\kappa = 45°$ and $\tau = 45°$.

To optimize with respect to the taper ratio, the two imposed conditions are that it must lie between 0 and 1,

$$0 \leq t_0/t_t \leq 1 \qquad (7.1)$$

Figure 7.1 shows the initial $C_P - \lambda_t$ base rotor curves for $t_0/t_t = 0.3$ and the same curve optimized with the taper ratio, as well as in Table 7.1 it is presented their respective curve area and power coefficient values.

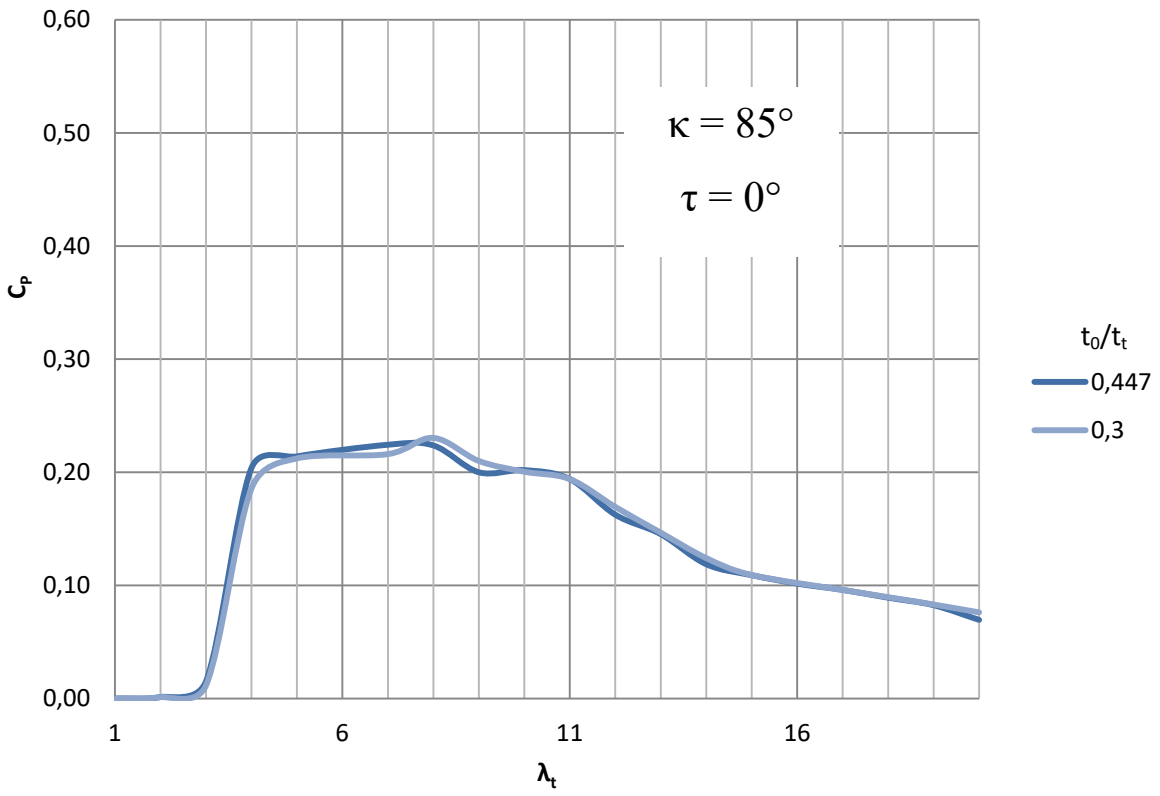

Figure 7.1 Power coefficient curves for the base rotor with t_0/t_t = 0.3 and with an optimum taper ratio (from Blade Element Momentum Spread Sheet)

Table 7.1 Area and C_{Pmax} for t_0/t_t = 0.3 and $(t_0/t_t)_{max}$

Taper Ratio	$t_0 / t_t = 0.3$	$(t_0 / t_t)_{max} = 0.447$
Area	2.607	2.619
C_{Pmax}	0.230	0.224

In Figure 7.2 they are shown aerodynamic efficiency curves for the second analysed rotor: κ = 60° and τ = 30. There is shown the comparison between the curve for t_0/t_t = 0.3 and the optimized curve. In Table 7.2 they are shown the maximum values of each of these curves.

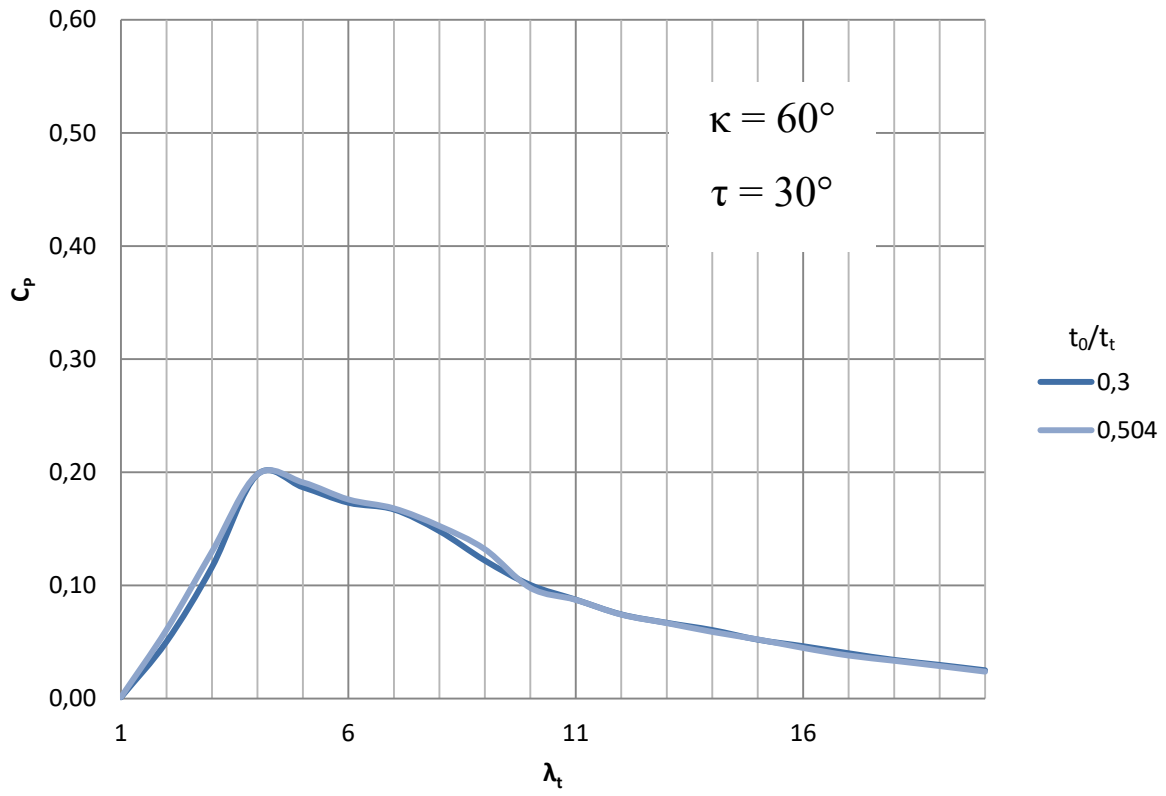

Figure 7.2 Power coefficient curves for κ = 60° and τ = 30° with t_0/t_t = 0.3 and with an optimum taper ratio (from Blade Element Momentum Spread Sheet)

Table 7.2 Area and C_{Pmax} for t_0/t_t = 0.3 and $(t_0/t_t)_{max}$

Taper Ratio	$t_0 / t_t = 0.3$	$(t_0 / t_t)_{max} = 0.504$
Area	1.770	1.799
C_{Pmax}	0.198	0.198

Finally, the optimization for the third rotor, κ = 45° and τ = 45°, is presented in Figure 7.3 and Table 7.3. It can be inferred from these charts that the optimization regarding the taper ratio has not a big influence on the established rotors, in order that the curve areas are practically the same.

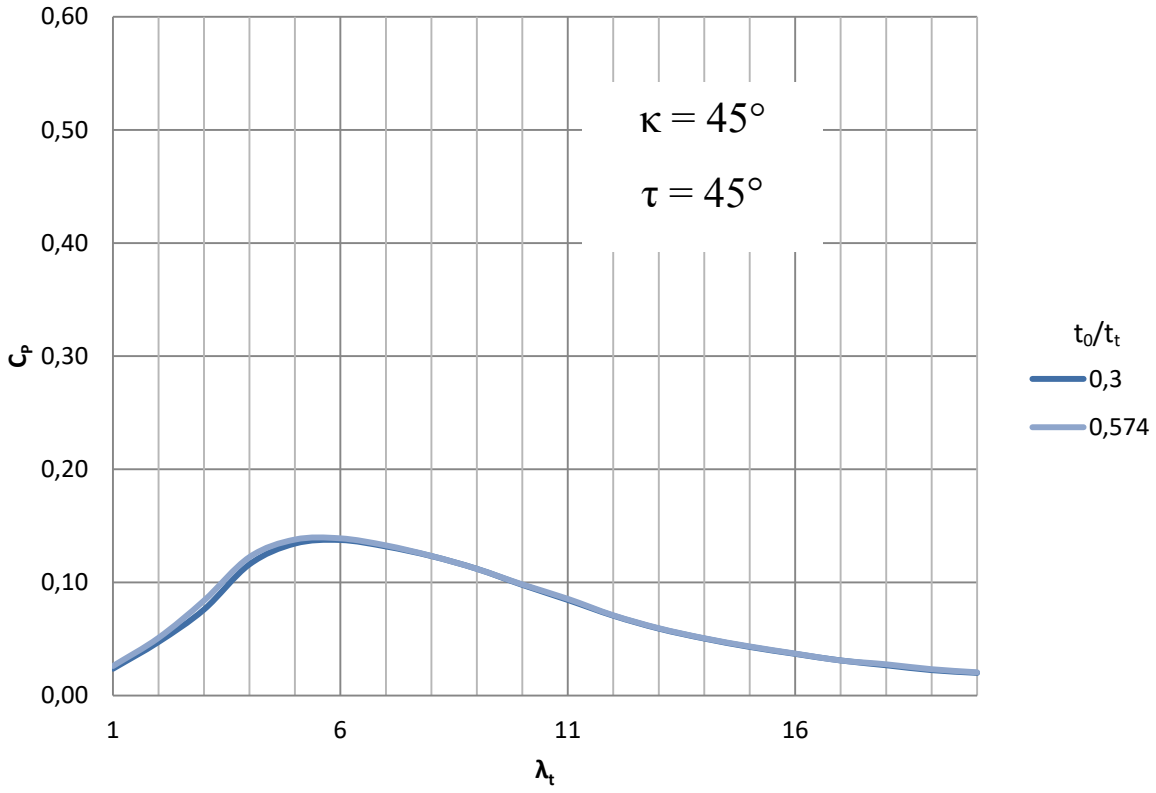

Figure 7.3 Power coefficient curves for κ = 45° and τ = 45° with t_0/t_t = 0.3 and with an optimum taper ratio (from Blade Element Momentum Spread Sheet)

Table 7.3 Area and C_{Pmax} for t_0/t_t = 0.3 and $(t_0/t_t)_{max}$

Taper Ratio	$t_0 / t_t = 0.3$	$(t_0 / t_t)_{max} = 0.511$
Area	1.450	1.473
C_{Pmax}	0.138	0.139

7.2 Optimum Number of Blades

The optimization with the number of blades is going t be applied on the same three rotors. To carry it out, its main condition is that the number of blades must be lower than ten and higher than 1.

$$0 \leq z \leq 10 \qquad (7.2)$$

The upper limit of this condition should be analysed regarding cost aspects, so it can be known how economically viable is to install a great number of blades.

The base rotor is optimized with the number of blades obtaining the curves in Figure 7.4. Their maximum values are shown in Table 7.4. Results of the optimization on the other two rotors are represented in Figure 7.5, Figure 7.6, Table 7.5 and Table 7.6.

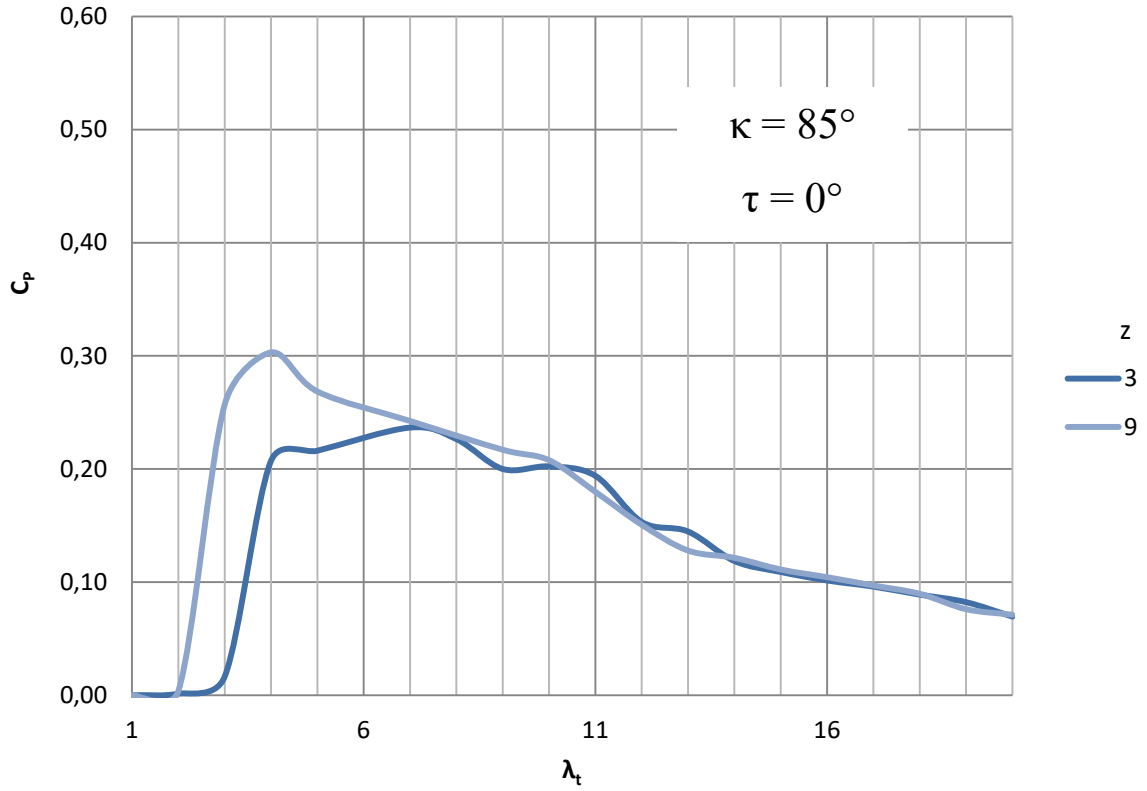

Figure 7.4 Power coefficient curves for the base rotor with z = 3 and with an optimum number of blades (from Blade Element Momentum Spread Sheet)

Table 7.4 Area and C_{Pmax} for z = 3 and z_{max}

Number of blades	z = 3	z_{max} = 9
Area	2.612	3.103
C_{Pmax}	0.237	0.303

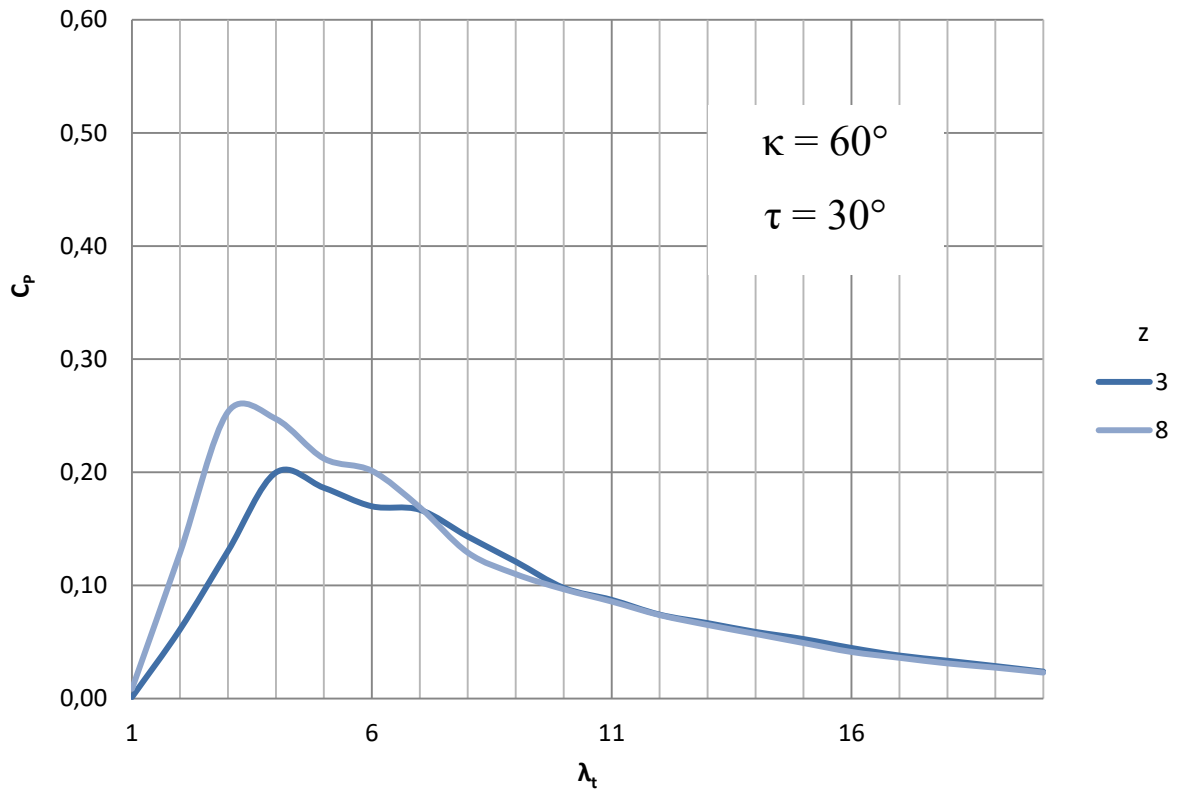

Figure 7.5 Power coefficient curves for κ = 60° and τ = 30° with z = 3 and with an optimum number of blades (from Blade Element Momentum Spread Sheet)

Table 7.5 Area and C_{Pmax} for z = 3 and z_{max}

Number of blades	z = 3	z_{max} = 8
Area	1.800	2.040
C_{Pmax}	0.202	0.253

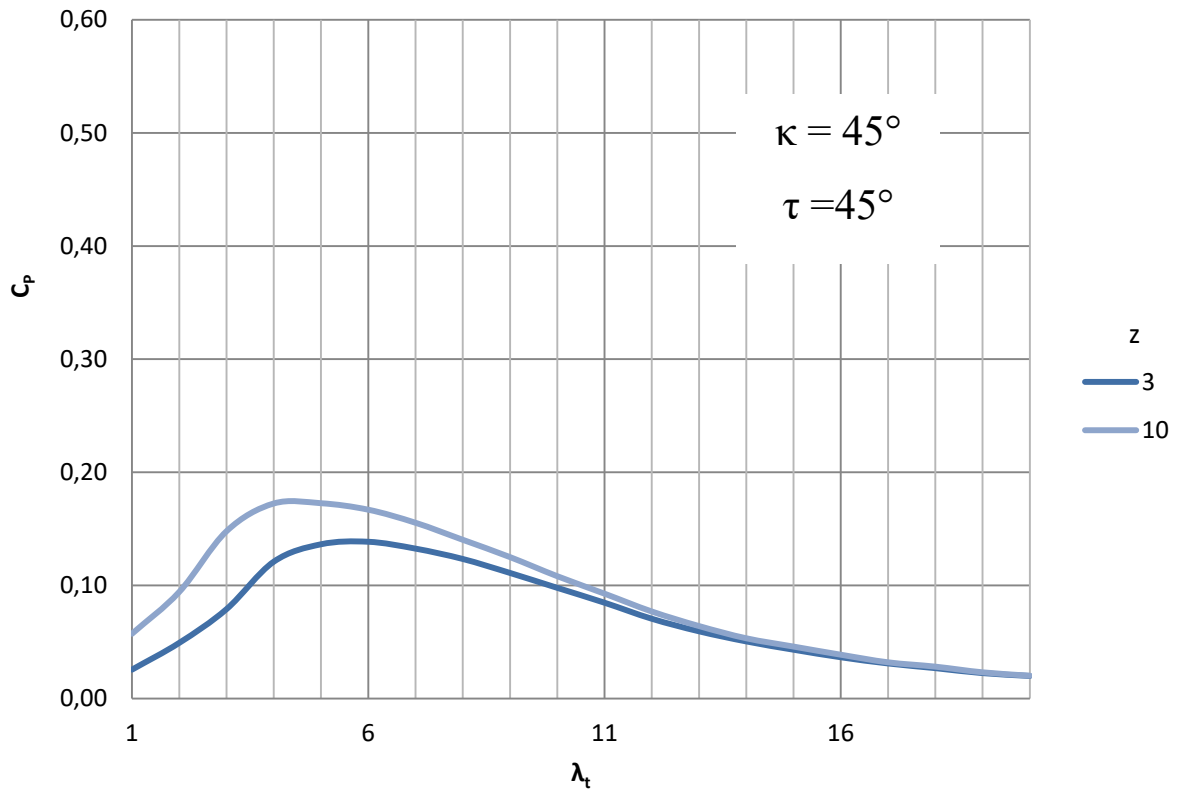

Figure 7.6 Power coefficient curves for κ = 45° and τ = 45° with z = 3 and with an optimum number of blades (from Blade Element Momentum Spread Sheet)

Table 7.6 Area and C_{Pmax} for z = 3 and z_{max}

Number of blades	z = 3	z_{max} = 10
Area	1.800	2.040
C_{Pmax}	0.202	0.253

As it can be observed, optimizing with respect to number of blades has a greater influence on the analysed rotors. It is important to remark that all three optimizations return values of z around 9, confirming that, the higher the number of blades is, the more effective the rotor will be, as it was explained in 6.1.3.

8 Summary

This thesis covers the preliminary design of a wind turbine rotor, being the aerodynamic efficiency the scope of it.

It has been shown different tools that help rotor design, although these do not fulfil the whole requirements of this work. Therefore, it has been developed a new design tool: Blade Element Momentum Spread Sheet. This program has been implemented in Excel based on the one developed in Fortran 95 by **Lindemann 1985**.

For the rotor analysis, it has been introduced an additional geometrical configuration based on the Wagner-Rotor (**Wagner**). They appear two installation angles: the cone angle, κ, and the axis angle, τ, which will influence strongly the wind turbine performance.

The Blade Element Momentum Theory has been the basis for all wind turbine calculations since its first development by Glauert (**Glauert 1935**). The theory is based on dividing a rotor blade into several elements, being those the units for the calculations, called Blade Elements. All the aerodynamic equations are applied on each element, taking into account its position on the blade to know its relative speed. The influences of all elements are summed for all blades within the rotor, obtaining the final non-dimensional power output.

They have been stablished the two different operations of wind turbines: fixed-speed and variable-speed wind turbines. These configurations determine the design from its beginning, so it is important to set how the wind turbine will work. In the fixed-speed performance, blades are pitched negatively, so when a rated wind speed is reached, blades enter into stall. In variable-speed wind turbines, when wind speed increments and a rated power output is reached, blades are pitched positively, so that the power is limited and reduced for growing wind speeds.

With Blade Element Momentum Spread Sheet they can be compared different rotor configurations. The user introduces its requirements, as geometrical parameters or rotation speed, and obtains the wind turbine power curves: $C_P - \lambda_t$ and C_P - V_w. These curves give information about the power output of the turbine and allow the user to observe the influence of the different parameters in order to obtain the desired power levels and compare different designs.

As a remarkable design aspect, it has been observed that the most efficient rotors are those with high cone angles and low axis angles.

9 Conclusions and Recommendations

From the previous analysis, the following conclusions can be drawn:

1. Wind energy is a growing sector, with a huge development in the last 30 years. It is very relevant due to its attractive attribute that the fuel is free and environment friendly. Moreover, there are no marketing risks, as the product is electrical energy, and projects do not need manpower investment. All these make wind energy one of the cheapest current sources of electrical energy.

2. Blade Element Momentum Theory is the aerodynamic base for all wind turbine calculations. However, there are many phenomena not fully understood due to several aspects that are unique for wind turbine aerodynamics, as unsteady conditions of wind, influence of stall during the operation, or influence of the three- and two-dimensional flow combination.

3. There are several current tools that help wind turbine calculations. However, they do not support them at a preliminary design level, and, besides, they do not introduce installation angles, which are one of the scopes of this thesis. Therefore, it has been created the Blade Element Momentum Spread Sheet to assist the needs of design set for this study.

4. It has been drawn how the trend in wind turbine performance has been the stall-operated fixed-speed design. Nevertheless, direction towards variable speed in new large wind turbines ends in better output power quality to the grid, together combined with pitch regulation. However, new paths in wind turbine design follow a combination between pitch regulation and stall within variable-speed wind turbines, which limits loads and fatigue and is almost universally employed in new large wind turbine designs.

5. Related to rotor design, it can be proved that the higher power coefficients are obtained for base-rotor-type wind turbines ($\kappa = 85°$, $\tau = 0°$) compared to rotors with other combinations of installation angles. Therefore, it can be demonstrated that the most effective rotor is the base rotor, with a high cone angle and a low axis angle. Also is remarkable within other combinations of installation angles that, as κ gets lower, the power curve gets more abrupt (less rounded), and as τ gets lower, they are obtained bigger maximums.

6. Chord distribution can be set as a trapezoid profile. The ideal blade produces an ideal reduction at every point, but is not constructively viable, since in the vicinity of the root it grows to enormous widths and requires unnecessarily material. Nevertheless, a trapezoid profile is very simple to manufacture and is only about 1% worse than the ideal blade.

7. The twist angle distribution has to be set as a compromise solution taking into account the desired results in power output that the user requires.

8. Pitching the blades has effect on the final power output. There are two types of pitching: stall and feather. It has been demonstrated with Blade Element Momentum Theory that negative pitch angle settings increase power outputs for same wind speeds, which at the end produces stall on the blade, commonly used in fixed-speed wind turbines, limiting loads and fatigue. When a positive pitch setting is introduced, power coefficients reduces at the same wind speed causing feather, which is used in variable-speed wind turbines to maintain a rated power output.

9. When designing a wind turbine, it can be observed that the higher the number of blades is, the more effective the rotor is. This can lead into the idea that a rotor should include a great number of blades; however it comes into play the manufacturing cost of the wind turbine. Wind energy should maintain a low producing cost in order to have a competitive advantage over other electric energy sources. Therefore, a further optimization taking into account the economic perspective must be done.

On the other hand, there are several future improvements that could be done by future analysts. Some of these are related to the Blade Element Momentum Spread Sheet:

1. Introduction of a more realistic airfoil transition along the blade. This could lead into a more accurate result that would help into an actual preliminary design.

2. Study of different twist angle distributions. It can be done by choosing another solution of twist distribution for a different combination of λ_t and θ_m, and fixing it as the constant nonlinear twist angle distribution forcing at the tip $\beta_t = 0°$. This can be done several times in order to observe which one gives a better power output.

3. Selection and introduction of a rate power level for each analysed wind turbine in order to set a pitching to stall (fixed speed) or to feather (variable speed) performance.

4. Introduction of the geometrical results into a CAD tool, so that the designed blade can be obtained in 3D.

5. Introduction of economic features, as manufacturing costs and operating profits, in order to optimize the wind turbine with commercial use aspects.

List of References

Auld 1995 AULD, D. J.; SRINIVAS, K.: Aerodynamics for Students, 1995. – URL: https://t1p.de/4okfh

Burton 2001 BURTON, Tony; SHARPE, David; JENKINS, Nick; BOSSANYI, Ervin: *Wind Energy Handbook*. West Sussex, 2001

Betz 1927 BETZ, A.: *Tragflügel und hydraulische Maschinen. Handbuch der Physik*, vol.7, pp.256-259, Berlin, 1927

Drela 2004 Drela, Mark: *QPROP: Propeller/Windmill Analysis and Design*. – URL: https://web.mit.edu/drela/Public/web/qprop

Enercon ENERCON: Homepage. – URL: https://www.enercon.com

Epps 2010 EPPS, B.P.: *OpenProp – Integrated Rotor Design and Analysis.* Dartmouth College, School of Engineering, Hanover, NH, USA, 2012. – URL: https://openprop.engineering.dartmouth.edu

Franquesa 1989 FRANQUESA, Manuel: *Kleine Windräder : Berechnung und Konstruktion*. Wiesbaden : Pfriemer, 1989

Freris 1990 FRERIS, L. L: *Wind Energy Conversion Systems*. New York : PrenticeHall, 1990. – URL: https://www.amazon.com/dp/0139605274

Glauert 1935 GLAUERT, H.: Airplane Propellers. In: DURAND, W. F.: *Aerodynamic Theory*, *Vol. IV*, 1935

Hermann 2004 HERMANN, Lutz: *Windkraft 3.41 – Programm zur Konstruktion und Berechnung von Windrädern*. – URL: http://www.bitpilot.de/#nr2

Hütter 1942 HÜTTER, Ulrich W.: *Beitrag zur Schaffung von Gestaltungsgrundlagen für Windkraftwerke*. Dissertation. Technische Hochschule Wien, 1942

Kerwin 2007 KERWIN, Justin E.: *Hydrofoils and Propellers*. MIT Open Courseware, Course 2.23: Cambridge, MA, USA : MIT, 2007. – URL: https://t1p.de/xbfcy

Lanchester 1915 LANCHESTER, F. W.: A Contribution to the Theory of Propulsion

and the Screw Propeller. In: *Journal of the American Society for Naval Engineers*, 1915.

Larrabee 1979 LARRABEE, E. E.: *Practical Design of Minimum Induced Loss Propellers. Wichita,* April 1st, 1979, Business Aircraft Meeting and Exposition. SAE Technical Paper 790585, 1979. – URL: https://doi.org/10.4271/790585

Lerbs 1952 LERBS, H.W. [Hamburgische Schiffbau Versuchsanstalt, Germany]: Moderately Loaded Propellers with a Finite Number of Blades and an Arbitrary Distribution of Circulation. *Transactions of the Society of Naval Architects and Marine Engineers*, vol. 60, no. 1, paper: T1952-1, 1952

Lindemann 1985 LINDEMANN, Dieter: *Zur aerodynamischen Berechnung eines Windenergie-Konverters am Beispiel des Wagner- Rotor*. Seminarvortrag. Hannover, Germany : Institut für Mechanik, Universität Hannover, 1985. – URL: https://nbn-resolving.org/urn:nbn:de:gbv:18302-aero1985-06-19.010

Lindemann 1988 LINDEMANN, Dieter: *Berechnung der reibungsfreien Strömung in Rotoren von Windkraftanlagen*. Hannover, Germany : Institut für Mechanik, Universität Hannover, 1988. – URL: https://nbn-resolving.org/urn:nbn:de:gbv:18302-aero1988-02-19.017

Marten 2010 MARTEN, David: *The QBlade Software*, 2010. – URL: https://qblade.org

Maheri 2006 MAHERI, A.; NOROOZI, S.; TOOMER, C.; VONNEY, J.: *Damping the Fluctuating Behavior and Improving the Convergence Rate of the Axial Induction Factor in the BEMT-based Aerodynamic Codes*. Bristol, UK : University of West England, 2006. – URL: https://www.researchgate.net/publication/277016534

Montgomerie 2004 MONTGOMERIE, B: *Methods for Root Effects, Tip Effects and Extending the Angle of Attack Range to +-180, with Application to Aerodynamics for Blades on Wind Turbine and Propellers*. FOI Swedish Defence Research Agency, Scientific Report FOI-R-1035-SE, 2004. – URL: https://www.foi.se/rest-api/report/FOI-R--1305--SE

Moragues 2003 MORAGUES, Jaime; RAPALLINI, Alfredo: *Energía Eólica*. Buenos Aires : Instituto Argentino de la Energía "General Mosconi", 2003.

URL: https://t1p.de/5vywp

Morris 2011 MORRIS, Lindsay: Direct Drive vs. Gearbox: Progress on Both Fronts. In: *Power Engineering*, vol. 115, no. 3, pp. 38-42, 2011.

Muljadi 2013 MULJADI, E.; SINGH, M.; GEVORGIAN, V.: *Fixed-Speed and Variable-Slip Wind Turbines Providing Spinning Reserves to the Grid*. Vancouver: National Renewable Energy Laboratory, 2013. – URL: https://www.nrel.gov/docs/fy13osti/56817.pdf

Özdemir 2013 ÖZDEMİR, Gökhan: *Variable speed versus fixed speed*. – URL: https://t1p.de/parbd

Rama 2016 RAMA, Usha: *Induction Generator as a Wind Power Generator*. – URL: https://t1p.de/v2iu2

Schenk 2007 SCHENK, Helmut: *Propeller Calculator*. – http://www.drivecalc.de/PropCalc

Schmitz 1956 SCHMITZ, Gerhard: Theorie und Entwurf von Windrädern optimaler Leistung. In: *Wissenschaftliche Zeitschrift der Universität Rostock*, 5. Jg. 1955/56, Rostock, Germany, 1956

Sheldahl 1981 SHELDAHL, Robert E.; KLIMAS, P. C.: *Aerodynamic Characteristics of Seven Symmetrical Airfoil Sections through 180-Degree Angle of Attack for Use in Aerodynamic Analysis of Vertical Axis Wind Turbines*. Albuquerue, NM, USA : Sandia National Lab, 1981. – URL: https://www.osti.gov/biblio/6548367

Stubblefield 2008 STUBBLEFIELD, J. M.: *Numerically Based Ducted Propeller Design using Vortex Lattice Lifting Line Theory*. Master Thesis. Massachusetts Institute of Technology. Department of Mechanical Engineering, 2008. – URL: http://hdl.handle.net/1721.1/45209

Tong 2010 TONG, Wei.: *Wind Power Generation and Wind Turbine Design*. Southhampton, Boston: WIT Press, 2010. – URL: https://n2t.net/ark:/13960/t56d9866g

Wagner WAGNER, G.: *Formelsammlung Windenergie.* List, Sylt, Germany : Dr.Wagner GmbH, Windenergy-Converter, 1982 (approximately)

Appendix A

Numeric Results from Blade Element Momentum Spread Sheet

The base rotor ($\kappa = 85°$, $\tau = 0°$) returns the following results:

Table A.1 Results for base rotor

$\kappa = 85°$	$\tau = 0°$	$L = 10$ m	$L_0 = 1$ m	$z = 3$	$\omega = 100$ rpm	$t_0/t_i = 0.5$
λ_t	C_{Pi}	η_P	$C_{Pi} \cdot \eta_P$	η_z	C_{PTot}	$C_P \cdot \Delta\lambda_t$
1.000	0.015	0.000	0.000	0.452	0.000	0.000
2.000	0.051	0.123	0.002	0.629	0.001	0.001
3.000	0.091	0.386	0.023	0.728	0.016	0.009
4.000	0.297	0.874	0.263	0.788	0.207	0.112
5.000	0.31	0.858	0.261	0.827	0.216	0.211
6.000	0.292	0.675	0.22	0.853	0.188	0.202
7.000	0.4	0.722	0.273	0.873	0.238	0.213
8.000	0.428	0.631	0.249	0.888	0.221	0.23
9.000	0.45	0.545	0.222	0.9	0.2	0.211
10,000	0.454	0.504	0.222	0.91	0.202	0.201
11.000	0.461	0.485	0.211	0.918	0.194	0.198
12.000	0.463	0.394	0.166	0.925	0.153	0.174
13.000	0.462	0.368	0.156	0.93	0.145	0.149
14.000	0.463	0.301	0.127	0.935	0.119	0.132
15.000	0.47	0.264	0.116	0.939	0.109	0.114
16.000	0.467	0.23	0.108	0.943	0.101	0.105
17.000	0.47	0.216	0.101	0.946	0.096	0.099
18.000	0.477	0.201	0.094	0.949	0.089	0.092
19.000	0.477	0.185	0.086	0.952	0.082	0.086
20.000	0.478	0.146	0.073	0.954	0.069	0.076

Table A.2 Maximum power coefficient and its tip speed ratio for the base rotor

C_{Pmax}	0.238
λt	7.000

The second rotor ($\kappa = 60°$, $\tau = 30°$) returns the following results:

Table A.3 Results for base rotor with $\kappa = 60°$, $\tau = 30°$

$\kappa = 60°$	$\tau = 30°$	L = 10 m	$L_0 = 1$ m	z = 3	$\omega = 100$ rpm	$t_0/t_i = 0.5$
λ_t	C_{Pi}	η_P	$C_{Pi} \cdot \eta_P$	η_z	C_{PTot}	$C_P \cdot \Delta\lambda_t$
1.000	0.034	0.124	0.003	0.452	0.001	0.001
2.000	0.143	0.447	0.096	0.629	0.06	0.031
3.000	0.236	0.668	0.178	0.728	0.13	0.095
4.000	0.333	0.727	0.244	0.788	0.192	0.161
5.000	0.36	0.607	0.218	0.827	0.18	0.186
6.000	0.391	0.509	0.193	0.853	0.165	0.173
7.000	0.445	0.437	0.192	0.873	0.167	0.166
8.000	0.449	0.349	0.158	0.888	0.14	0.154
9.000	0.455	0.279	0.134	0.9	0.121	0.131
10,000	0.462	0.223	0.109	0.91	0.1	0.11
11.000	0.468	0.188	0.093	0.918	0.085	0.092
12.000	0.476	0.161	0.08	0.925	0.074	0.08
13.000	0.48	0.144	0.072	0.93	0.067	0.07
14.000	0.481	0.126	0.063	0.935	0.059	0.063
15.000	0.484	0.11	0.055	0.939	0.052	0.055
16.000	0.486	0.095	0.047	0.943	0.045	0.048
17.000	0.487	0.081	0.04	0.946	0.038	0.041
18.000	0.488	0.07	0.035	0.949	0.033	0.036
19.000	0.489	0.06	0.03	0.952	0.029	0.031
20.000	0.49	0.05	0.025	0.954	0.024	0.026

Table A.4 Maximum power coefficient and its tip speed ratio for the second rotor

C_{Pmax}	0.196
λt	4.000

The third rotor ($\kappa = 45°$, $\tau = 45°$) returns the following results:

Table A.5 Results for base rotor with $\kappa = 45°$, $\tau = 45°$

$\kappa = 45°$	$\tau = 45°$	L = 10 m	$L_0 = 1$ m	z = 3	$\omega = 100$ rpm	$t_0/t_i = 0.5$
λ_t	C_{Pi}	η_P	$C_{Pi} \cdot \eta_P$	η_z	C_{PTot}	$C_P \cdot \Delta\lambda_t$
1.000	0.191	0.121	0.056	0.452	0.025	0.013

2.000	0.269	0.165	0.078	0.629	0.049	0.037
3.000	0.342	0.226	0.108	0.728	0.079	0.064
4.000	0.397	0.318	0.153	0.788	0.121	0.100
5.000	0.427	0.342	0.165	0.827	0.136	0.129
6.000	0.445	0.336	0.162	0.853	0.139	0.137
7.000	0.458	0.316	0.152	0.873	0.133	0.136
8.000	0.464	0.29	0.138	0.888	0.123	0.128
9.000	0.467	0.259	0.123	0.900	0.111	0.117
10,000	0.469	0.228	0.107	0.910	0.098	0.104
11.000	0.475	0.194	0.092	0.918	0.085	0.091
12.000	0.475	0.163	0.076	0.925	0.071	0.078
13.000	0.477	0.139	0.064	0.93	0.059	0.065
14.000	0.480	0.119	0.054	0.935	0.05	0.055
15.000	0.479	0.099	0.045	0.939	0.043	0.046
16.000	0.480	0.085	0.039	0.943	0.036	0.04
17.000	0.481	0.071	0.033	0.946	0.031	0.034
18.000	0.480	0.061	0.028	0.949	0.027	0.029
19.000	0.479	0.05	0.023	0.952	0.022	0.024
20.000	0.485	0.042	0.020	0.954	0.019	0.021

Table A.6 Maximum power coefficient and its tip speed ratio for the second rotor

C_{Pmax}	0.139
λt	6.000